MODELING AND MEASURING ELECTRODEPOSITION PARAMETERS NEAR ELECTRODE SURFACES TO FACILITATE CELL PERFORMANCE OPTIMIZATION

by

Abhijeet Shukla

A thesis submitted to the faculty of
The University of Utah
in partial fulfillment of the requirements for the degree of

Master of Science

Department of Metallurgical Engineering

The University of Utah

August 2013

The University of Utah Graduate School

STATEMENT OF THESIS APPROVAL

The thesis of **Abhijeet Shukla**

has been approved by the following supervisory committee members:

Michael L. Free	, Chair	**05/09/2013** Date Approved
Sivaraman Guruswamy	, Member	**05/09/2013** Date Approved
Manoranjan Misra	, Member	**05/09/2013** Date Approved

and by **Jan D. Miller** , Chair of

the Department of **Metallurgical Engineering**

and by Donna M. White, Interim Dean of The Graduate School.

ABSTRACT

Unusual deposits of copper may cause short-circuits in copper electrowinning cells. The objectives of this thesis are to provide experimental and modeling data for near surface electrowinning that is pertinent to industrial electrowinning. A bench-scale electrowinning cell was set up to produce copper under the similar conditions used in industrial copper electrowinning to see the effect of various operating parameters such as Cu concentration in electrolyte, electrolyte temperature, current density, and guar concentration. A statistical analysis was performed to analyze the deposited thickness, surface roughness, and maximum feature height data. A finite element analysis-based simulation package (COMSOL Multiphysics) was used to validate the experimental data.

The statistical analysis of deposits obtained from the short-term and long-term experiments shows there is a significant effect of current density and temperature on the roughness of copper deposits. These experiments were performed using a number of small coupons, and linear maximum feature height was analyzed using various statistical distribution density functions. Extrapolation from the small length of the sample to a length of 1 meter was carried out to see the effect of operating parameters on short-circuit. Extrapolation for time was also carried out and it was found that, with 475 A/m^2 current density, 175 gm of guar per tonne of copper, 35 g/l of concentration of Cu, and 55°C temperature, the cell may be short-circuited by growth of copper in 12 days. On the other hand, with 325 A/m^2 current density, 250 gm of guar per tonne of copper cathode,

45 g/l of copper concentration, and 55°C temperature, short-circuiting is predicted in 23 days.

Linear maximum feature height data were compared to 3-dimensional surface feature height data using stacked 2-dimensional slices of maximum feature height with intervals of 0.05 cm per slice for 10 layers for two experiments (rough and smooth deposits). The 3-dimensional analysis of surface roughness was very similar to 2-dimensional line scan. Long-term experiments showed that short-circuit occurred after 9.5 days of experiment, which is 2.5 days less than the linear data prediction. Further validation was performed using an experiment with 475 A/m^2 current density, 175 gm guar per tonne of copper cathode, 35 g/L of Cu, and 55°C temperature. The first short-circuit in this test was observed after 8 days of experiment, as predicted by statistical analysis. These results were compared with the model predicted ratio of current density to limiting current density (i/i_L) and it was noted that model prediction is in proximity to the experimentally obtained data.

This study provides an industrial relevant baseline against which the new operating parameters can be compared. Results from the bench-scale copper electrowinning experiments, statistical analysis, and modeling show that operating parameters adjustments can reduce short-circuiting in copper electrowinning.

“JAI SAI BABA”

I dedicate my thesis work to my family. A special feeling of gratitude to my loving parents, **Mahesh Prasad Shukla** and **Rashmi Shukla,** whose words of encouragement and push for tenacity ring in my ears. My sisters **Kamana** and **Bhawana** have never left my side and are very special.

TABLE OF CONTENTS

LIST OF TABLES

ACKNOWLEDGEMENTS

I would sincerely like to express my heartfelt gratitude towards Dr. Michael L. Free for providing me with such a wonderful opportunity to work on this project. His constant guidance, persistence, and words of encouragement have been like the pillars of inspiration for me, throughout my stay at the University of Utah. Words of wisdom have always been helpful and appreciated at each stage of research, leading to its completion.

I would also like to express my sincerest thanks and gratitude to members of my supervisory committee, Dr. Sivaraman Guruswamy and Dr. Manoranjan Misra, for their invaluable inputs and suggestions. They took time out of their extremely busy schedules and helped me in pursuing my research diligently, leading to its completion.

I would like to extend my heartfelt gratitude and thanks to Thien Vethosodsakda for his immense contribution during preparation of the thesis. He performed the concluding set of experiments for my thesis to perfection and documented them for my ease (Section 5.2 and 5.3) in proper format. Lauryn Hansen has also helped me throughout the preparation of this thesis, and hence, I would like to express my gratefulness towards her. She has played a major role in getting this project to its completion.

I would like to extend my gratitude to fellow lab mates and research group members, Mark Robison, Prashant Sarswat, and Soumya Kar, for their precious help and personal insights into the various problems and obstacles faced during research work.

These people deserve a special mention as they have supported me through thick and thin, all the way along.

I would also like to thank AMIRA and the collaborating companies for sustaining the research work for all these years, through valuable financial support and co-ordination. I would also like to express my sincere thanks to Ms. Evelyn Wells and Ms. Kay Argyle for valuable administrative support.

Lastly, I would like to express my gratitude towards my parents, siblings, friends, and all those who had indubitable faith in my abilities, and for the limitless support I received from them, throughout my research work.

CHAPTER 1

INTRODUCTION

1.1 Background and Motivation

Electrowinning is the process of recovering metal from solution by electrolysis. Two electrodes are placed in a solution containing metal ions, and electric current is passed between them to deposit the metal on the negative electrode called the cathode. In the process of recovering the metal from an aqueous solution with metal ion, oxygen is evolved at the positive electrode called the anode. Operating parameters such as current density, concentration of metal ion, and temperature are generally chosen to give a dense, compact electrodeposit. Additives are included in the electrolyte solution to improve the quality of electrodeposited metal. About 20% of the world's copper production is based on hydrometallurgical processes, with electrowinning being one of the important steps. The electrowinning process has been in existence since the 1800s and it has evolved due to research and developments. Electrowinning is an energy-intensive process and as such, it accounts for a significant part of copper production costs.

In a typical copper electrowinning operation, the electrolytic cells are rectangular tanks containing 20-50 cathodes and a nearly matching number of anodes. An additiona anode is required in each cell in order to ensure plating occurs on both sides of each cathode. The anodes are usually made from lead calcium alloys and the modern

traditional cathodes for copper electrowinning are made of stainless steel. Conventional electrowinning plants use a variety of Walker configuration-based intercell bars designed to ensure a common voltage for every cathode–anode pair of a cell[1].

The copper electrowinning process consumes a large amount of energy. Electrical resistance or disruption, like loose electrode busbar contacts and short-circuits between electrodes, can increase the energy consumption and decrease the amount and quality of copper produced[2]. The uniformity of current distribution in an electrowinning cell affects the industrial operation performance.

Electrowinning objectives include copper production rate and smooth cathode deposit[3]. These objectives can be achieved by optimizing the process parameters such as current density, electrolyte temperature, electrolyte concentration, and concentration of additives. Proper adjustment of the process parameters allows somewhat higher current density, and correspondingly increases the production of copper without short-circuiting.

1.2 Problem Statement

The electrowinning process is significantly affected by process parameters such as current density, electrolyte temperature, electrolyte concentration, and concentration of additives. Industry can be operated at relatively high current density giving a high rate of copper production, but increased current density increases the possibility of short-circuiting in the cell. During the operation at high current density, dendrites and other protruding electrodeposited structures form at the cathode. Such structures can grow from the cathode to the anode and cause short-circuiting. An additive such as Guar is often added to the electrowinning cell to slow undesirable growth at the cathode surface.

However, high current density often causes short-circuits in the cell because of the bent or misaligned cathode. Short-circuiting in the electrowinning cell causes high energy consumption and loss in copper production. Short-circuit that occurs in the electrowinning cell as a consequence of undesirable outward growth increases copper production costs.

1.3 Aim

The objectives of this study are to provide experimental and modelling data for near surface electrowinning that is pertinent to industrial electrowinning. Improved modelling is accompanied by experimental validation and statistical analysis. The model was designed to provide output data that includes primarily deposit profile, short-circuit tendency, and roughness information as a function of input parameters. Modelling was validated using a bench-top electrowinning cell. Measurements of cathode deposit profiles are used to compare with model predictions. Measured electrodeposit data were used with statistical evaluations to produce electrode location-based probability maps for short-circuiting based on appropriate statistical functions.

1.4 Hypotheses

In view of the reported problem of short-circuiting and high energy consumption associated with the high current density operation, the adjustment of operating parameters may be altered to reduce these adverse effects. Research to reduce the short-circuiting in the electrowinning cell is ongoing, but much of it is focused on changing the busbar electrode design. However, adjustment of operating parameters may also be a good way

to mitigate short-circuiting. Therefore, a number of experiments with varying operating parameters were performed in this study to prove or disprove this hypothesis. High and low values of current density, electrolyte temperature, electrolyte concentration, and additive concentration were used to test cathode deposits outcome such as roughness and maximum feature height.

1.5 Research Questions

- ✓ What affects unusual growth of deposits?
- ✓ What is the relationship between operating parameters and cathode deposit roughness and maximum feature height?
- ✓ What are other effects of changing the operating parameters?

1.6 Objectives

- ✓ To set up a laboratory-scale electrowinning cell where cathode deposit can be obtained to analyze the effect of different operating parameters.
- ✓ To develop an electrowinning cell model using finite element analysis-based simulation tool to validate the experimentally obtained results.
- ✓ To analyze the morphology of the copper deposit obtained from various experiments.
- ✓ To compare the cathode deposits obtained with varying parameters.
- ✓ To assess the reliability of modeling results.
- ✓ To compare the modeling and experimental results in terms of deposit thickness and current density distribution.

1.7 Research Layout

The rest of this thesis will be organized as follows:

- ✓ Theoretical Background
- ✓ Literature Review
- ✓ Experimental Procedure
- ✓ Results and Discussions
- ✓ Conclusion and Recommendation

CHAPTER 2

THEORETICAL BACKGROUND

2.1 Electrochemical Thermodynamics

2.1.1 Electrochemical Processes

Electrode processes are chemical reactions that involve the transfer of charge, usually electrons across the interface between an electrode and an electrolyte. For electrochemical reactions to occur, an anode, a cathode, ionic contact between the electrodes via an electrolyte, and electronic contact are necessary. At the anode, oxidation of species occurs, which is a loss of electrons while at the cathode, a simultaneous reduction process occurs. This reaction consumes those electrons provided by the oxidative process. Unless these electrons can be consumed, the anodic reaction cannot occur[4].

2.1.2 Electrode Potential

Electrochemical reactions that characterize a metal-solution interface occur at the surface of the metal, when a metal is immersed in a given solution. This leads to corrosion of the metal. The reactions create an electrochemical or equilibrium potential called electrode potential, or open circuit potential, or *E* (corrosion) potential. The potential of a metal is the means by which the anodic and cathodic reactions are kept in

balance. Since the open circuit potential ends up at the potential where the cathodic and anodic currents are equal, it can also be referred to as a mixed potential.

2.1.3 Nernst Equation – Measurement of Electrode Potential

Electrode potentials can be calculated from the Nernst equation when the activity of metal cations is not at unit activity (nonstandard conditions):

$$E_{cell} = {E^0}_{cell} - \frac{2.303\,RT}{nF}\log\frac{c_r}{c_o} \tag{2.1}$$

where, ${E^0}_{cell}$ is the standard potential (the equilibrium potential when all reactants and products are at their standard states), n is the number of electrons participating in the reaction, R is the gas constant, T is temperature, c_r and c_o are the concentrations of the reduced and oxidized species, respectively. The thermodynamic equation can also be written in terms of a ratio of activities.

2.2 Electrochemical Kinetics

2.2.1 Electrochemical Polarization

Polarization is the potential change from the equilibrium half-cell electrode potential caused by a net surface reaction or an applied potential. This causes current to flow via electrochemical reactions that occur at the electrode surface. The amount of current is controlled by the kinetics of the reactions and the diffusion of reactants both towards and away from the electrode.

The extent of polarization is measured by the overpotential, η. For anodic polarization, electrons are removed from the metal and a deficiency results in a positive

potential change due to the slow liberation of electrons by the surface reaction, and η_a must be positive. For cathodic polarization , the cathodic overpotential η_c, electrons are supplied to the surface, and a buildup in the metal due to the slow reaction rate causes the surface potential, E, to become negative compared to the equilibrium half-cell electrode potential, E_{eq} . Thus, η_c is negative by definition[5].

Over potential is determined from equations 2.2 and equation 2.3 shows that overpotential is related to current density:

$$\eta = E - E_{eq} \qquad (2.2)^{6}$$

$$\eta = C \log i + D \qquad (2.3)^{5}$$

Equation 2.3 is known as the Tafel equation, where C and D are constants and *i* is the cell current.

2.2.2 Faraday's Law of Electrolysis

According to Faraday's law of electrolysis, the mass of the metal deposited at the cathode (or dissolved from the anode) is proportional to the quantity of electricity.

If 'm' is the mass or amount is a substance deposited or liberated and 'I' is the current in amperes, which passes for't' seconds, then according to the law

$$m \propto It \qquad (2.4)$$

In another way,

$$m = \frac{MIt}{nF} \tag{2.5}$$

where,

M = Molecular weight of the substance

n = Number of electrons

F = Faraday's constant

2.2.2.1 Applications of Faraday's Law

2.2.2.1.1 Weight of deposit

Weight of deposits can be calculated using the equation number 2.5.

2.2.2.1.2 Thickness of deposit

The deposit thickness can be calculated using Faraday's law. To calculate the thickness of deposited layer, the weight of metal plated m is determined first using equation (2.5) and the density ρ (in g/cm^3) of the metal is noted. Then the following equation is used to calculate the thickness of deposited layer:

$$T = \frac{m}{a \times \rho} \tag{2.6}$$

where, 'a' is the plated area in square centimeters[7].

2.2.3 Butler – Volmer Equation

The Butler-Volmer equation assumes the concentration at the electrochemical interface is equivalent to the bulk concentration. If mass transport becomes a limiting factor, this assumption will no longer be valid. Thus, the bulk concentration, which is implicit in the i_0 value (i_0 is a direct function of bulk concentration), must be multiplied by the surface concentration divided by the bulk concentration. This procedure effectively replaces the bulk concentration term inherent in i_o with the desired surface concentration. The resulting Butler-Volmer equation is:

$$i = i_0 \left[\frac{C_{sa}}{C_{ba}} exp\left(\frac{\alpha_a F\left(E - E_{eq}\right)}{RT} \right) - \frac{C_{sc}}{C_{bc}} exp\left(\frac{-\alpha_a F\left(E - E_{eq}\right)}{RT} \right) \right] \qquad (2.7)$$

where the "*s*" subscript denotes the surface concentration, "*b*" represents bulk concentration, "*a*" represents anodic, and "*c*" represents cathodic[8].

2.3 Electrowinning of Copper

Commercial electrowinning generally entails:

- ✓ Immersing metal cathodes and inert, conductive anodes in an aqueous solution of Copper sulphate containing free sulphuric acid ($CuSO_4$-H_2SO_4-H_2O electrolyte), applying an electrical potential between the anodes and cathodes,
- ✓ Plating pure metallic copper from the electrolyte onto the cathodes.

Cathodes may be stainless steel blanks or copper 'starter sheets' and the anode is made of Pb and Sn alloy. Copper is electrodeposited on the cathodes for about one week, after which harvesting is done while water dissociates into hydrogen ions and oxygen at

the anode[3]. An additive such as Guar is added in to electrolyte solution to obtain smooth surface deposit.

2.3.1 Electrowinning Reactions

During electrowinning of copper, the following reactions occur at the electrodes

Cathode:

$$Cu^{2+} + 2e^{-} \rightarrow Cu \qquad E^0 = +0.34\ V \quad (2.8)$$

Anode:

$$H_2O \rightarrow H^+ + OH^- \rightarrow \frac{1}{2}O_2 + 2H^+ + 2e^- \qquad E^0 = 1.23\ V \quad (2.9)$$

Equation 2.9 above is known as the oxygen evolution reaction (OER). Thus, an oxygen evolution reaction is an electrode reaction in which oxygen gas is produced at the anode of an electrolytic cell by the oxidation of hydroxyl (OH^-) ions or the oxidation of the water molecules of an aqueous solution[9].

2.3.2 Oxygen Evolution

Oxygen evolution is one of the most important technological reactions in electrochemistry taking place in many industrial processes. It is based on water electrolysis and it is included in metal electro-winning, cathodic protection, and electro-organic synthesis. Oxide-based anodes are more frequently used for the oxygen evolution in acid media[10]. The OER affects the economies of the copper electrowinning process.

Furthermore, this reaction enhances the harsh corrosive environment inside an electrowinning cell.

The overall electrowinning reaction is the sum of reactions 2.8 and 2.9 in the presence of sulfate ions[3].

$$Cu^{2+} + {SO_4}^{2-} + H_2O \rightarrow Cu + \frac{1}{2} O_2 + 2H^+ + {SO_4}^{2-} \qquad E_{cell} = 0.89\ V \quad (2.10)$$

If the applied potential is greater than the difference between the two half-cell reactions, electrodeposition of the metal will occur. The rate of electrodeposition depends on the applied potential and the associated electrochemical reaction kinetics. A significant overvoltage is needed to allow the water decomposition to occur at a reasonable rate. The overpotential for the metal deposition is generally not as large. If the voltage is not greater than the difference between the half-cell voltages plus the reaction overpotentials and solution and contact resistance voltage drops, no electrowinning occurs. The applied potential can be expressed mathematically as[8]:

$$\Delta V_{applied} = \Delta V_{Half\ Cell} + \Delta V_{cathodic\ overpotential} + \Delta V_{anodic\ overpotential} + \Delta V_{sol+cont.+misc.} \quad (2.11)$$

which is more commonly written using different terms as:

$$V_{applied} = E_{anodic} - E_{cathodic} + \eta_{anodic} + \eta_{cathodic} + IR_{solution} + IR_{others} \quad (2.12)$$

in which E is the specified half-cell potential, I is the overall current, η is the overpotential, and R is the resistance of the medium specified (V = IR - Ohm's Law).

2.3.3 Electrowinning Products

The main copper electrowinning products are:

- ✓ Pure copper metal at the cathode
- ✓ Oxygen gas at the anode
- ✓ Regenerated sulfuric acid in the solution

The copper is manually or machine-stripped from the stainless steel cathode blanks, washed, and sent to the market or the entire copper 'starter sheet' is washed and sent to the market. The oxygen enters the atmosphere while the acid is recirculated to the solvent extraction circuit[3].

2.3.4 Acid Mist

At the inert anode, water molecules are electrolyzed and oxygen bubbles are formed on the surface of the anode. These oxygen bubbles grow and eventually detach from the surface and rise in the bulk of the solution. These bubbles burst at the free surface of the solution and produce highly acidic droplets. The fine droplets become airborne and form an acid mist throughout the tankhouse of the electrowinning plant. There have been many attempts to eliminate or minimize acid mist in copper electrowinning operations. Polyethylene balls, suction hoods, mats, brushes and wipers, chemical reagents, and forced ventilation are examples of such attempts[11].

2.3.5 Current Density

Copper plating rate increases with increasing current density. However, excessive current density gives rough, nodular cathode deposits and decreased copper purity. Therefore, each plant chooses its current density based on a balance between these opposing factors[9].

2.3.6 Electrolyte Concentration

Electrowinning electrolyte typically contains 44 kg Cu^{2+} and 170 kg H_2SO_4 per m^3 as it enters an electrowinning cell. It contains about 5 kg Cu^{2+} less per m^3 as it leaves the cell[3].

2.3.7 Additives

Many electrowinning plants dissolve guar gum in their electrolytes (about 250 g/t of cathode copper) or glue[3]. Guar promotes dense, level copper deposits with minimum impurity entrainment[12]. Cobalt sulfate solution is also added to provide about 150 ppm Co^{2+} in electrowining electrolyte. Co^{2+} promotes O_2 evolution at the anode rather than lead oxidation. This minimizes lead contamination of the depositing copper and extends anode life[13]. Chloride ions are either naturally present in electrowinning electrolyte or are added as HCl at low levels. They promote dense, fine grain, low impurity copper deposits on the cathode[3].

2.3.8 Maximizing Copper Purity

The three main impurities in electrowon copper are[3]:

a) Lead (1 or 2 ppm) from anode corrosion product entrapment

b) Sulphur (4 or 5 ppm) from lead sulphate anode corrosion product and electrolyte entrapment and

c) Iron (1 or 2 ppm) from electrolyte entrapment.

According to Maki (1999)[14], cathode purity may be maximized by:

a) Straight vertical equispaced cathodes and anodes with no anode-cathode contact

b) Immediate thorough washing of the deposited copper

c) Frequent removal of anode corrosion products from the bottom of the electrowinning cells

d) Iron in electrolyte below 2 kg/m^3 to minimise iron in cathode copper.

2.3.9 Maximizing Current Efficiency

Current efficiencies in modern electrowinning plants can often be higher than 90%. The unused current is wasted by:

a) anode/cathode short circuits

b) stray current to the ground

c) reduction of Fe^{3+} to Fe^{2+} at the cathode and re-oxidation of Fe^{2+} to Fe^{3+} at the anode.

High current efficiency is important because it maximizes copper plating rate and minimizes electrical energy consumption[3].

2.4 Electrowinning Cell Disturbances

The copper electrowinning cell disturbances can be divided into two categories, mechanical and electrical.

2.4.1 Mechanical Disturbances

The mechanical disturbances consist of electrode shape errors and electrode positioning inaccuracies. The thickness of the electrowinning anode varies due to manufacturing method, creating one type of disturbance. Additionally, mechanical disturbances can also be caused by bent or misaligned electrodes[15].

2.4.2 Electrical Disturbances

Electrical disturbances include stray currents, loose contact, and short-circuits. Electrical disturbances increase the energy consumption and deteriorate the quality of produced cathode copper. The short-circuit develops between an anode and a cathode because of the unusual growth of deposits that happens due to locally increased cathode current density or nonuniform cathode copper deposition[15].

2.5 Modeling and Simulation

Modeling and simulations are cost-effective ways for understanding, optimizing, and controlling electrodeposition processes. A typical simulation yields the current distribution at the surface of the electrodes and the thickness and composition of the deposited layer. They are used to study important parameters such as: cell geometry,

electrolyte composition, electrode kinetics, operating voltages and currents, as well as temperature effects.

COMSOL Multiphysics™ is a finite element analysis, solver, and simulation software package for various physics and engineering applications, especially coupled phenomena, or multiphysics. The Electrodeposition Module uses the computational capability of COMSOL Multiphysics™ to simulate electrodeposition processes. Easy-to-use physics interfaces are provided for primary, secondary, and tertiary current distribution models, while very accurate geometric representations of deposited layer buildup are included as model parameters. The shape of the electrode can also be simulated with moving boundaries

The Electrodeposition Module is applicable to a variety of diverse applications including; metal deposition for electronics and electrical parts, corrosion and wear protection, decorative electroplating, electroforming of parts with thin and complex structure, and metal electrowinning[16].

2.5.1 The Electrodeposition, Tertiary Nernst – Planck Interface

The Electrodeposition, Tertiary Nernst-Planck (edtnp) interface, describes the current and potential distribution in an electrochemical cell taking into account the transport charged species (ions) in the electrolyte through diffusion, migration, and convection. This physics interface further assumes that the electroneutrality condition is valid in the electrolyte. Under these assumptions, the contributions to the transport of current in the electrolyte are from diffusion and migration of ions.

The interface also describes how the geometry of the cell is affected due to the deposition of species on the electrodes. Surface species, adsorbed on the electrode surfaces and their impact on the deposition processes, can also be modeled by the interface. When this interface is added, these default physics nodes are also added to the Model Builder—Electrolyte**,** Free Deformation**,** Zero Normal Mesh Velocity**,** Electric Insulation**,** No Flux, and Initial Values[17]**.**

2.5.1.1 External Depositing Electrode

The External Depositing Electrode node is used to define the surface and deposited metal concentration-dependent variables, as well as the electrode currents and reactions present on an external boundary of an electrolyte domain. Electrodes of an electrowinning cell are defined as External Depositing Electrode in the model.

The External Depositing Electrode node sets up boundary conditions for the dependent variables of the adjacent electrolyte domain. In addition, it also creates surface source terms for the depositing concentrations. When solving for a deforming geometry, it also sets a condition for the normal velocity of the boundary, based on the reaction rates, densities, and molar masses of the depositing species. When this node is added, these default physics nodes are also added to the Model Builder**.** Model Builder includes Surface Properties**,** Electrode Reaction, No Flux, and Initial Values[17]**.**

2.5.2 Laminar Flow Interface

The Laminar Flow (spf) interface has the equations, boundary conditions, and volume forces for modeling freely moving fluids using the Navier-Stokes equations as

well as solving for the velocity field and the pressure. The main feature is Fluid Properties, which adds the Navier-Stokes equations and provides an interface for defining the fluid material and its properties.

When this interface is added, these default nodes are also added to the Model Builder—Fluid Properties**,** Wall (the default boundary condition is No slip), and Initial Values[18].

2.5.2.1 Volume Force

The volume force node defines the force used in Navier Stokes equation depending on the domain selected for the modeling. It helps to include the effect of gravity in the model.

2.5.2.2 Pressure Point Constraint

The Pressure Point Constraint feature adds a pressure constraint at a point. If it is not possible to specify the pressure level using a boundary condition, the pressure must be set in some other way, for example, by specifying a fixed pressure at a point[18]. Figure 1 shows an image of the list of physics used for the modeling of copper electrowinning cell in COMSOL Multiphysics™.

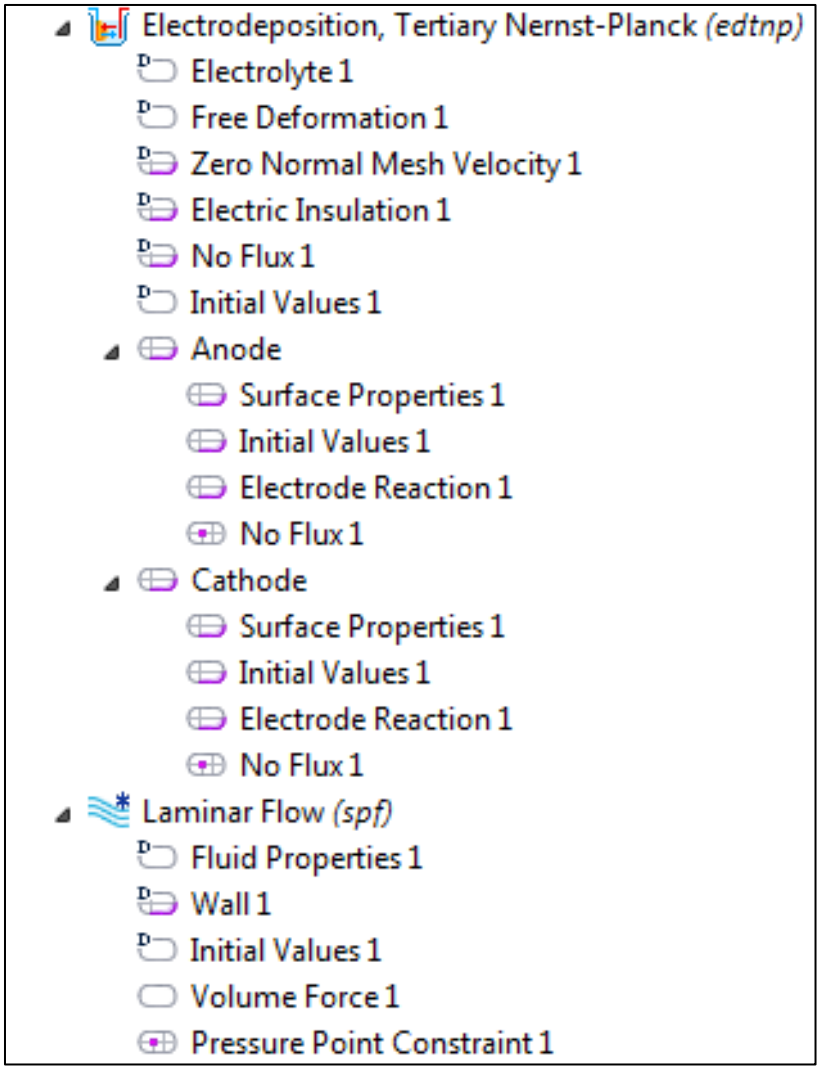

Fig. 1. List of physics used for the modeling of copper electrowinning cell in COMSOL Multiphysics™

CHAPTER 3

LITERATURE REVIEW

3.1 Energy Consumption in Copper Electrowinning Cell

The power requirements for the copper electrowinning operations are very high and depend primarily upon the applied voltage, as shown in equation 3.1:

$$P = ViA \tag{3.1}$$

where,

P = Power require

i = Current density

A = Total area of electrowinning surface

The amount of metal produced in copper electrowining operations depends upon the atom and amount of current that passes through the cell. The energy (kWhr/tonne) needed to electrowin the metal is expressed as:

$$Energy\left(\frac{kWhr}{tonne}\right) = \frac{V\,(n)26800}{M_w\beta} \times 100 \tag{3.2}$$

where,

V = Applied voltage

n = Number of electrons

M_w = Molecular weight of copper

β = Current efficiency (%)

The energy required for a copper electrowinning operation varies between 1300 and 2400 kWhr/tonne for the typical values of applied potential and current efficiencies (85-95%)[8]. The reason for the low current efficiencies is[19]:

- ✓ Inadequate circulation of the electrolyte
- ✓ Poor connections
- ✓ Circuit leakages
- ✓ Short-circuitry of the electrode caused by the dendritic growth of the copper during deposition.
- ✓ Parasitic reactions such as reduction of Fe^{3+} in to Fe^{2+}.

3.1.1 Short-circuit in Electrowinning Cell – Previous Investigations

In a copper electrowinning cell, short-circuit occurs mainly due to the following reasons:

- ✓ Misalignment of the electrodes
- ✓ Bent cathodes
- ✓ Unusual dendritic growth of electrodeposited copper.

A significant amount of research work is being carried out to reduce the short-circuiting in copper electrowinning operations, but most of it is focused on the

misalignment of electrodes which causes uneven current distribution. This thesis explores the idea of reducing the unusual dendritic growth of electrodeposited copper by optimizing the operating parameters. Figure 2 shows metallurgical short-circuits observed at the surface of a cathode in copper electrowinning operation[20]. The nodule shown in the picture was grown out of the cathode copper deposit and came into contact with an anode causing short-circuiting in the cell. The edges of the cathode are covered with the Teflon strips to prevent edge deposition.

3.1.1.1 Optical Intercell Bar

Eduardo P. Wiechmann, Anibal S. Morales, and Pablo Aqueveque have suggested an evolved Optibar intercell bar for copper electrowinning processes with current sensing capabilities. This technology upgrades the advantages of the conventional Optibar by providing a complete measuring system using magnetic sensors inside the capping board. One of the primary achievements of this bar is to limit short-circuit currents to a maximum of 1.5 p.u. of the actual process current. However, low-current short-circuits are more difficult to detect. Thus, conventional short-circuit detection instruments like gaussmeters and infrared cameras become ineffective[20].

3.1.1.2 Bypass-Backup Connection System

Eduardo P. Wiechmann, Luis G. Muñoz, Pablo E. Aqueveque, Guillermo A. Vidal, and J.A. Henríquez proposed a system for current mode segmented intercell bars. These bars are immune to short-circuits but sensitive to open circuits and dirty contacts. This new system adds segmented sidebars to interconnect in groups the otherwise

electrically insulated cathode and anode hanger ends. The combination of a segmented main bar with these sidebars offers immunity to short-circuits, open circuits and bypasses dirty contacts.

3.2 Effect of Operating Parameters

Studies have been performed to understand the effect of individual parameters on the deposition and surface morphology of electrodeposited copper. This thesis shows an overall effect of all the operating parameters together.

3.2.1 Effect of Copper Concentration in Electrolyte

The effect of copper concentration in electrolyte was studied by Das and Krishna. They observed a marginal increase in current efficiency during increase in Cu^{2+} concentration keeping the temperature and iron concentration constant. This may be due to the fact that when the Cu concentration in the cell is increased, the solution viscosity increases. This increase in viscosity impedes distribution of Fe^{3+} over the cathode surface[21]. They also noticed that the power consumption increased with decreasing Cu^{2+} concentration throughout the temperature range they studied. A similar trend was observed by Yuness Khouraibchia and Michael Moats too[22].

The similar study was performed by Ashour Owais on electrowinning of copper powder. He found that the efficiency is better in higher copper concentration than in lower concentration. His experiments show that the energy demand is lower at higher concentration of copper with better productivity. The explanation of this can be that increasing the Cu ion concentration in electrolyte will feed a sufficient and constant

amount of Cu^{2+} to the cathode surface, which improves the deposition rate and consequently the efficiency[23].

3.2.2 Effect of Temperature

Copper electrowinning is industrially carried under a wide range of temperature varying from 25°C to 65°C[24]. Therefore, there is no optimum temperature to operate electrowinning plants. The best temperature is determined by the other operating parameters specific to each plant. The effect of temperature on copper electrowining is significant.

It is shown by the Ashour[23] that increasing electrolyte temperature from 35°C to 65°C increases the current efficiency and consequently decreases the energy demand. He found that the particle size of the produced copper powders is finer with increase of the electrolyte temperature.

In addition, Krishna and Das studied the effect of electrolyte temperature on surface morphology of electrodeposited copper and they found that there is no change in size and shape of the grains though the temperature was raised from 30°C to 60°C. They found a number of fine pores at the surface of cathode deposit at lower temperature but the pore size was increased with decreases in number[21].

It has been recorded by Mishra and Cooper that changing the electrolyte temperature under the same parameters affects the quality of copper cathode significantly[25]. According to Pradhan, the surface roughness became more pronounced at higher temperature than in lower temperature[26].

A significant amount of research has been carried to see the effect of temperature on cathode deposits and it can be concluded that a vigorous control and optimization of temperature with other operating parameters is required to produce high-quality copper cathode.

3.2.3 Effect of Additives

The process of electrochemical crystal growth cannot be achieved under "ideal" conditions, i.e., without additives, due to the crystallographic properties of the substrate and depositing metal[27]. In copper electrowinning chloride ions and Guar are commonly used as additives to produce dense and high ductility copper cathodes. The organic additives significantly affect the current – potential relationship due to their interactions with the components of the electrolyte system, including with chloride ions.

3.2.3.1 Effect of Chloride Ions

According to the Bijaylaxmi Panda[28], the presence of added chloride ion in the electrolyte solution containing 150 ppm of Co^{2+} ion was found to increase the anode and the cell potentials and decrease the cathode potential. It has been reported from many authors that adding chloride ions in electrolyte solution has different effects on deposition of copper. From an electrochemical perspective, chloride acts as both polarizer and depolarizer. Ilgar and O'Keefe found that addition of 20 ppm of chloride ion slightly polarizes the electrode reaction at lower overpotentials[29].

In addition, it has been reported by Wang and O'Keefe that chloride at less than 5 ppm acts as a polarizer with the formation of CuCl. They suggested that if the

concentration of chloride is higher than 20 ppm, it acts as a depolarizer. Similar conclusions were reported by Yao, Fabricius, and Lakshmanan[30].

Finally, chloride ions are added to the electrolyte solution in the form of HCl. The concentration of chloride ions should never be greater than 30 ppm because it causes chlorine gas evolution, according to the following equation:

$$2Cl^- + \frac{1}{2}\,O_2 + H_2O \rightarrow\ Cl_2 + 2OH^- \qquad (3.3)$$

This leads to pitting corrosion of the top of the stainless steel blade, causing the depositing copper to stick and resist detachment[3].

3.2.3.2 Effect of Organic Additives

Guar is the industry standard organic additive used in copper electrowinning as a weak leveling agent for about 40 years to produce bright and dense copper deposit. The success of this reagent leads to its wide use at most copper electrowinning operations, as surveyed by Robinson et al.[24] at an average dosage of 250 g/tonne of copper cathode. The addition of Guar-like organic additives reduces the grain size of deposited copper[23].

Cobalt sulfate is also added to provide almost 150 ppm of Co^{2+} in electrowinning electrolyte. Co^{2+} promotes O_2 evolution at the anode rather than Pb oxidation. This minimizes Pb contamination of the depositing copper and extends anode life[13]. The presence of Co^{2+} decreases the anode potential and remarkably mitigates the corrosion of Pb anode with a smooth deposit of copper in the cathode. Current efficiency is also found to be higher in the presence of Co^{2+}.

3.2.4 Effect of Current Density

Current density is the most important parameter in the metal electrowinning because it controls the amount of electrodeposited metal at the cathode. It affects other characteristics of an electrowinning operation such as current efficiency and morphology of deposited copper. The optimum current density used by most industries is between 280 A/m^2 to 340 A/m^3. Copper plating rate increases with increasing current density. However, excessive current density gives rough, nodular cathode deposits and decreased copper purity. A higher current density can be obtained by using various types of forced circulation.

Increasing the current density beyond the limiting current density causes the deposits to become powder. The operating current density is usually less than the 50% of limiting current density. This limit is due to an uneven current distribution in the cell even though the leveling agents are present in the electrolyte solution. It has been reported by Subbaiah and Kammel that the limiting current can be increased by increasing the electrolyte circulation, Cu concentration, and air sparging in the cell[31].

It has also been shown by Das and Krishna[21] that at 30°C to 40°C, the current density increases slowly up to 600 A/m^2, beyond which it is almost constant. However, in the case of 60°C, an increase in the current efficiency was observed up to current density of 1050 A/m^2. An increase in power consumption per tonne of copper is also observed with increasing current density at each of the temperatures studied. A marked change of cathode deposit was found with increasing current density and temperature. An acceptable deposit was obtained at comparatively higher current density with rising

temperature. When a rough cathode deposit was obtained beyond 450 A/m^2 at 30°C it was possible to achieve a smooth deposit even at current density of 750 A/m^2 at 60°C.

3.2.5 Effect of Ferric Ion Concentration

Copper bearing ores are always associated with the iron and this iron is present when the ores are leached via hydrometallurgical operations. These leached solutions are then passing through the solvent extraction step for their purification, but the final electrolyte ends up having some amount of Fe^{3+} in it. These solutions containing Fe^{3+} are directly used in the electrowinning step. The presence of Fe^{3+} in the electrolyte causes a loss in current efficiency and increase in the energy consumption[21].

The behavior of iron during electrowinning of copper from sulfate electrolytes is well known and its effects on the performance of the copper electrowinning process has been reported by Anderson (1973)[32], Gruenfelder (1960)[33], Greenwalt (1924)[34], Mantell (1960)[35], Winmand (1975)[36], and Adrian F. Gil (1996)[37]. Das and Krishna (1996)[21] have studied the effect of ferric ions and other parameters on copper electrowinning under conditions close to those used in industrial operations. They suggested that:

- ✓ The current efficiency drops at any flow rate when Fe^{3+} concentration is raised beyond about 1 g/l.
- ✓ A comparatively higher fall in the current efficiency is observed when both flow rate and Fe^{3+} concentration are high.
- ✓ About 90% current efficiency can be achieved if the ratio Fe^{3+}/Fe^{2+} can be maintained if concentration of iron in the electrolyte is less than 1.0.

- ✓ A marked change in cathode deposit is found with increasing current density and temperature. Smooth deposits at higher Fe^{3+} concentrations can be achieved when both the temperature and the applied current density are higher.

3.3 Acid Mist Control

Acid mist is generated during the copper electrowinning process due to the oxygen bubble formation at the anode. These bubbles rise to the top of the cell and burst and make a cloud of acid. There are many factors which affect the production of acid mist, such as current density, ambient temperature, electrolyte temperature, ambient pressure, and electrolyte composition[38].

Reza Al Shakarji et al.[11] have performed a statistical analysis to see the effect of various parameters on acid mist generation. They suggested that acid mist was found to increase with temperature and current density. In contrast, addition of FC-1100 to the solutions decreased the amount of acid mist. However, it is critical to note that it is the ability of FC-1100 to increase the surface elasticity and surface viscosity, not its ability to reduce surface tension, which is responsible for the reduction of acid mist generation. The bubble burst mechanism at the free surface of the solution, which is mainly influenced by surface elasticity and surface and bulk viscosity of the solution, proved to be a critical factor in the amount of acid mist generated.

3.4 Modeling and Simulation – Previous Investigation

A mathematical model can be a very helpful tool to understand and improve the various phenomena inside an electrolysis cell. Mathematical modeling has been

performed to better understand the velocity field inside an electrolysis cell, gas bubble distribution analysis, current distribution, and mass transfer rate analysis by many authors using different techniques and tools such as finite element analysis and computational fluid dynamics. The ultimate goals of these models are to make estimation of real-world phenomena.

3.4.1 Electrolyte Circulation in an Electrowinning Cell

As mentioned earlier in this thesis, oxygen gas evolves at the anode of a copper electrowinning cell that drives electrolyte to circulate between two electrodes. The bubbles evolved at an anode rise through the electrolyte and by a "gas lift" effect (a reduction in effective electrolyte density in the region of high gas fraction resulting in a buoyancy of this region); upflow of electrolyte occurs near the anode (see Figure 3). Most of the gas bubbles disengage from the electrolyte at the electrolyte surface and the electrolyte returns downward, sweeping with it some of the bubbles, particularly smaller ones. The bubble distribution has an effect on the effective conductivity of the electrolyte, which in turn leads to a nonuniform current distribution in the cell. Nonuniformity in current results in nonuniform metal deposition at the cathode and also in nonuniformity in gas generation at the anode. The latter has an effect on the bubble distribution[39].

Jennings et al. [40] investigated a plane parallel forced flow electrowinning cell and concluded that electrolytically evolved bubbles do not enhance the mass transport. The observed enhancement is because of the increase in the velocity of the electrolyte. Ettel and coworkers[41] measured local mass transfer coefficients in electrowinning cells of

dimensions comparable to industrial practice. They found that the mass transfer coefficient was nearly uniform in the bottom half of the cell and increased with height in the top half. They associated this with the contacting of the cathode by the anode bubble wedge in the top of the cell. This result appears to contradict that of Jennings et al.

The effect of bubbles on conduction has been studied by many authors and a technique that can be used to measure the gas void fraction in electrolyte has been done. In addition to the free floating bubbles, those adhering to the anode can have an effect on cell resistivity. Sides and Tobias[42] proposed a relationship for the effective conductivity of the layer of electrolyte containing the adherent bubbles. This relationship was further corrected by Vogt and Kuhn[43].

Tobias[44] proposed a cell model that predicts current distribution and cell voltage by taking into account the bubble resistivity in the bulk electrolyte and linear polarization at the electrodes. He used the Bruggeman equation to calculate the electrolyte resistivity. The bubble fraction was calculated under the assumption of uniform horizontal dispersion of the bubbles, and bubble velocity was assumed to be equal to the free rise velocity of the monosized bubbles. The Tobias[44] result depicts the nonuniformity of current density produced by the bubbles and the influence of electrode polarization in decreasing this nonuniformity.

Even for the simple case of an electrowinning cell using plane parallel electrodes, it appears that there is uncertainty concerning current distribution and electrolyte velocity distribution[39]. One of the aims of this study is to provide the means for predicting the current distribution and the electrolyte recirculation velocities. It is worth mentioning that

most of the past studies have dealt with the stagnant electrolyte and gas being evolved at both the electrodes.

3.4.2 Modeling of a Copper Electrolysis Cell Group

A sufficiently accurate computational model of an electrolysis cell group can provide many practical benefits such as product development. Laitinen and Tanttu have done extensive modeling and simulation work of a copper electrowining cell group for various designs of intercell busbar (ICBB). For their modeling, they used a simplified geometry of an electrowinning cell. The model was solved in two steps. In the first step, only the electric potential is solved and in the second step, electric potential and temperature is solved together. They found a short-circuit in their cell that causes linear change in electric potential between short-circuited electrodes[2].

Detailed models of some parts of electrolysis cell have been developed using computational fluid dynamics (CFD), including modeling of bubbles and droplets[45], and modeling of the current density distribution at vertical gas-evolving electrodes[46]. These models have restricted the geometry size due to the computational demand of the CFD modeling, and are therefore inadequate to predict phenomena at a cell group level. This study focuses on all aspects of a copper elctrowinning cell such as electrolyte circulation, bubble void fraction, and short-circuit tendency. To our knowledge, this kind of simulation has not been done by any other author.

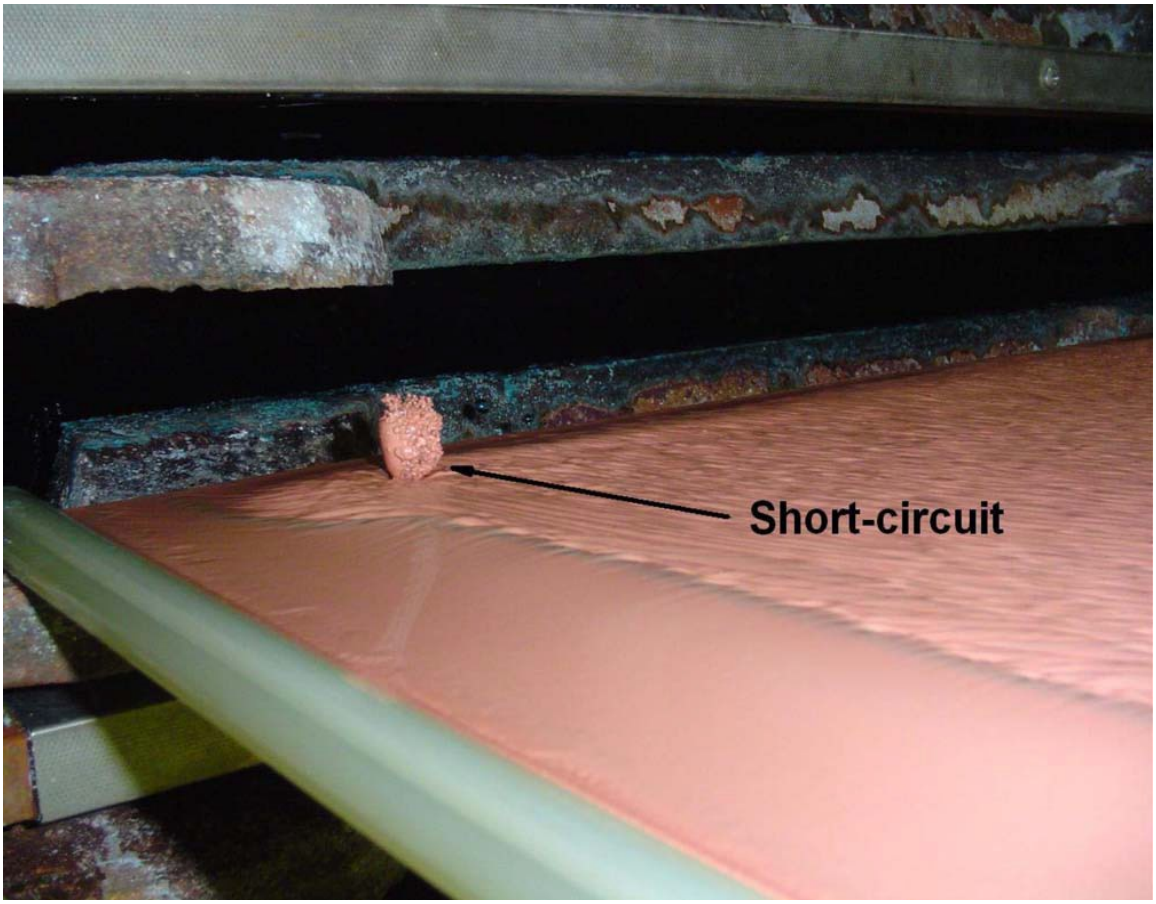

Fig. 2. Metallurgical short-circuit observed at the surface of a cathode in copper electrowinning cell[20].

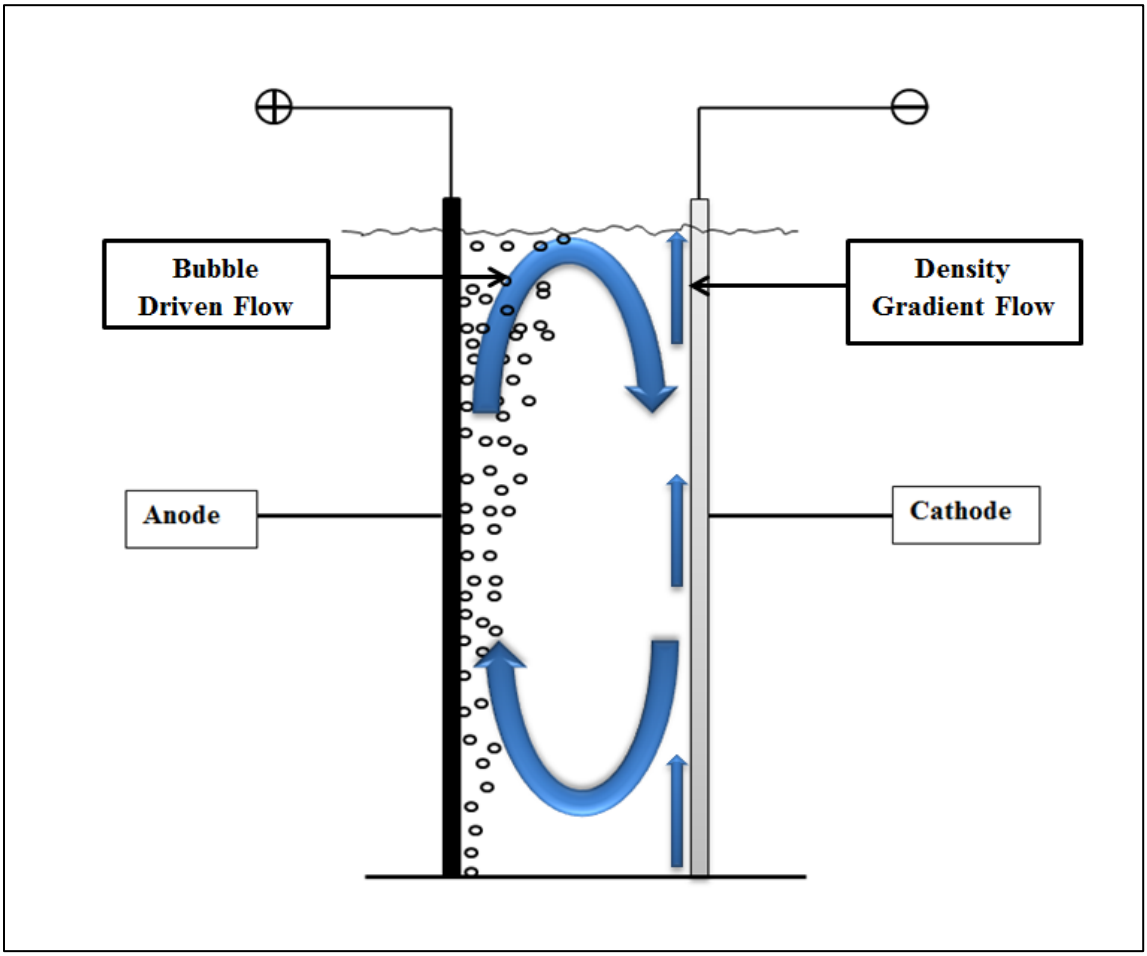

Fig. 3. Schematic diagram showing bubble-driven electrolyte recirculation and density gradient flow in copper electrowinning cells[39].

CHAPTER 4

EXPERIMENTAL PROCEDURE

4.1 Experimental Design for Copper Electrowinning

A bench top electrowinning test cell (15.5cm x 13cm x 10.5cm) with a cathode (9.0cm x 8.0cm) and an anode (8.5cm x 8.0cm) was constructed and operated to simulate industrial processing. The following studies were conducted to evaluate the performance of various parameters. The parameters that were taken into consideration include copper concentration in electrolyte solution, guar concentration, current density, temperature, and time.

- ✓ A 2^4 experimental design was devised to evaluate the effects of these parameters on copper electrowinning under industrial conditions as well as to verify model results.
- ✓ Simulation work is carried out using the COMSOL Multiphysics™ electrodeposition module (finite element analysis-based simulation tool).
- ✓ The maximum deposit feature height, which is the precursor to short-circuiting, was measured and predicted using various forms of density functions.

The experimental design selected for this work uses high and low levels of variables to evaluate parameter effects on electrowinning cell performance. Table 1 shows the 2^4 experimental design parameters.

Electrowinning experiments were carried out for 5 hours for the complete set of parameters. A smaller number of tests were performed at 20 and 80 hours for conditions that showed the greatest range of roughness in the 5-hour tests. Table 2 shows the details of the operating conditions. The net electrolyte volume in the electrowinning cell was 2.1 L (without electrodes) and the flow rate of the recirculating electrolyte was maintained constant at 11.67 mL/min. Calculated amount of guar was dosed initially for 2.1 L of solution directly into the electrowinning cell then dosed constantly using a NE 4000 (New Era pump systems) series syringe infusion pump. The electrolyte temperature was kept constant at the desired temperature using a temperature bath. Copper was replenished using pure copper filings in a separate vessel to recycle the electrolyte. Figure 4 shows the eletrowinning cell setup used for 5-hour experiments.

A 316L stainless steel plate of thickness 1 mm (Figure 5) and a Pb alloy plate of thickness 1.5 mm were used as the cathode substrate and anode, respectively. The back side and the edges of the cathode were coated using a high-quality finger nail polish to prevent deposition in these areas. The stainless steel substrate was thoroughly washed with acetone and water, then soaked in the electrolyte solution for an hour and washed again with distilled water before each experiment. The distance between the electrodes was 25 mm. Guar was dissolved in water at room temperature, under stirring, for 6 hours prior to addition in the electrowinning cell.

The copper sheets harvested from the electrowinning cell were stripped from the cathode at the end of each test. These sheets were cut in different pieces and mounted to measure the thickness and roughness of the deposits. The surface roughness evaluation includes analysis of variance and statistical inference using Minitab® software. The

adequacy of the model was checked using residual analysis as described by Montgomery[47].

An optical microscope (Amscope – ME 520T) was used to take images of the cross-sections and thickness was measured using image analysis software, ToupView®. The harvested copper sheets were cut into three sections (top, middle, and bottom) and these sections were once again sliced into three pieces (1 cm away from the left edge, center of the sheet, and 1 cm away from the right edge). Thickness and roughness were measured along the cross-sections. Figure 6 shows the schematic diagram of sections of copper sheet chosen for analysis, and Figures 7, 8, and 9 show a cross-section of a piece of copper sheet harvested and mounted in epoxy from the electrowinning cell to measure the average roughness, average thickness, and maximum feature height. The current efficiency and cell voltage variation with different parameters is shown in Tables 3, 4, and 5 for 5, 20, and 80 hours.

4.2 FEA Modeling of a Copper Electrowinning Cell

A finite element analysis-based simulation package, COMSOL Multiphysics™, was used for the modeling of copper electrowinning cell. COMSOL allows coupling of several physical phenomena to model together such as electrodeposition and laminar flow. In addition, it includes a number of predefined application modes, which makes modeling easier. The Electrodeposition Module is intended to investigate the influence of different parameters in an electrodeposition cell or on the thickness and composition of deposited layers. A typical simulation yields the current distribution in the electrodeposition cell and at the surface of the electrodes.

4.2.1 Model Assumptions

This section contains the list of assumptions that are used for the modeling and simulation of copper electrowinning cell. Figure 10 shows a model geometry used for the simulation of copper electrowinning cell. The important assumptions about the electrowinning cell modeling are:

- ✓ The electrolyte is considered to be composed of only Cu^{2+}, SO_4^{2-}, H^+, and Fe^{3+} ions to make the model simple. Other species are ignored because their effect is very small on the electrodeposition of copper.
- ✓ The flow is considered to be laminar and incompressible.
- ✓ The electrolyte conductivity and density are affected by the concentration of all the ions included in the electrolyte, temperature of the electrolyte solution, mixing of the electrolyte solution, and bubble formation at the anode.
- ✓ The efficiency of oxygen formation at the anode is considered to be 100%.
- ✓ Study is considered to be time-dependent and modeling is performed for 5, 20, and 80 hours which are similar to experimental run time.
- ✓ The tertiary current distribution is considered to include the effect of solution resistivity, activation overpotential, and concentration overpotential.
- ✓ The volume force is considered to be vertical adjacent to the anode boundary to incorporate the effect of bubble rise in the electrolyte.
- ✓ The void fraction is assumed to be 10% at the top of the anode, decreasing linearly to zero at the bottom of the anode[48]. The region where void fraction is applied is the area immediately adjacent to the anode, extending 3 mm into the solution.

The mesh generator discretizes the domains into triangular mesh elements. If the boundary is curved, these elements represent only an approximation of the original geometry. The sides of the triangles are called mesh edges, and their corners are mesh vertices. A mesh edge must not contain mesh vertices in its interior boundary; that makes simulation difficult[18].

The boundaries defined in the geometry are discretized (approximately) into mesh edges, referred to as boundary elements (or edge elements), which must conform to the mesh elements of the adjacent domains. The geometry vertices are represented by vertex elements.

COMSOL allows using the default mesh system according to the shape of the geometry. For example, for a fluid-flow model, you obtain a somewhat finer mesh than the default with a boundary layer mesh along the no-slip boundaries. In this study, a finer mesh size is used to see the effect of laminar flow and electrodeposition of copper. Figure 11 depicts a meshed geometry of the simulated model.

The computational power used by the simulation is dependent on the geometry and mesh. In order to maximize computational resource utilization, a 2D geometry was used.

4.2.2 Model Geometry and Meshing

A 2D geometry is devised to simulate the copper electrowinning cell. The geometry includes an anode (A), cathode (B), electrolyte (C), and void fraction generated because of the bubble formation at the anode (D). Anode and cathode are modeled as a single straight line. The dimensions of the components used in the geometry are the same

as the cell used for the experiment of copper electrowinning. Table 6 shows the dimensions of the component.

4.2.3 Parameters and Equations

The parameters and equations considered for the simulation of copper electrowinning cell are given in Table 7 and 8.

Table 1. 2^4 Experimental design parameters

	Low Level	High Level
Current Density (A/m^2)	325	475
Copper Concentration (g/L)	35	45
Electrolyte Temperature (^0C)	35	55
Guar (g/ton of copper cathode)	175	325

Table 2. General experimental conditions used for copper electrowinning.

Current Density (A/m^2)	325/475
Deposition Area (cm^2)	80
Sulfuric Acid Concentration (g/L)	180
Iron Concentration (g/L)	2
Chloride Ion Concentration (ppm)	20
Cobalt Concentration (ppm)	100
Electrolyte Net Volume (L)	2.1
Cell Dimensions (L×W×H)	15.5×13×10.5
Electrolyte Flow Rate (mL/Min)	11.67
Guar Addition (gm/tonne of copper cathode)	175/325

Table 3. Various parameters for 5-hour electrowinning experiment.

Exp No	Temperature (^{0}C)	Cu Conc (g/l)	Guar Conc (g/tonne of Cu)	Current Density (A/m^2)	Amount of Deposited Cu (g)	Current Efficiency (%)	Cell Voltage (V)
1	35	35	175	325	15.19	91.52	1.98
2	55	35	175	325	15.01	90.43	1.99
3	35	45	175	325	14.98	90.25	1.91
4	55	45	175	325	15.14	91.22	1.88
5	35	35	175	475	21.98	90.44	2.09
6	55	35	175	475	22.6	92.99	1.94
7	35	45	175	475	22.72	93.48	2.16
8	55	45	175	475	23.16	95.29	2.11
9	35	35	325	325	15.42	92.90	1.98
10	55	35	325	325	15.02	90.49	1.82
11	35	45	325	325	15.22	91.70	1.98
12	55	45	325	325	15.06	90.73	1.81
13	35	35	325	475	21.02	86.49	2.11
14	55	35	325	475	22.72	93.48	1.88
15	35	45	325	475	22.66	93.24	2.13
16	55	45	325	475	22.81	93.85	1.89

Table 4. Various parameters for 20-hour electrowinning experiment.

Exp No.	Temperature (^{0}C)	Cu Conc (g/l)	Guar Conc (g/tonne of Cu)	Current Density (A/m^2)	Amount of Deposited Cu (g)	Current Efficiency (%)	Cell Voltage (V)
1b	35	35	175	325	60.16	90.61	1.96
3b	35	45	175	325	60.2	90.67	1.92
5b	35	35	175	475	91.39	94.01	2.04
7b	35	45	175	475	91.35	93.97	2.02
9b	35	35	325	325	60.41	90.99	1.94
11b	35	45	325	325	60.3	90.82	1.95
13b	35	35	325	475	90.52	93.11	2.06
15b	35	45	325	475	90.73	93.33	2

Table 5. Various parameters for 80-hour electrowinning experiment.

Exp No.	Temperature (^{0}C)	Cu Conc (g/l)	Guar Conc (g/tonne of Cu)	Current Density (A/m^2)	Amount of Deposited Cu (g)	Current Efficiency (%)	Cell Voltage (V)
3c	35	45	175	325	226.5	91.85	1.98
7c	35	45	175	475	353.4	90.88	2.06
11c	35	45	325	325	243.5	91.69	1.99
15c	35	45	325	475	349.6	89.90	2.04

Table 6. Dimensions of component used in 2D geometry.

Component	Measurement (cm)
Anode	8.5
Cathode	9
Distance between Electrodes	3
Void Fraction (At the top of the cell)	0.3
Void Fraction (At the bottom of the cell)	0

Table 7. Parameters considered for the simulation of copper electrowinning cell.

Parameter	Value
Cu Concentration	35/45 (g/l)
Iron Concentration	2 (g/l)
Acid Concentration	180 (g/l)
Temperature	35/55 (°C)
Exchange Current Density	0.2 (A/m^2)
Relative Equilibrium Potential (versus Cu^{2+}/Cu)	0 (V)
Anode Potential	0.135 (V)

Table 7. Contd.

Parameter	Value
Cathode Potential	-0.135 (V)
Anode Symmetry Factor	1.5
Cathode Symmetry Factor	0.5
Net Species Charge	2
Charge on Cu ion	2
Charge on Sulfate ion	-2
Diffusivity of Cu ion	8.66e-11 (m^2/s)
Diffusivity of Sulfate ion	8.66e-11 (m^2/s)
Diffusivity of Iron	7.26e-8 (m^2/s)
Area of Cathode (A_c)	6.8e-3 (m^2)
Width of Anode (W_a)	0.08 (m)
Atmospheric Pressure (P)	101325 (Pa)
Diameter of Bubble (d)	50e-6 (m)
Gap between Electrodes (g_e)	0.03 (m)

Table 8. Equations considered for the simulation of copper electrowinning cell[48-49].

Parameter	Equation
Electrolyte conductivity containing oxygen bubbles (σ)	$\sigma_0\ (1-\varepsilon)^{3/2}$
Electrolyte conductivity without oxygen bubble (σ_0)	$10^5 \times (3200 + 7.3 \times [Cu] - 5.6[Acid] - 14.6[T])^{-1}$
Void faction (ε)	$\frac{3\,J_c A_c RT\eta}{W_a FPg\rho d^2 g_e}$
Kinematic viscosity (η)	$(700 - 8.3[Cu] + 16[Acid] - 18[T])^{-1}$
Density of the electrolyte (ρ)	$1022 + 2.24[Cu] + 0.55[Acid] - 0.58[T]$
Dynamic viscosity (μ)	$\frac{Density\ (\rho)}{Kinematic\ Viscosity\ (\eta)}$

where,

[x] = Concentration of the species

J_c = Cathode current density

R = Gas constant

g = Acceleration due to gravity

F = Faraday constant

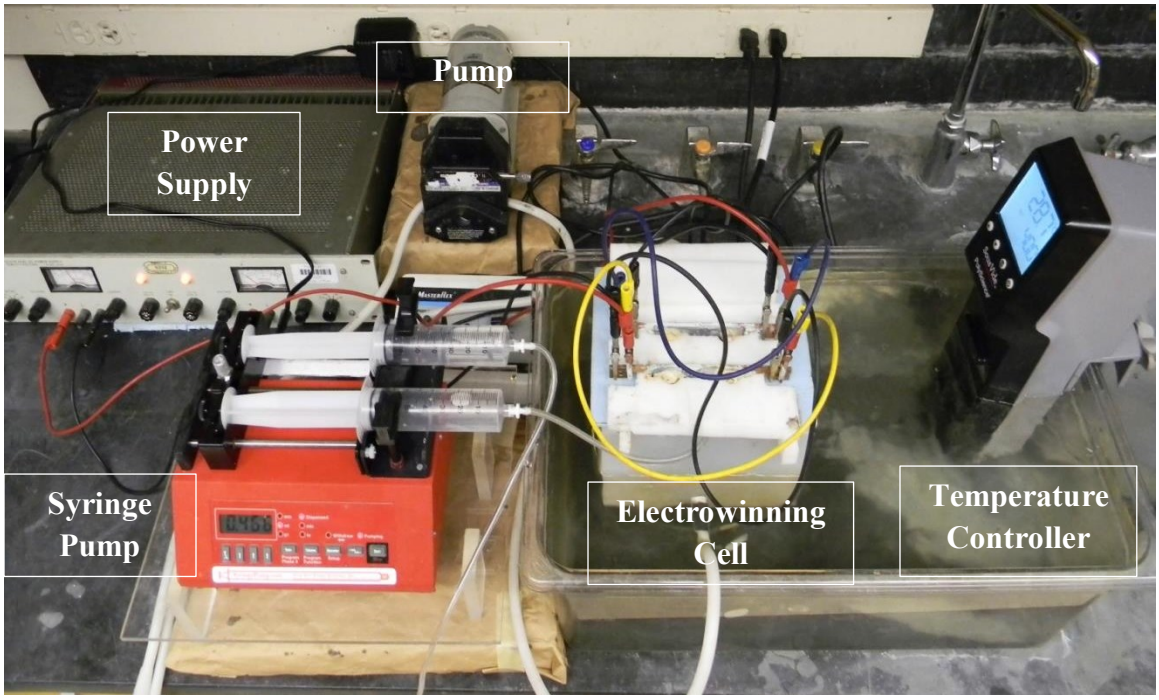

Fig. 4. Electrowinning cell setup used for 5, 20, and 80 hours of experiment.

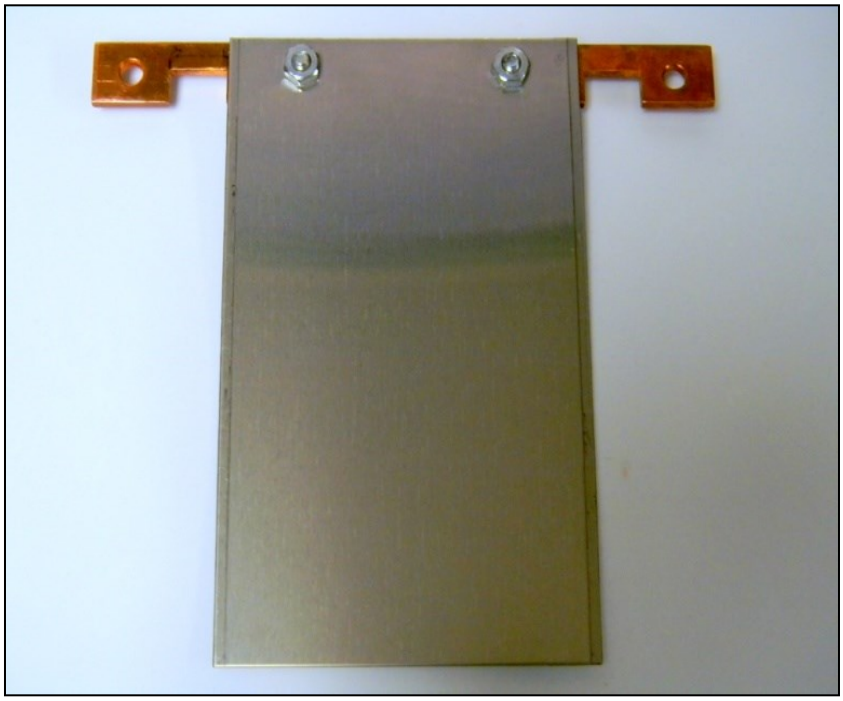

Fig. 5. 316L Stainless steel used as cathode.

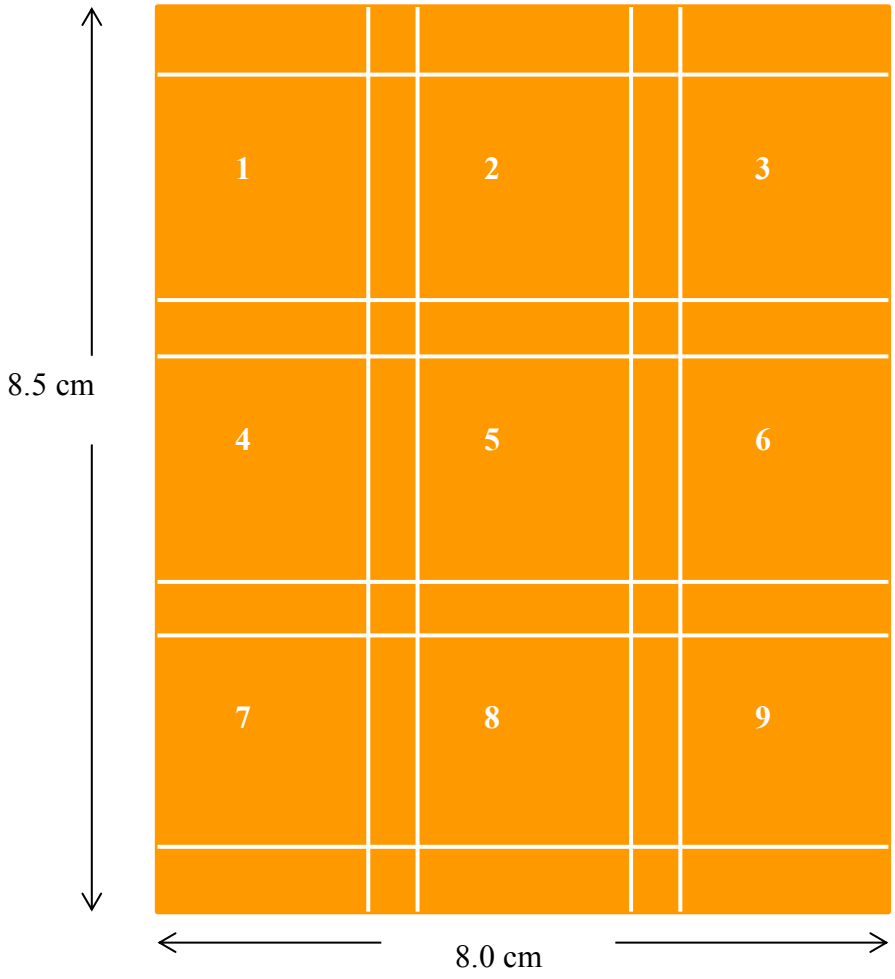

Fig. 6. Schematic diagram of cross-section of a copper sheet harvested from an electrowinning cell test. Numbers identify the sections taken for the analysis.

Fig. 7. Measurement of average roughness of the cross-section of a piece of copper sheet harvested from the electrowinning cell. The upper bar shows the baseline and the small vertical lines show the feature height.

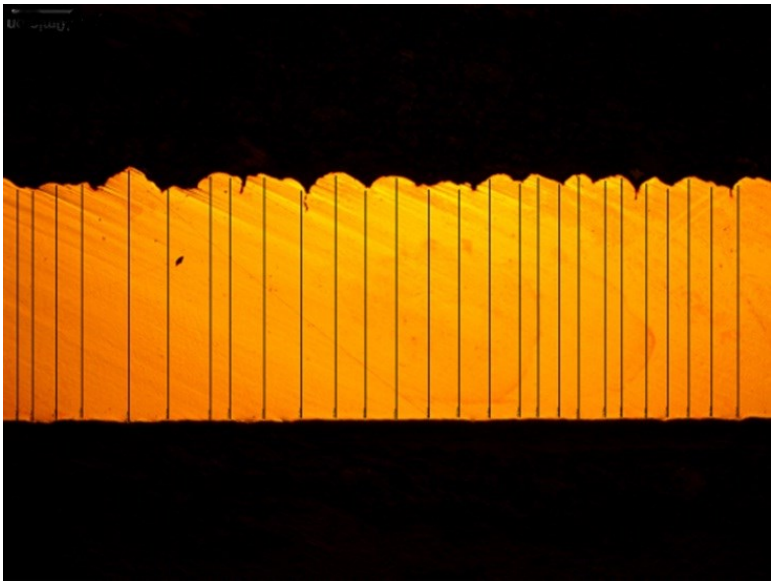

Fig. 8. Measurement of average thickness of the cross-section of a piece of copper sheet harvested from the electrowinning cell. The vertical lines show the height at systematically measured locations.

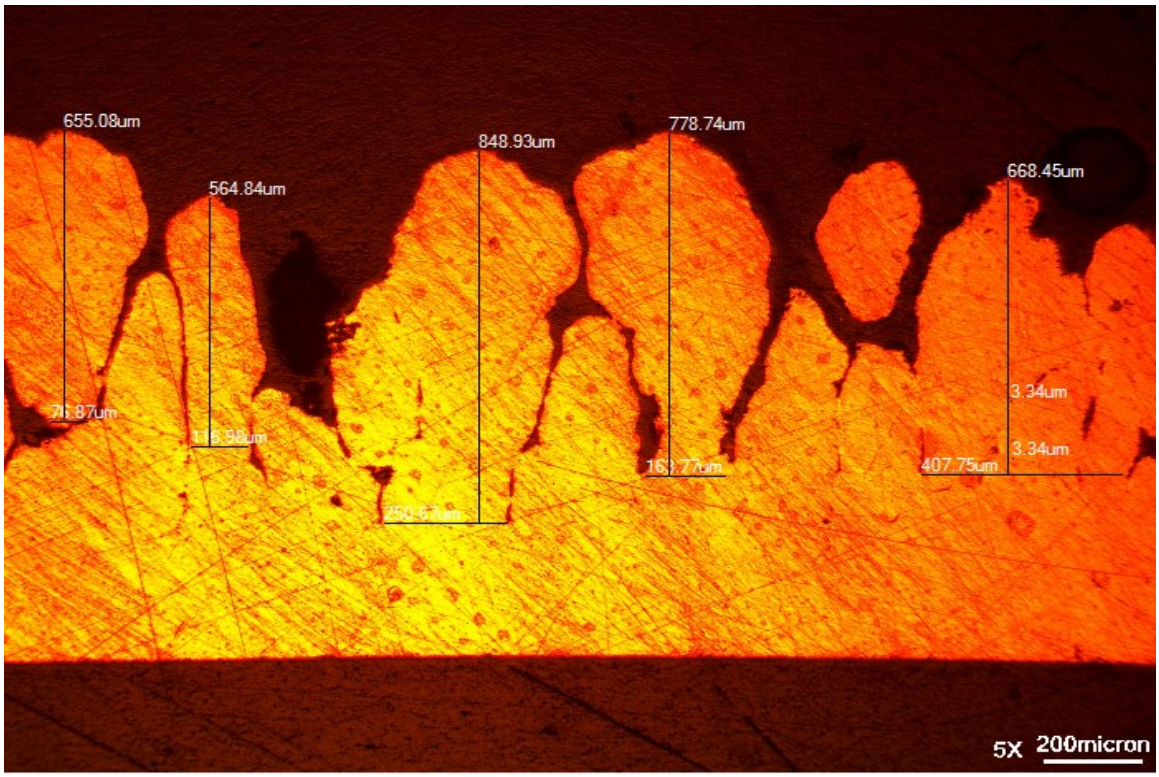

Fig. 9. Measurement of maximum feature height of the cross-section of a piece of copper sheet harvested from the electrowinning cell. The vertical lines show the height at systematically measured locations.

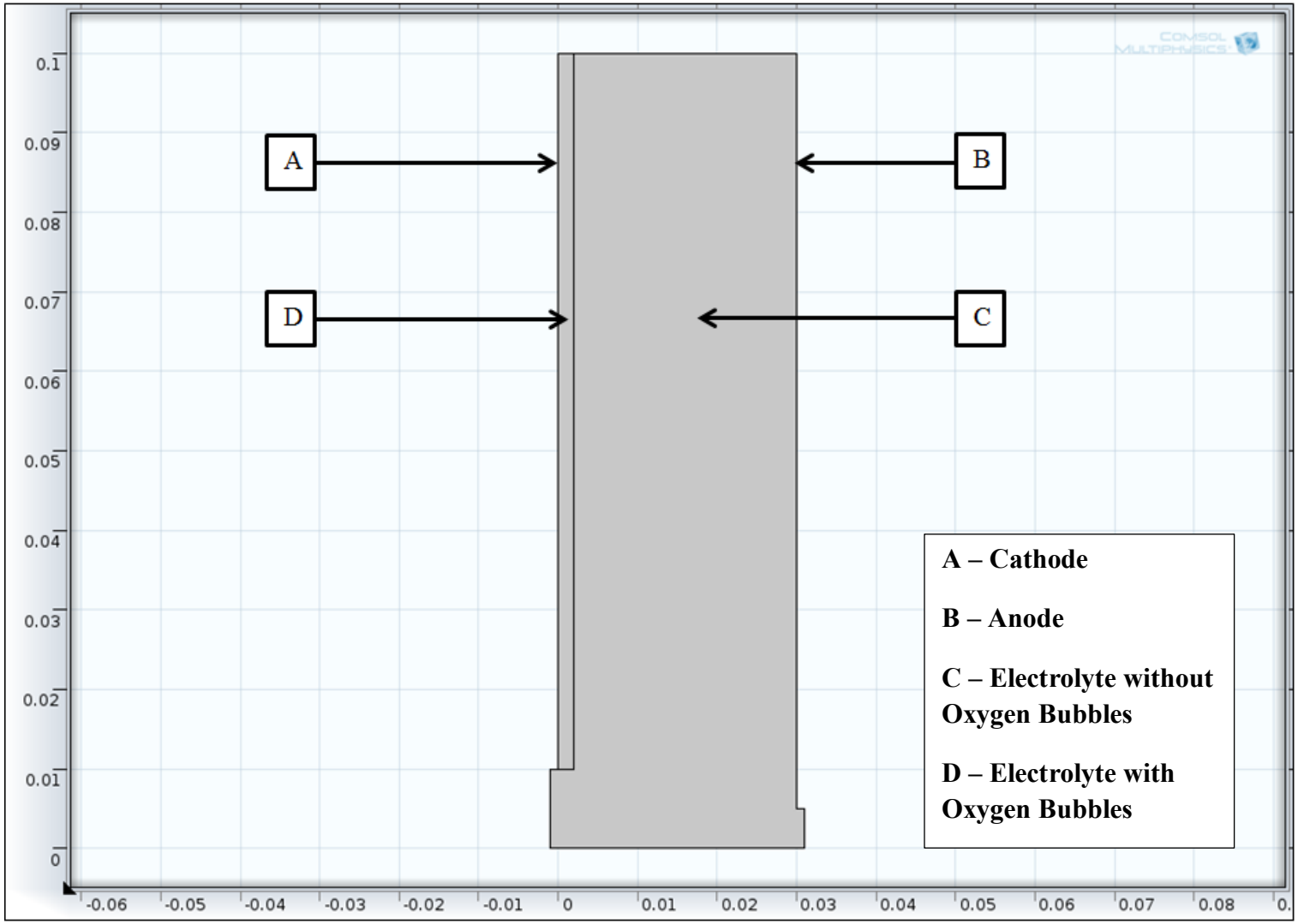

Fig. 10. Model geometry used for the simulation of copper electrowinning cell.

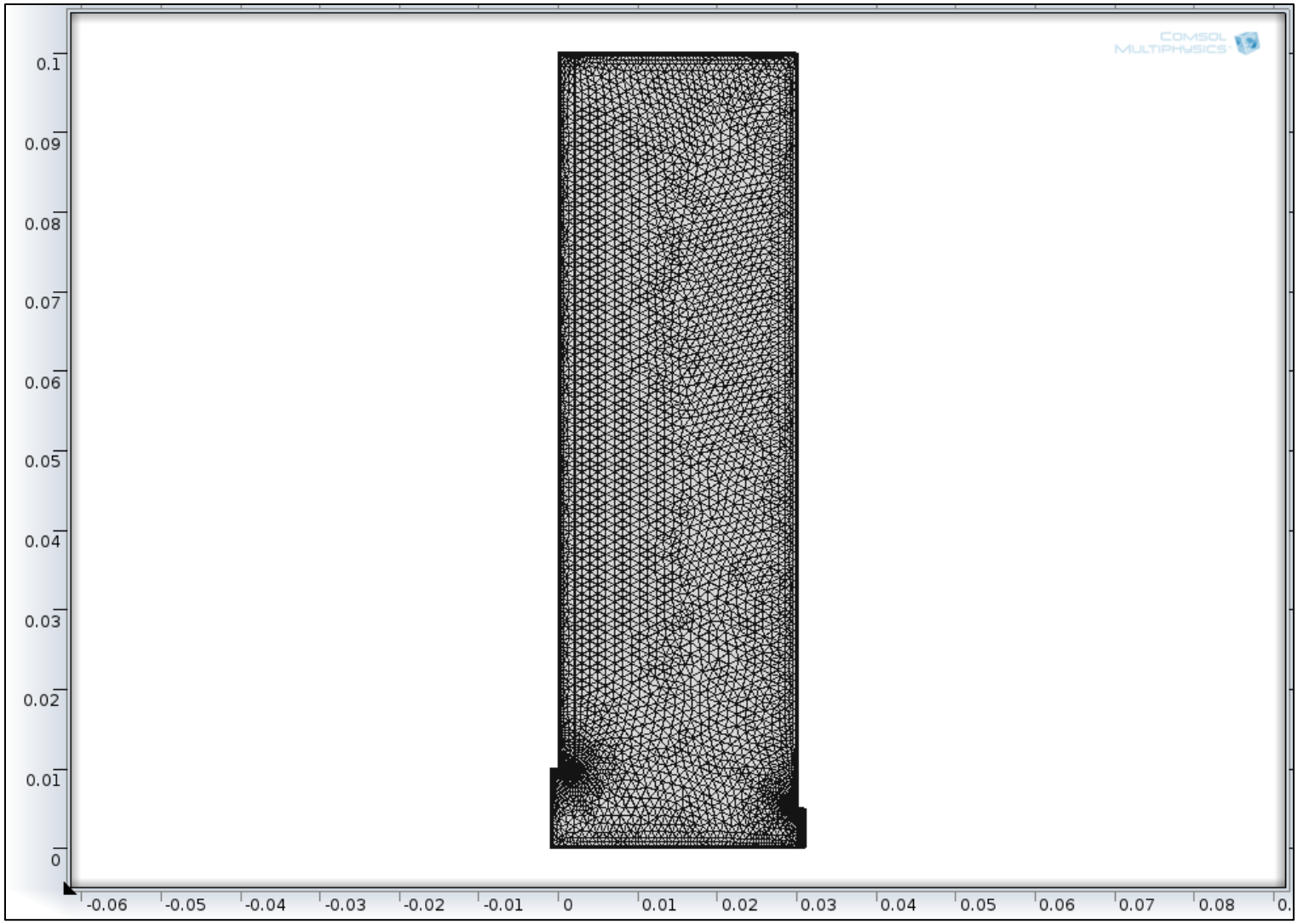

Fig. 11. A typical mesh distribution used for the simulation of copper electrowinning cell.

CHAPTER 5

RESULTS AND DISCUSSIONS

5.1 Analysis of Deposits

Initial analysis of deposits obtained from the short-term and long-term experiments shows there is a significant effect of current density on the roughness of the deposits, as expected. Figures 12-16 are sample images of deposits obtained from electrowinning experiments. The deposit shown in Figure 12 is bright and very smooth with no nodules at the edges or in the center of the deposit. Deposits which were obtained at high levels of variable parameters and longer time experiments are shown in Figures 13-16.

Smoother deposit can be seen with low levels of current density and temperature, whereas rough deposits are observed with high levels of these parameters. Dendritic and discontinuous copper deposits can be seen in the image, which was obtained with 475 A/m^2 of current density (Figure 15). The electrowinning experiments that showed the greates tendency of rough deposits were performed for 80 hours and similar growth trends were obtained. Figure 16 shows the 80-hour electrowinning experiments results. One of the experiment was carried out with tilted cathode to see the effect of misalignment of the cathode on short-circuiting tendency of the copper electrowinning cell.

5.2 Maximum Roughness Feature Height Prediction

Undesirable roughness can cause short-circuiting between cathodes and anodes. Short-circuiting will occur first where the maximum electrodeposit feature height reaches a length, which when coupled with the base deposit thickness, reaches across the gap between the cathode and anode. Maximum feature height prediction utilizes lifetime prediction principles from fields such as corrosion. Copper cathodes were produced and cut into 9 sections, as described previously. Each section was analyzed for maximum feature height by cross-sectional optical microscopy. A series of feature height data was collected and maximum values, which are likely to lead to eventual short-circuiting, were collected and evaluated using distribution functions. In probability theory and statistics, the cumulative distribution function (CDF), or just distribution function, describes the probability that a real-valued random variable x (here maximum feature height) with a given probability distribution will be found at a value less than or equal to x. In the case of a continuous distribution, it gives the area under the probability density function from minus infinity to x. The selected distribution functions are used for extreme value-based predictions, and they include log-normal, exponential, double exponential, and Weibull density functions. The most appropriate function was selected based on the highest correlation coefficient squared value with experimental data. Extrapolation of short-term, small sample area data was made. Deposition time was extrapolated from 5, 20, and 80 hours to 168 hours. Sample size effects were extrapolated from approximately 1 mm to an application size of 1 meter. However, this stage of the analysis includes only a line scan across an electrode that has been evaluated. A 2-dimensional analysis is discussed later.

5.2.1 Cumulative Maximum Feature Height Data

Roughness feature height data can be converted to a cumulative or distribution format by sorting the data from smallest to largest and determining the proper cumulative probability fraction, F(x), value, which is equal to:

$$F(x) = Order\ Number \times \frac{1}{N+1} \tag{5.1}$$

N is the maximum value order number. Order number is the number of the maximum feature measurement in sequence of lowest to highest maximum feature height. The maximum feature height is the maximum electrodeposit feature height measured from the nearest valley to the neighboring peak in a single microscope image. The cumulative fraction is based on integration of a distribution density function. The distribution of maximum feature height of Experiment 5 (rough surface) and Experiment 11 (smooth surface) after 5 hours of experiment in the middle of the cathode plate is shown in Table 9.

5.2.2 Determination of the Best Distribution Function Fit of the Data

Functions that are used for extreme value-based predictions include log-normal, exponential, double exponential, and Weibull functions. Selected extreme value statistical density functions are shown in the following equations:

5.2.2.1 Log-Normal Density Function

$$f(x) = \frac{1}{\sigma x\sqrt{2\pi}} exp\left[-\frac{(\ln x - \mu^2)}{2\sigma^2}\right] \tag{5.2}$$

5.2.2.2 Exponential Density Function

$$f(x) = \frac{1}{\beta}\exp\left(\frac{-x}{\beta}\right); x > 0; \beta > 0 \tag{5.3}$$

5.2.2.3 Double Exponential Density Function

$$f(x) = \frac{1}{\alpha} exp\left[\frac{-(x-\lambda)}{\alpha} - exp\frac{(x-\lambda)}{\alpha}\right] \tag{5.4}$$

5.2.2.4 Weibull Density Function

$$f(x) = \alpha\beta x^{\beta-1}\exp\left(-\alpha x^{\beta}\right); x > 0;\ \beta > 0 \tag{5.5}$$

Experimental F(x), the cumulative probability of finding a feature height below *x*, and *x*, the maximum feature size, were plotted in log-log scale to determine which distribution function fits the data best. Other comparisons were made in a linearized form by rearranging equations and testing the fit using the following equations:

5.2.2.5 Linearized Exponential Distribution Function

$$-\ln\left(1 - F(x)\right) = \lambda x \tag{5.6}$$

5.2.2.6 Linearized Double Exponential Density Function

$$\ln(-\ln F(x)) = -\frac{(x-\lambda)}{\alpha} \tag{5.7}$$

5.2.2.7 Linearized Weibull Density Function

$$\ln\left[ln\left(\frac{1}{1-F(x)}\right)\right] = \alpha\ln(x) - \alpha\ln(\beta) \tag{5.8}$$

The edge of the cathode and the middle area of the cathode were evaluated separately. The density function plot of Experiment number 1 at 5 hours (low temperature, low copper concentration, low current density, and low guar) is representative of the other experiments. Figures 17-20 show the fits of the experimental data to the linearized cumulative distribution functions. The data show a reasonably linear trend as expected for each set of data. However, Figures 17-20 indicate there is a difference in the distribution function for the edge and middle areas of the cathode.

The edge of the cathode shows higher roughness feature peaks than the middle area. The extreme values at the end of the function, which contains the maximum values, are the area of interest for preventing short-circuiting problems. The edge area distribution data for Experiment 1 at 5 hours were plotted to test the related fit to each cumulative distribution function. The plots are shown in Figures 21 to 24.

The graphical function fitting shows that the most appropriate function is the Weibull distribution function. Alpha and beta values for the Weibull function can be calculated based on the slope and intercept of a linear trend line equation. Alpha represents shape parameter, beta represents the scale factor, and the cumulative determines the form of the distribution and to perform a probability distribution it is false. Predicted probability functions for Experiment 1 at 5 hours and 20 hours are shown in Figure 25.

5.2.3 Extrapolation of Short-term, Small Sample Linear Data into Long-term, Long Linear Roughness Feature Height Prediction Data

These experiments were performed using a limited number of small coupons and linear roughness feature height measurements, which simulate key parameters from industry. Extrapolation from the small length of the sample to a length of 1 meter was carried out. A schematic diagram showing coupon positions on the experimental cathode is shown in Figure 26.

The analysis length for the small measured sample is 2.66 cm. Equivalent testing for the industrial size cathode would require 25 samples:

$$T_{full-scale} = \frac{Length_{full-scale}}{Length_{small-scale}} = \frac{66.66}{2.66} = 25.06 \tag{5.9}$$

Now, 25.06 samples are required to match the entire length of industrial size cathode; The probability of maximum feature height that occurs in only 1 of 25 samples that would be equivalent to one line scan of an industrial sample can be calculated by:

$$F\left(x_{full-scale}\right) = 1 - \frac{1}{T_{full-scale}} = 1 - \frac{1}{25.06} = 0.96 \tag{5.10}$$

The feature height extrapolation line at F(x) = 0.96 is shown as a horizontal red line in Figure 27. This is the probability of having one feature out of the 25.06 needed to complete one industrial scale line scan across an electrode. Extrapolation to the intersection of the Weibull functions to the F(x) = 0.96 line gives the associated value of

maximum expected feature height as illustrated by the associated vertical red line intersection with the X- axis.

The extrapolation from Experiment 5 (the roughest condition) to larger industrial length gives heights of 300, 1215, and 2450 for 5 hours, 20 hours, and 80 hours, respectively.

The relationship between time and the maximum feature height is found using a plot of log time (hours) versus log maximum feature height (microns). Experiment 5 (the most rough condition) and Experiment 11 (the smoothest condition) were plotted and compared in Table 10, and Figures 28 and 29.

Based on Figures 28 and 29, the maximum feature height along a 1-meter line scan of an industrial size cathode for 168 hours (7 days) can be calculated from the equation:

$$H_{\max feature} = \mathrm{k}t^{m} \tag{5.11}$$

$$\log\left[H_{\max feature}\right] = \log k + \mathrm{m}\log t \tag{5.12}$$

where $H_{\max\ feature}$ is maximum feature height (microns)

t is time (sec)

m is slope

k is a constant

Thus, the plot of log $H_{\max\ feature}$ versus log t gives a slope of m and an intercept of log k. These values can be used to obtain the final equation.

The results of the maximum feature height prediction at 7 days are 4819 microns at the rough condition and 931 microns at the smooth condition. From this approach, possible total growth distance can be calculated by

$$H_{total\ growth} = H_{Plating\ Thickness} + H_{\max feature} \tag{5.13}$$

Thickness of copper deposition can be calculated from Faraday's Law:

$$H_{Plating\ Thickness} = \frac{it\beta M_w}{n\rho F} \times 100 \tag{5.14}$$

$$H_{total\ growth} = H_{Plating\ Thickness} + H_{max\ feature} \tag{5.15}$$

$$H_{total\ growth} = \frac{it\left(\frac{\beta}{100}\right)M_w}{n\rho F} + kt^m \tag{5.16}$$

where

ρ is density of copper (g/cm^3)

i is current density (A/m^2)

A is area of cathode (m^2)

t is time (sec)

β is current efficiency (%)

M_w is atomic weight of copper

n is the number of electrons

F is Faraday's constant (96485 C/mole)

Short-circuiting occurs when the total growth of electrodeposit plus the maximum feature height exceeds the electrode separation distance. Based on 2.5 cm electrode

separation distance and 95% current efficiency, the predicted times to short-circuiting of Experiments 5 and 11 are presented in Figure 30.

Figure 30 illustrates that reducing current density from 475 A/m^2 to 325 A/m^2, increasing copper concentration from 35 g/L to 45 g/L, and increasing guar concentration from 175 g/t to 325 g/t extends the time to short-circuiting by a factor of 2. Time to short-circuiting can be calculated by

$$T_{short} = \frac{D_{electrode\ Separation}}{R_{growth}} \tag{5.17}$$

$$R_{growth} = \frac{H_{total\ growth}}{t} \tag{5.18}$$

where,

T_{short} is time to short-circuiting (sec)

$D_{electrode\ separation}$ is distance between electrodes (m)

R_{growth} is rate of growth (m/s)

From calculations, time to short-circuiting are 12 days and 23.63 days for experiment 5 (475 A/m^2, 35 g/L copper, and 175 g/t of guar) and 11 (325 A/m^2, 45 g/L copper, and 325 g/t of guar), respectively.

5.2.4 Linear Data to Area Data Correction

The initial measurement of short-circuiting is based on a linear line scan analysis, but it is necessary to validate this measurement by measuring the maximum feature height across the full sample length. Testing for copper electrowinning is nearly always performed using a limited number of small coupons, which are tested for only a fraction of a typical useful harvesting time, or they are performed using extreme techniques that

accelerate short-circuiting. Successful extrapolation of resulting test data to real-world short-circuiting can in many cases be made using appropriate extrapolation. Coupons of copper cathode from Experiment 5 and Experiment 11 were repolished (to penetrate into the sample) layer by layer in small increments of 0.05 cm for 10 layers. The resulting data collectively provide an area scan. The measured maximum feature height data are shown in Figures 31and 32.

Figure 31 shows the layer-by-layer measurement of maximum feature height of the sample harvested from the electrowinning cell with the condition of Experiment 5. It is evident that the increase in maximum feature height from the initial line scan measurement in converting to an effective area scan is 12.1%, 9.6%, and 6.1% for 5, 20, and 80 hours of experiment, respectively. Similarly, it is evident from Figure 32 that the increase in maximum feature height from the initial measurement to the more complete effective area scan is 6.1%, 4.8%, and 2.9% for 5, 20, and 80 hours of experiment with the conditions of Experiment 11, respectively. Thus, this increases the percentage effect of maximum feature height changing from a line scan to an area scan. Table 11 shows the extrapolated results of this analysis.

From the analysis of percentage increase in maximum feature height, it can be seen that for 2.66 x 0.5 cm^2 measured area, the percentage increase from a corresponding line scan is 25.8%, 20.2%, and 12.6% with the conditions of Experiment 5. With the conditions of Experiment 11, extrapolated maximum feature height for 2.66 x 0.5 cm^2 measured area compared to a line scan is 12.6%, 10%, and 5.8% for 5, 20, and 80 hours of experiment, respectively. The time to short-circuit correction analysis is performed based on these calculations.

5.2.5 Extrapolation of Short-term, Small Sample Area Data into Long-term, Full-scale Area Data for Maximum Feature Height Prediction

The area of the sample taken for analysis is 2.66 x 0.5 cm^2. Equivalent testing for the industrial size cathode would require 7519 samples that can be calculated using following formula

$$T_{full-scale} = \frac{Area_{full-scale}}{Area_{small-scale}} = \frac{1\ m^2}{0.000133\ m^2} = 7519 \tag{5.19}$$

Furthermore, the probability of maximum feature height that occurs in only one sample out of the 7519 samples can be calculated from the following equation.

$$F(x_{full-scale}) = 1 - \frac{1}{T_{full-scale}} = 1 - \frac{1}{7519} = 0.9999 \tag{5.20}$$

The extrapolated feature height extrapolation line at F(x) = 0.9999, which is shown in red, to full-scale area for Experiment 5 is shown in Figure 33.

The corrected maximum feature heights for industrial size cathodes are 440 µm, 2500 µm and 3900 µm for 5 hours, 20 hours, and 80 hours, respectively. Time to short-circuiting for corrected maximum feature height is calculated by the same approach as previously calculated for the linear data and is shown in Figure 34. The calculated time to short-circuiting for the extreme rough electrode surface condition is 9.5 days, which is 2.5 days earlier than the calculated time to short-circuiting from linear data (12 days). On

the other hand, the calculated time to short-circuiting for smooth condition shows very small difference from line scan compared to area scan.

5.2.6 Time to Short-Circuiting Verification Test

Objective of this test is to verify the time to short-circuiting prediction for various experimental conditions. The experiment was carried out in a copper electrowinning cell for the extreme rough condition of Experiment 5 (475 A/m^2, 35 g/L copper, and 175 gm guar per tonne of copper cathode and 55°C temperature) and 2.5 cm electrode distance. The first short-circuiting occurred after 8 days of deposition, as shown in Figure 35. After short-circuiting, undesirable growths were cut out to continue the test and verify the next short-circuiting, as shown in Figure 36. The second and third short-circuiting occurred after 9 days and 10 days of electrodeposition, respectively, as shown in Figure 37 and 38. Time to short-circuiting prediction after area data correction gives very good correlation between the predicted result and experimentally obtained result.

5.3 Statistical Analysis of Cathode Deposits

Cathode deposits were cut and mounted to measure the thickness and roughness. An optical microscope was used to take images of the cross-sections, and thickness was measured using image analysis software (ToupView®). Initial analysis shows that the higher current density deposits are rougher and thicker compared to low current density deposits. Tables 12-15 show the average thickness and roughness of cathode deposits for the conditions of roughest (35g/L Cu, 175 g of Guar/tonne of Cu, 35°C temperature, and 475 A/m^2) and smoothest (45g/L Cu, 325 g of Guar/tonne of Cu, 35°C temperature, and 325 A/m^2 of current density) deposits.

In order to explore the effect of individual parameters such as the concentration of Cu, concentration of guar, temperature, and current density, a factorial design of experiments was established. In most factorial experiments, each factor has only two levels (high and low). An experiment using 4 factors A, B, C, and D with 2 levels (high and low) results in 16 experiment combinations. A set of tests that follow the factorial design approach with electrodeposition variables tested at high (+) and low (-) levels is presented in Table 16. The values of main effect parameters and interactions are indicative of how strong an individual factor affects the response variable. The null outcome indicates the neutrality of effect parameter.

The relative effect of parameters is shown below:

A. (-y1+y2-y3+y4-y5+y6-y7+y8-y9+y10-y11+y12-y13+y14-y15+y16)/16

B. (-y1-y2+y3+y4-y5-y6+y7+y8-y9-y10+y11+y12-y13-y14+y15+y16)/16

C. (-y1-y2-y3-y4+y5+y6+y7+y8-y9-y10-y11-y12+y13+y14+y15+y16)/16

D. (-y1-y2-y3-y4-y5-y6-y7-y8+y9+y10+y11+y12+y13+y14+y15+y16)/16

A positive relative effect indicates enhancement of response variable due to increment of the associated factor. An experimental matrix designed for Cu concentration, guar concentration, temperature, and current density as factors and the maximum feature height per sample as the response variable was shown in Table 15. Figure 39 shows the effect of different parameters on the maximum feature height of the sample based on the data in Table 16. The data suggest that changing the current density has a significant effect on the maximum feature height and changing the guar concentration has the least effect on it. Figures 40-42 show the contour plots of maximum feature height with respect to Cu concentration, guar concentration, temperature, and

electrical current density. Figure 43 and 44 show the ANOVA analysis of the effect of individual parameters and interaction between these parameters.

Figures 45 and 46 show the thickness map of copper deposit obtained at high and low levels of current density. Analysis of these maps provides the thickness and roughness across copper sheets. It also provides a way to compare to modeling predictions to facilitate model validation. Copper deposits are thicker and rougher at the edges, whereas middle sections of deposits are thinner and smoother. Higher current density areas near edges result in rougher, thicker deposits.

5.4 Mathematical Modeling

A mathematical model using a finite element analysis-based software package, COMSOL Multiphysics, has been developed to predict the electrolyte velocity field, current distribution, and mass transfer rates in electrowinning cells with vertical planar electrodes. In this work, laminar flow of the electrolyte solution was taken into account. Modeling was performed on a 2D geometry and work is in progress to simulate a 3D mathematical model of an electrowinning cell. Simulation results are similar to the experimental results.

In electrowinning cells, the gas evolved at the anode is a major factor in determining electrolyte flow near the anode. In the development of the model, a single phase fluid approach was used to treat the gas and its interaction with electrolyte. Transport of bubbles within an aqueous electrolyte occurs predominantly by two mechanisms[39]:

i. The bubbles rise through the electrolyte due to their buoyancy,

ii. They are transported because the electrolyte itself is in motion with a time averaged velocity.

Gas bubbles in aqueous electrolytes are typically small and have small rise velocities. In the bulk of the fluid, mechanism (i) is typically negligible compare to mechanism (ii). In bulk electrolyte, bubbles can be treated as part of the liquid phase, and the liquid can be given a velocity based on bubble rise.

Figure 47 shows a COMSOL-predicted current distribution plot which is in proximity to the experimentally obtained results. The computations are performed for the fluid flow and concentrations across the planar vertical electrodes. The height of the cathode is 8.5 cm and height of anode is 8 cm, which is the same as our experimental setup. The triangular shaped boundary adjacent to the anode surface shows the region with bubble, which is taken directly from the work of A. Filzwieser, K. Hein, and G. Hanko[48]. The average size of the gas bubble was assumed to be 50 μm, which is measured experimentally by Reza Al Shakarji[11]. Figure 48 shows the velocity distribution of fluid between two electrodes. Ziegler and Evans have also shown the same velocity distribution in their model[39]. The corresponding current density distribution along the cathode surface is shown in Figure 49.

Figure 48 shows a 2D geometry for area between planar vertical electrodes in an electrowinning cell. The left side of the rectangle is the anode and the right side denotes the cathode of an electrowinning cell. In Figure 48, the color bar shows the velocity magnitude between two electrodes and in Figure 49, the curve shows the current density distribution along the cathode surface. X and Y axes denote the dimensions of geometry, which is in units of meters.

The roughness data measured from the experimental work and the model-predicted ratio of current density to the limiting current density (i/i_L) were then plotted against the distance from cathode bottom because COMSOL cannot measure the roughness of the cathode deposit directly. The simulation was performed for 20 hours and the limiting current density was then calculated from the data generated from the model using the equation given below:

$$i_L = \frac{D_{Cu} \times n \times F \times C_{Cu}}{\delta} \tag{5.19}$$

where,

i_L = Limiting current density

D_{Cu} = Diffusivity of copper ion

n = Number of electrons

F = Faraday constant

C_{Cu} = Bulk concentration of copper sulfate

δ = Boundary layer thickness

The boundary layer thickness was calculated from the following equation, available in the literature:

$$\delta = 3 \times l^{\frac{1}{2}} \times U^{\frac{-1}{2}} \times \nu^{\frac{1}{6}} \times {D_{Cu}}^{\frac{1}{3}} \tag{5.20}$$

where,

l = Length of the cathode

U = Relative velocity of the bubbles

ν = Kinematic viscosity

All the parameters needed to calculate the limiting current density can be obtained from the computer simulated model. The limiting current density was then calculated for the two different copper sulfate concentrations. The ratio of current density and limiting current density was then calculated for three different heights of cathode; 1 cm from the bottom of the cathode, 4 cm from the bottom of the cathode, and 8 cm from the bottom of the cathode. These regions were chosen for the analysis because the roughness measured experimentally was also at the same height. Figures 50 and 51 show the comparison of the results obtained experimentally and theoretically. These i/i_L values are then plotted against the average roughness. The experiment with 35 g/l of copper, 55^oC temperature, 475 A/m^2, and 175 g of guar per ton of copper cathode is supposed to produce the roughest deposit at the cathode, which is also predicted from the computer-simulated model since the i/i_L values are fairly close to the experimentally measured roughness at different cathode heights.

The same plots were obtained for the smoothest copper deposit at the cathode surface for the experimental condition of 45 g/l of Cu, 55^0C temperature, 325 A/m^2 current density, and 325 g of guar per ton of copper cathode (Figures 52, 53). The results obtained from the computer simulation are in proximity to the experimentally obtained data. A similar procedure was made for the maximum feature height for the above-mentioned experiments (Figures 54-57). The results show a similar trend of model-

predicted i/i_L values with respect to maximum feature height at different regions of the sample. A similar comparison was made for the thickness for the above-mentioned experiments (Figures 58-61). The results show a similar trend to the model-predicted i/i_L values with respect to maximum feature height at different regions of the sample.

Finally, the model predicted average thickness was compared with the experimentally measured average thickness and results are presented in Figure 62. Note that the model predicts the measured data well, indicating the model is a reasonable predictor of the experimental data.

5.5 Short-Circuiting Analysis with Tilted Cathode

Misalignment of the electrodes and bent cathodes cause short-circuits in copper electrowinning cells. To see the effect of a tilted cathode on the time to short-circuit, an experiment was carried out with a tilted cathode. A cathode was tilted 1.5 cm at the bottom to make the electrode separation distance 1 cm. The anode remained straight with an electrode separation of 2.5 cm at the top. The electrowinning cell setup is shown in Figure 63 with the new arrangement of electrodes. The experiment was carried out for the extreme rough condition of experiment 5 (i.e., 475 A/m^2 of current density, 35 g/L of Copper, 175 gm guar per tonne of copper cathode, and 55°C temperature). The first short-circuit occurs after 3 days of electrodeposition, which is significantly earlier than the experiment without the tilted cathode (Figure 64). It is evident from the experimental result that if care is taken to properly arrange the electrodes in a copper electrowinning operation, short-circuits can be largely avoided. A statistical analysis and multiphysics modeling will be carried out to validate this study in the future.

Table 9. The distribution of maximum feature height of Experiment 5 (rough surface) and Experiment 11 (smooth surface) at 5 hours of experiment and in the center of the cathode plate.

Order	Roughness height data of Experiment 5 (µm)	Roughness height data of Experiment 11 (µm)	F(x)
1	67	24	0.032
2	68	24	0.064
3	69	25	0.096
4	70	26	0.128
5	72	26	0.160
6	73	27	0.192
7	75	28	0.224
8	76	29	0.256
9	79	30	0.288
10	81	31	0.320
11	83	31	0.352
12	85	32	0.384
13	86	33	0.416
14	90	33	0.448
15	92	34	0.480
16	94	35	0.512
17	96	35	0.544
18	98	35	0.576

Table 9. Contd.

Order	Roughness height data of Experiment 5 (µm)	Roughness height data of Experiment 11 (µm)	F(x)
19	100	36	0.608
20	101	36	0.640
21	103	36	0.672
22	107	37	0.704
23	109	37	0.736
24	111	38	0.768
25	115	38	0.800
26	118	39	0.832
27	119	40	0.864
28	121	40	0.896
29	125	41	0.928
30	128	42	0.960

Table 10. Maximum feature heights based on extrapolation for Experiment 5 (the most rough condition) and Experiment 11 (the smoothest condition).

Time (hours)	Experiment 5 feature height (µm)	Experiment 11 feature height (µm)
5	300	105
20	1215	211
80	2550	617

Table 11. Extrapolated percentage increase in maximum feature height measure for 2.66 x 0.5 cm^2 measured area.

Experiment No.	Measurement Area (cm^2)	Maximum Feature height	Initial measurement	% increase compared to initial line scan for one measurement	Extrapolated maximum feature height for 2.66 x 0.5 cm^2 measured area	% increase compared to initial line scan for 10 measurements
5 (5 hours)	2.66 x 0.05	287 µm	256 µm	12.1	256 x 1.121 x 1.121 = 322 µm	25.8
5 (20 hours)	2.66 x 0.05	570 µm	520 µm	9.6	520 x 1.096 x 1.096 = 625 µm	20.2
5 (80 hours)	2.66 x 0.05	1788 µm	1685 µm	6.1	1685 x 1.061 x 1.061 = 1897 µm	12.6
11 (5 hours)	2.66 x 0.05	86 µm	81 µm	6.1	81 x 1.061 x 1.061 = 91 µm	12.6
11 (20 hours)	2.66 x 0.05	110 µm	105 µm	4.8	105 x 1.048 x 1.048 = 115 µm	10.0
11 (80 hours)	2.66 x 0.05	360 µm	350 µm	2.9	350 x 1.029 x 1.029 = 370 µm	5.8

Table 12. Average thickness of copper deposit obtained with 35g/L Cu, 175 g of Guar/tonne of Cu, 35°C temperature, and 475 A/m^2 of current density for 20 hrs.

	1cm from Left Edge	Center	1cm from Right Edge
Top(1cm from top)	784µm	514 µm	785 µm
Middle(5 cm from top)	894 µm	610 µm	907 µm
Bottom(1cm from bottom)	956 µm	620 µm	959 µm

Table 13. Average thickness of copper deposit obtained with 45g/L Cu, 325 g of Guar/tonne of Cu, 35°C temperature, and 325 A/m^2 of current density for 20 hrs.

	1cm from Left Edge	Center	1cm from Right Edge
Top(1cm from top)	467µm	237 µm	493 µm
Middle(5 cm from top)	507 µm	249 µm	498 µm
Bottom(1cm from bottom)	556 µm	279 µm	587 µm

Table 14. Average roughness of copper deposit obtained with 35g/L Cu, 175 g of Guar/tonne of Cu, 35°C temperature, and 475 A/m^2 of current density for 20 hrs.

	Average Roughness
Top(1cm from top)	62.41 μm
Middle(5 cm from top)	73.23 μm
Bottom(1cm from bottom)	81.79 μm

Table 15. Average roughness of copper deposit obtained with 45g/L Cu, 325 g of Guar/tonne of Cu, 35°C temperature, and 325 A/m^2 of current density for 20 hrs.

	Average Roughness
Top(1cm from top)	22.004 μm
Middle(5 cm from top)	23.76 μm
Bottom(1cm from bottom)	26.405 μm

Table 16. A four-factor, two-level experimental design matrix for 5-hour electrowinning tests.

Test	Temp. (^oC)	Dissolved Cu (g/l)	Current Density (A/m^2)	Guar (g/tonne Cu)	Maximum Feature Height (µm)
1	35	35	325	175	245
2	55	35	325	175	240
3	35	45	325	175	390
4	55	45	325	175	245
5	35	35	475	175	450
6	55	35	475	175	880
7	35	45	475	175	480
8	55	45	475	175	620
9	35	35	325	325	340
10	55	35	325	325	540
11	35	45	325	325	170
12	55	45	325	325	175
13	35	35	475	325	560
14	55	35	475	325	770
15	35	45	475	325	690
16	55	45	475	325	495

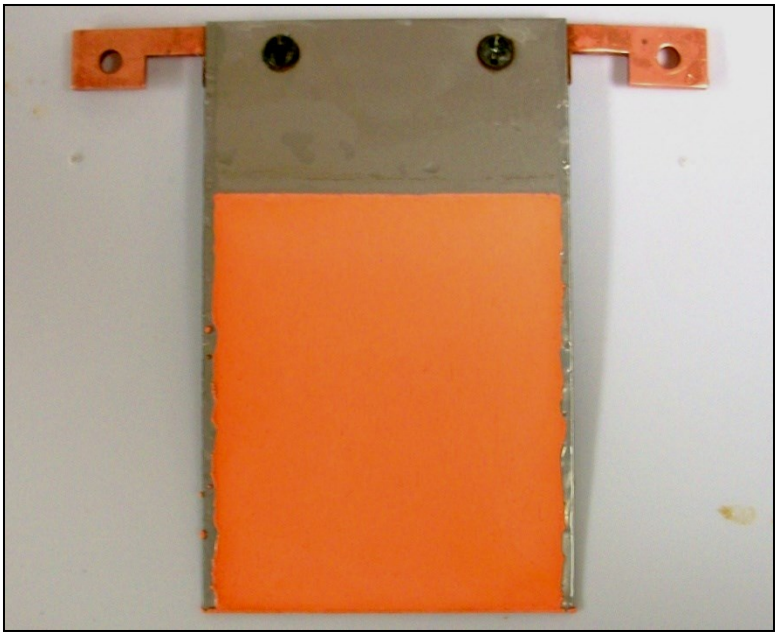

Fig. 12. Copper deposit obtained with 45g/L Cu, 325g of Guar/tonne of Cu, 35°C temperature, and 325 A/m^2 of current density for 5 hrs.

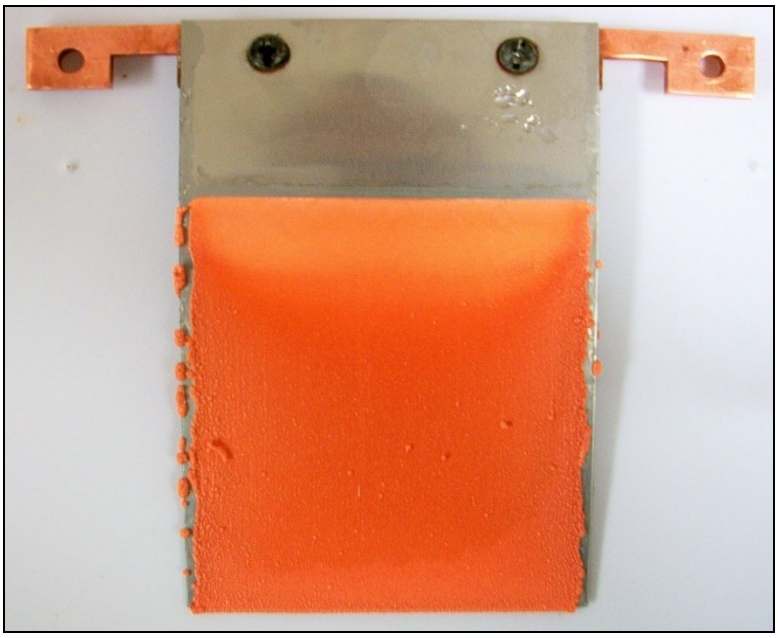

Fig. 13. Copper deposits obtained with 35g/L Cu, 175g of Guar/tonne, 35°C temperature, and 475 A/m^2 of current density for 5 hrs.

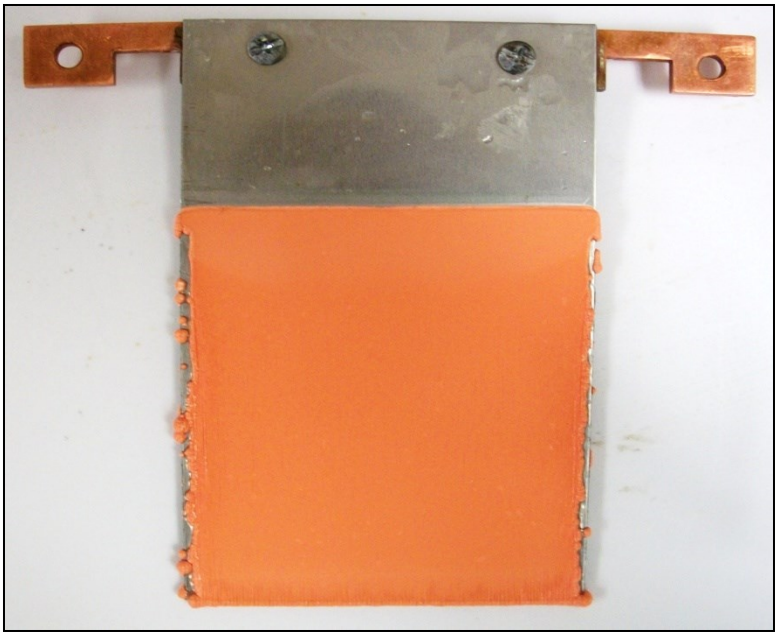

Fig. 14. Copper deposit obtained with 45g/L Cu, 325g of Guar/tonne of Cu, 35°C temperature, and 325 A/m^2 of current density for 20 hrs.

Fig. 15. Copper deposit obtained with 35g/L Cu, 175g of Guar/tonne of Cu, 35°C temperature, and 475 A/m^2 of current density for 20 hrs.

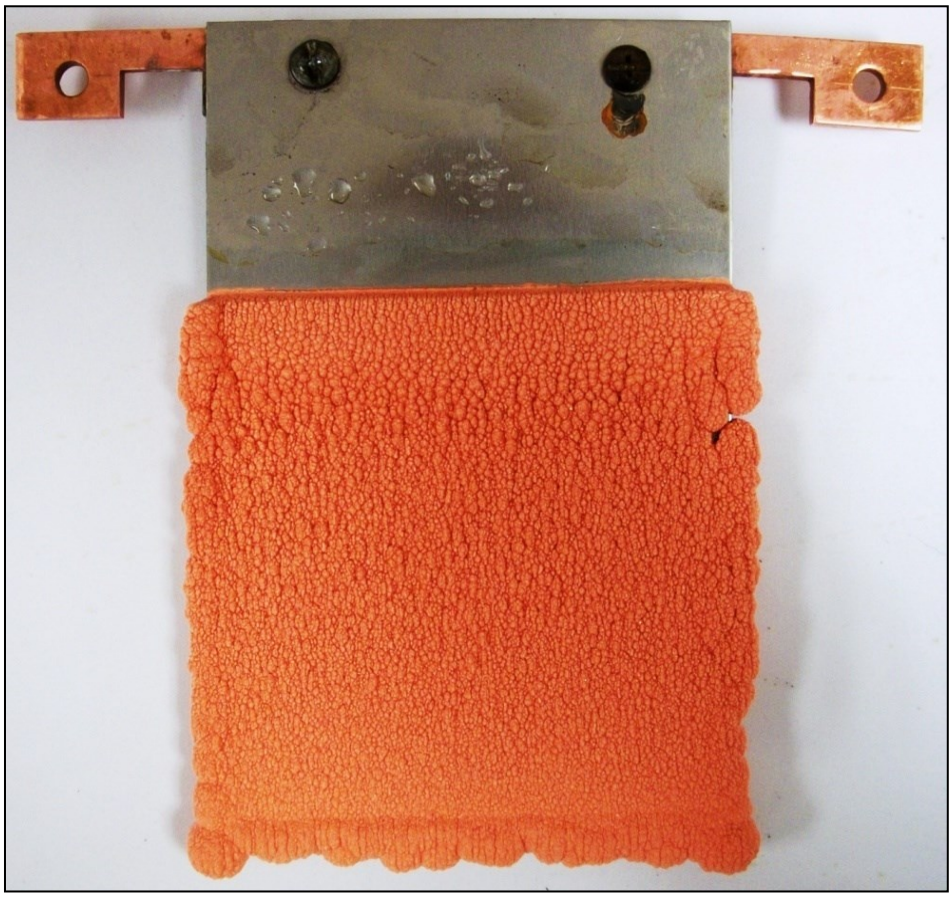

Fig. 16. Copper deposit obtained with 35g/L Cu, 175g of Guar/tonne of Cu, 35°C temperature, and 475 A/m^2 of current density for 80 hrs.

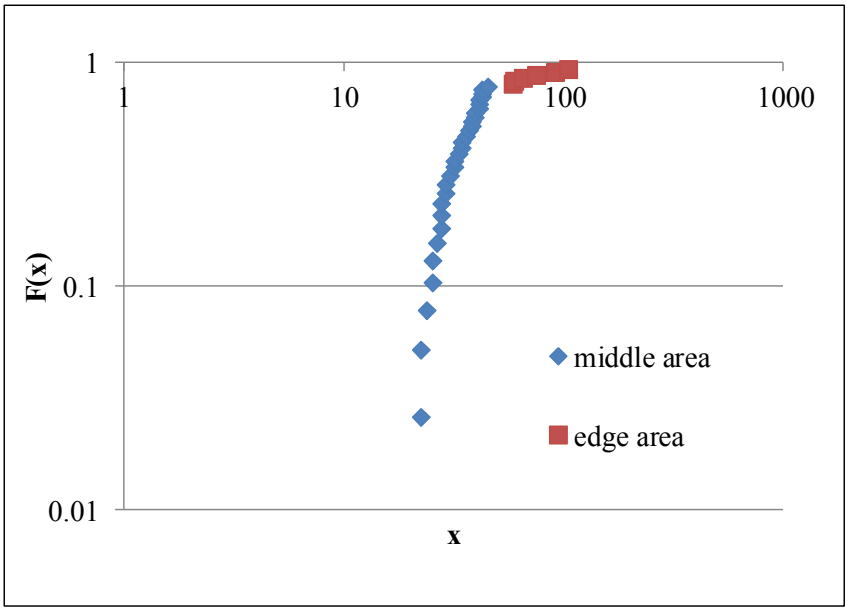

Fig. 17. Log-normal distribution data for Experiment 1 at 5 hours (low temperature, low copper concentration, low current density, and low guar).

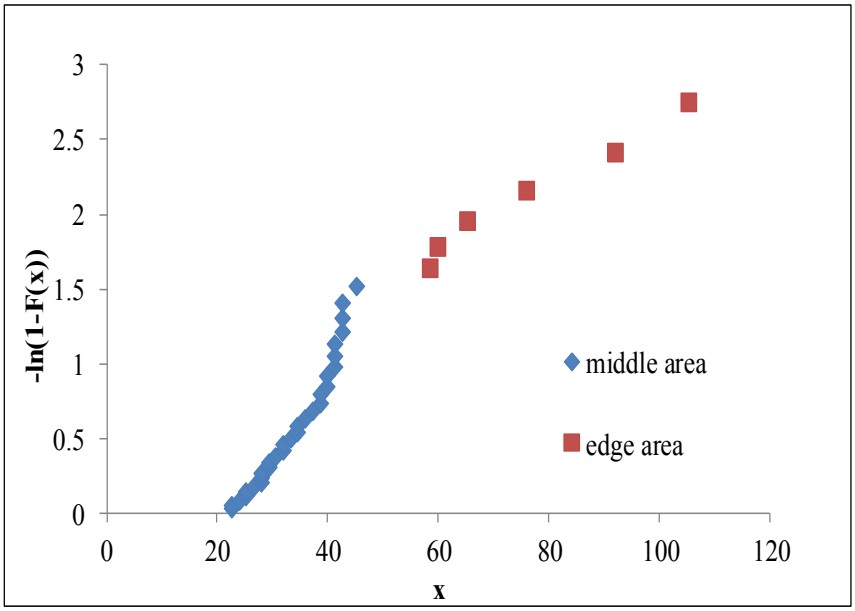

Fig. 18. Exponential distribution data for Experiment 1 at 5 hours (low temperature, low copper concentration, low current density, and low guar).

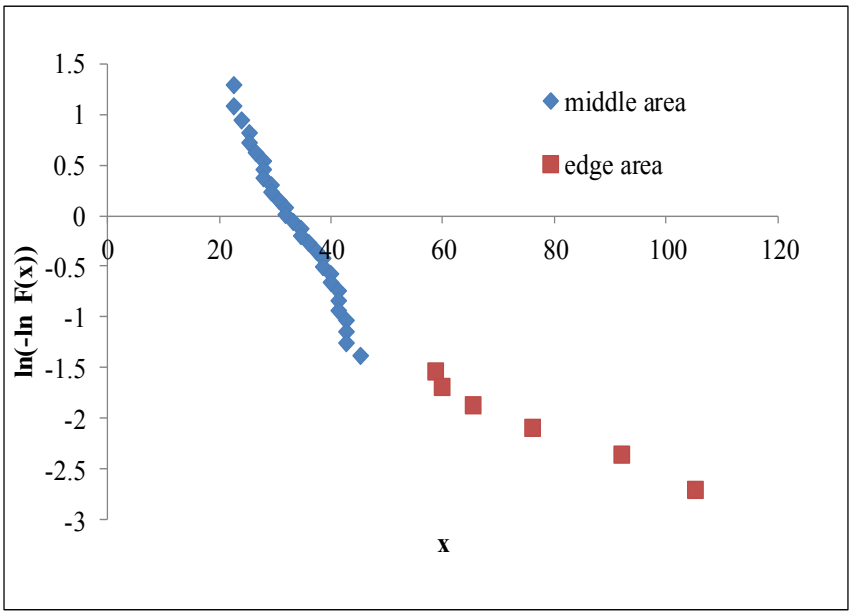

Fig. 19. Double exponential distribution data for Experiment 1 at 5 hours (low temperature, low copper concentration, low current density, and low guar).

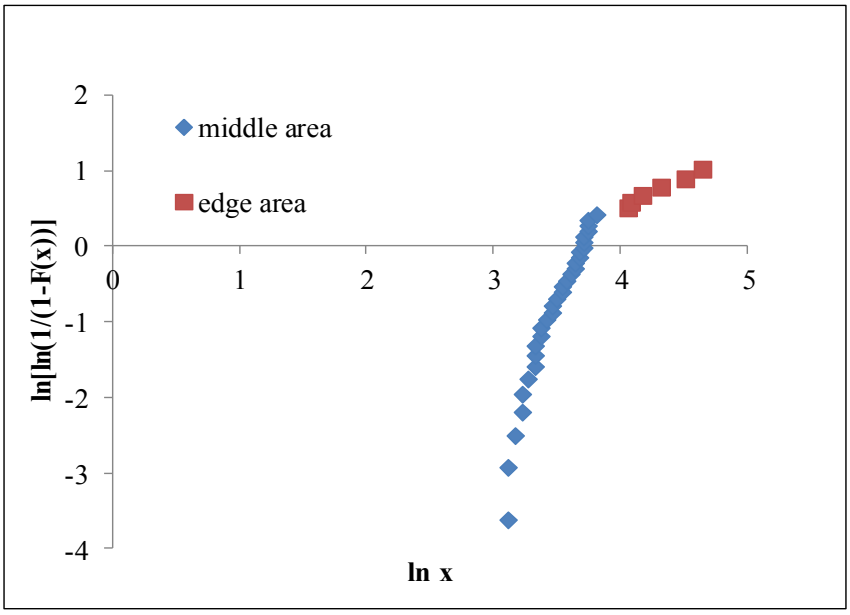

Fig. 20. Weibull distribution data for Experiment 1 at 5 hours (low temperature, low copper concentration, low current density, and low guar).

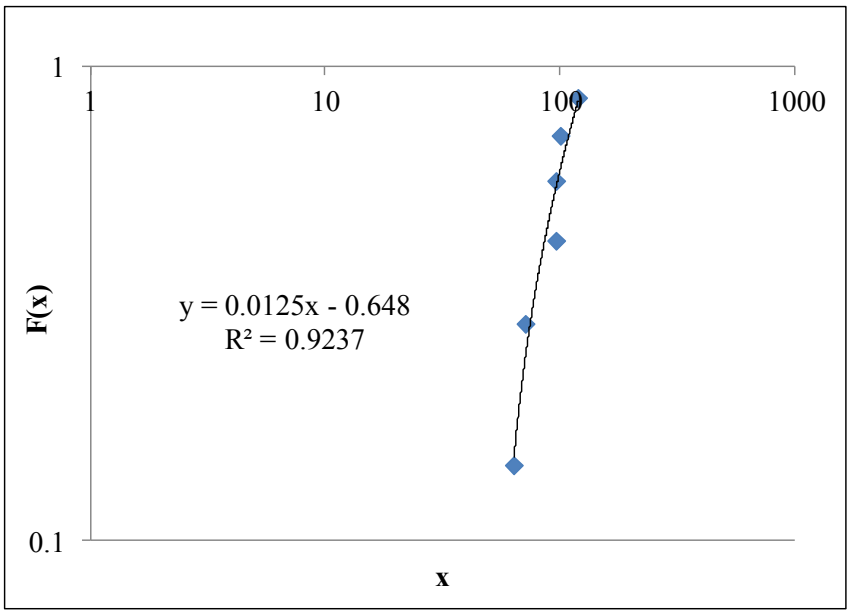

Fig. 21. Log-normal distribution edge area data for Experiment 1 at 5 hours (low temperature, low copper concentration, low current density, and low guar).

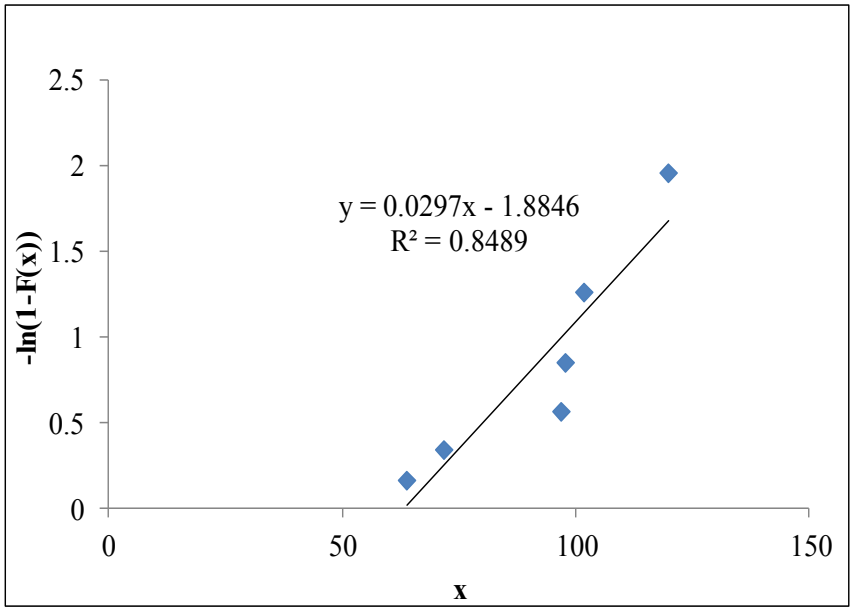

Fig. 22. Exponential distribution edge area data for Experiment 1 at 5 hours (low temperature, low copper concentration, low current density, and low guar).

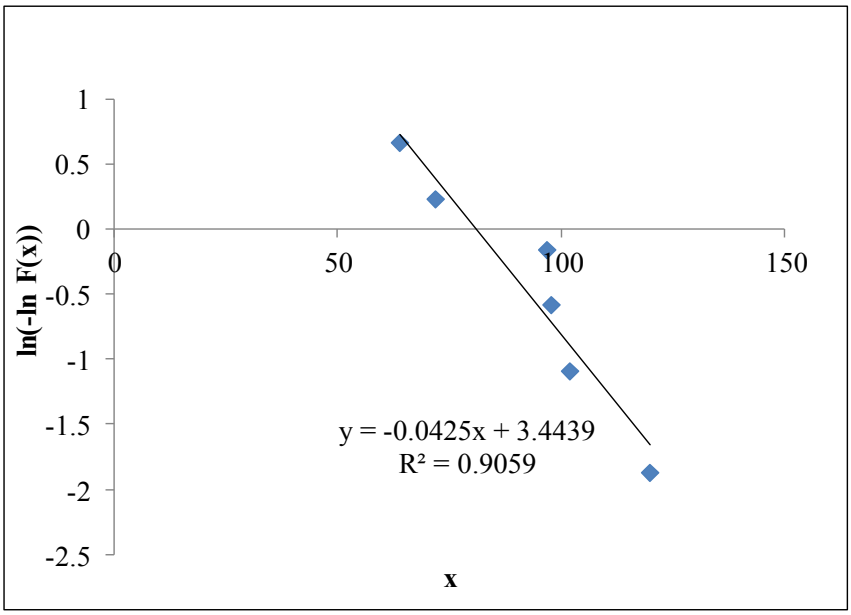

Fig. 23. Double exponential distribution edge area data for Experiment 1 at 5 hours (low temperature, low copper concentration, low current density, and low guar).

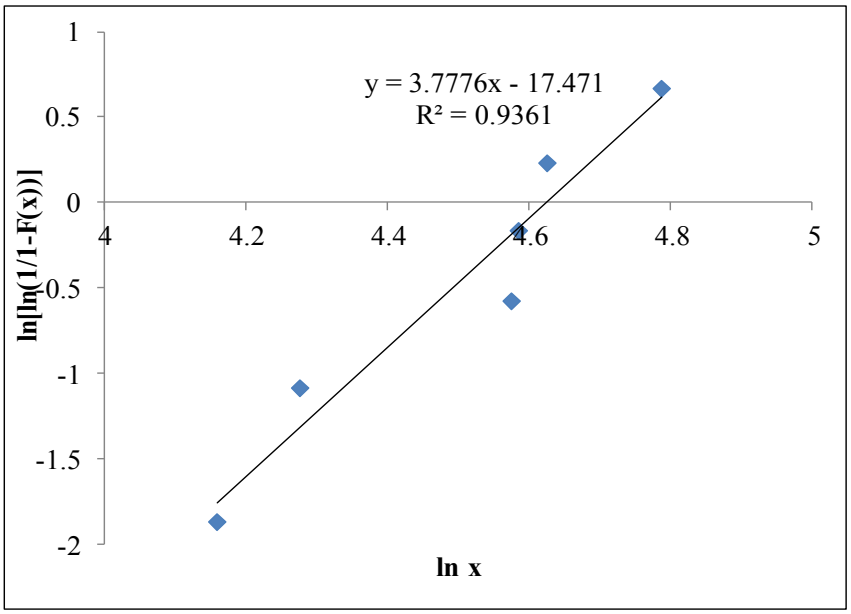

Fig. 24. Weibull distribution edge area data for Experiment 1 at 5 hours (low temperature, low copper concentration, low current density, and low guar).

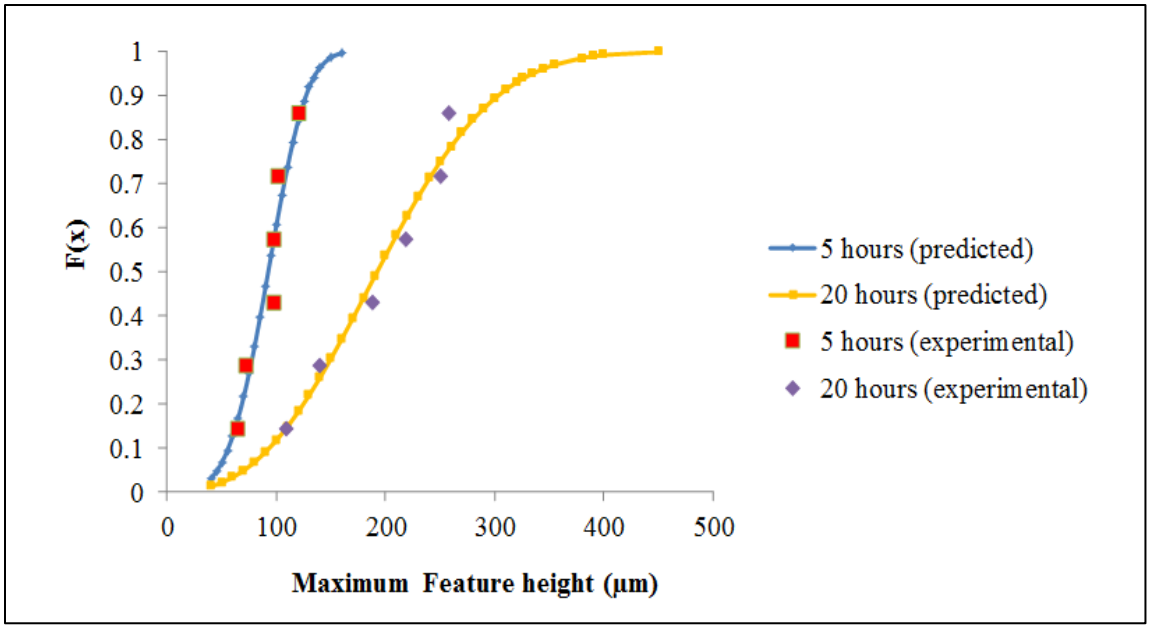

Fig. 25. Predicted and experimental probability functions for experiments (low temperature, low copper concentration, low current density, and low guar) at 5 hours and 20 hours.

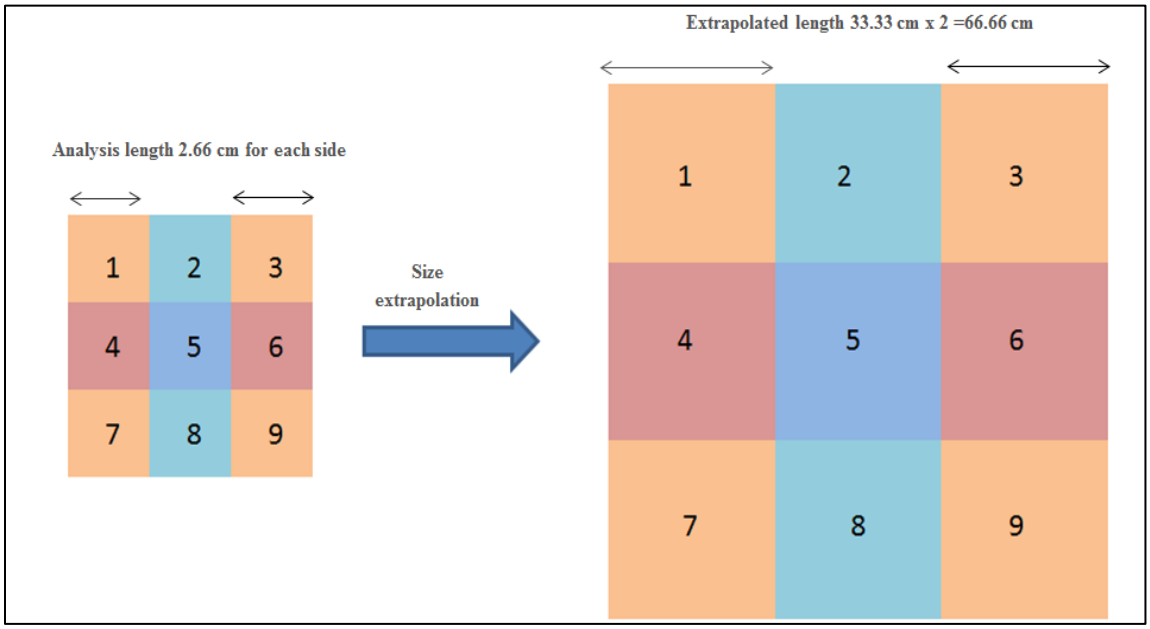

Fig. 26. Schematic diagram showing coupon (sample) positions of the experimental cathode and the associated extrapolation from sample coupons to an industrial scale electrode.

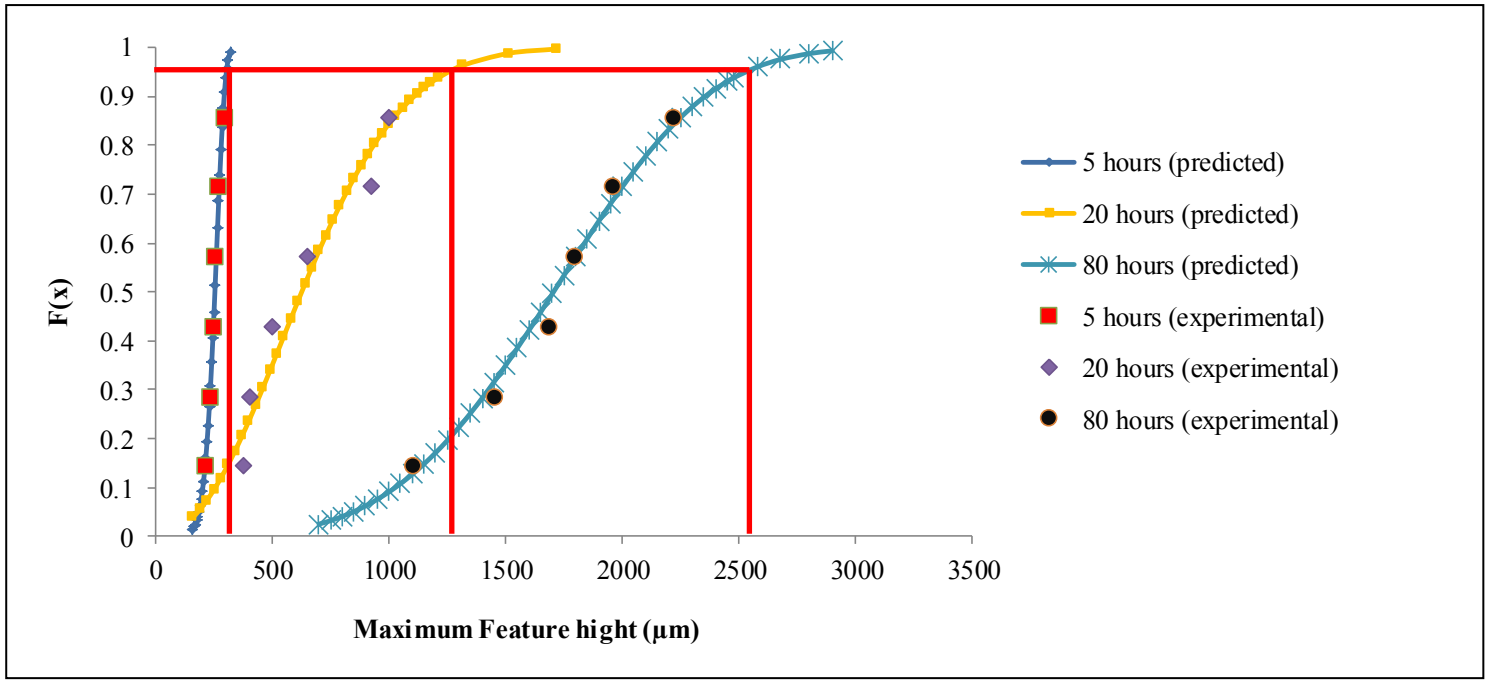

Fig. 27. The feature height extrapolation line at F(x) = 0.96, which is shown in red, from small samples to industrial size cathode for Experiment 5 (low temperature, low copper concentration, high current density, and low guar).

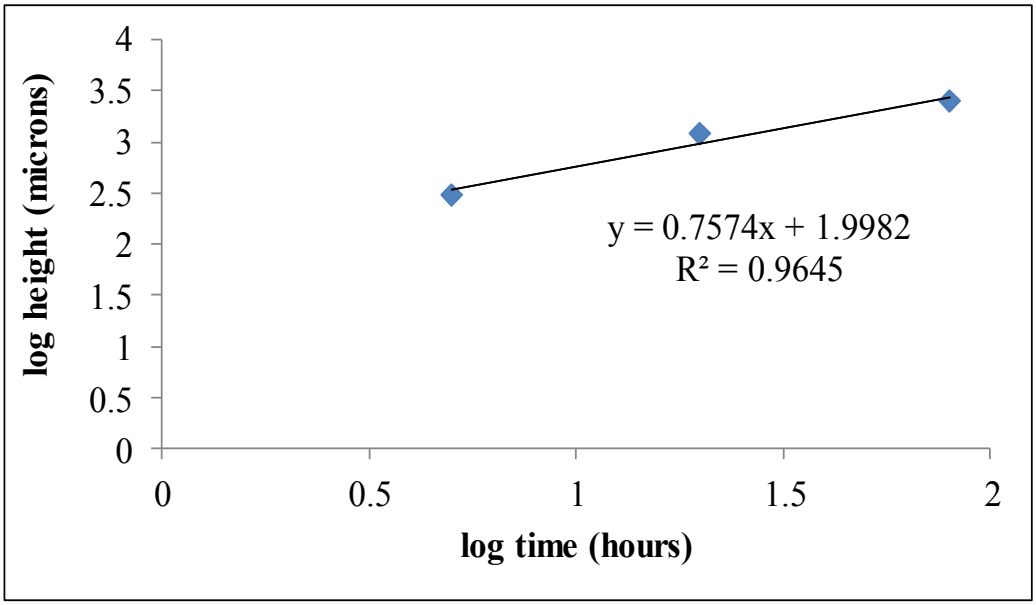

Fig. 28. Experiment 5 (the roughest condition) plot of log time (hours) vs log maximum feature height (microns) at industrial size cathode.

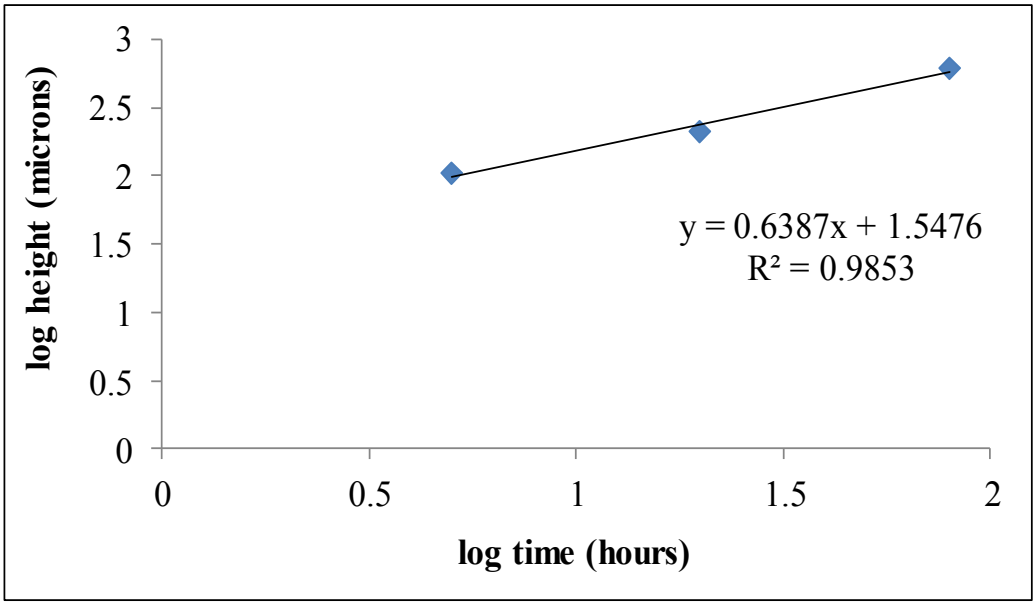

Fig. 29. Experiment 11 (the smoothest condition) plot of log time (hours) vs. log maximum feature height (microns) at industrial size cathode.

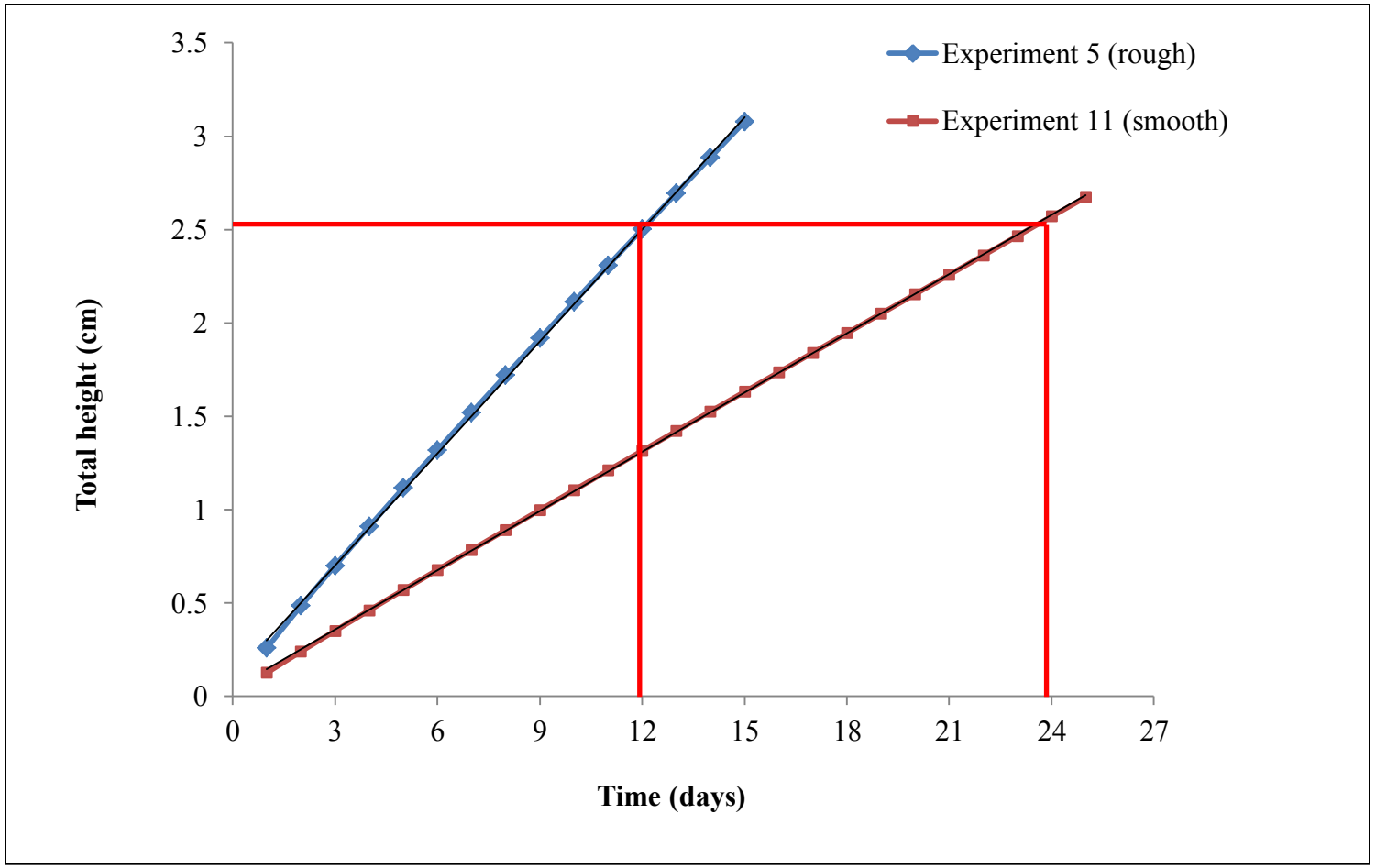

Fig. 30. Predicted time to short-circuiting of Experiments 5 (475 A/m^2) and 11 (325 A/m^2) for area of 1 m^2 deposition, 2.5 cm electrode distance, and 95% current efficiency.

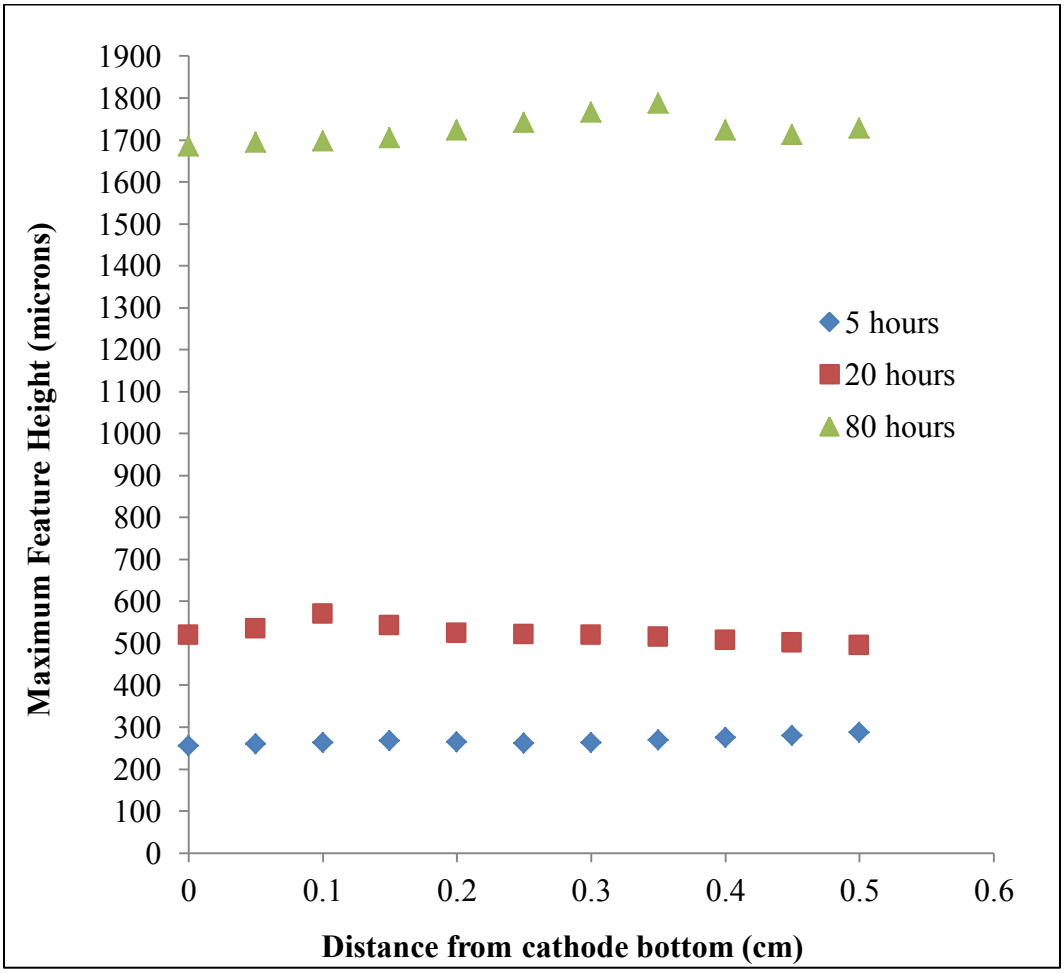

Fig. 31. Measured maximum feature height for each layer of a coupon from Experiment 5 (Extreme rough condition) for 5, 20, and 80 hours.

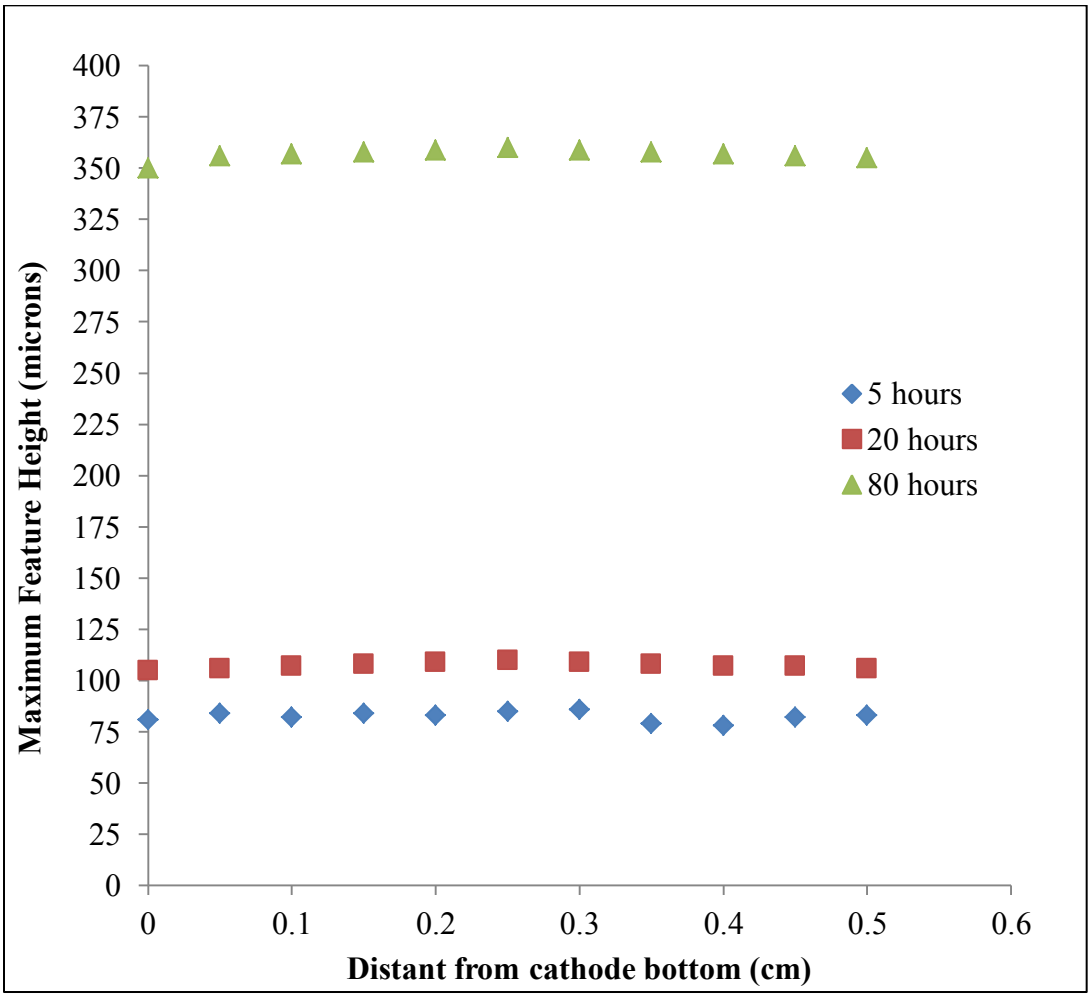

Fig. 32. Measured maximum feature height for each layer of a coupon from Experiment 11 (Extreme smooth condition) for 5, 20, and 80 hours.

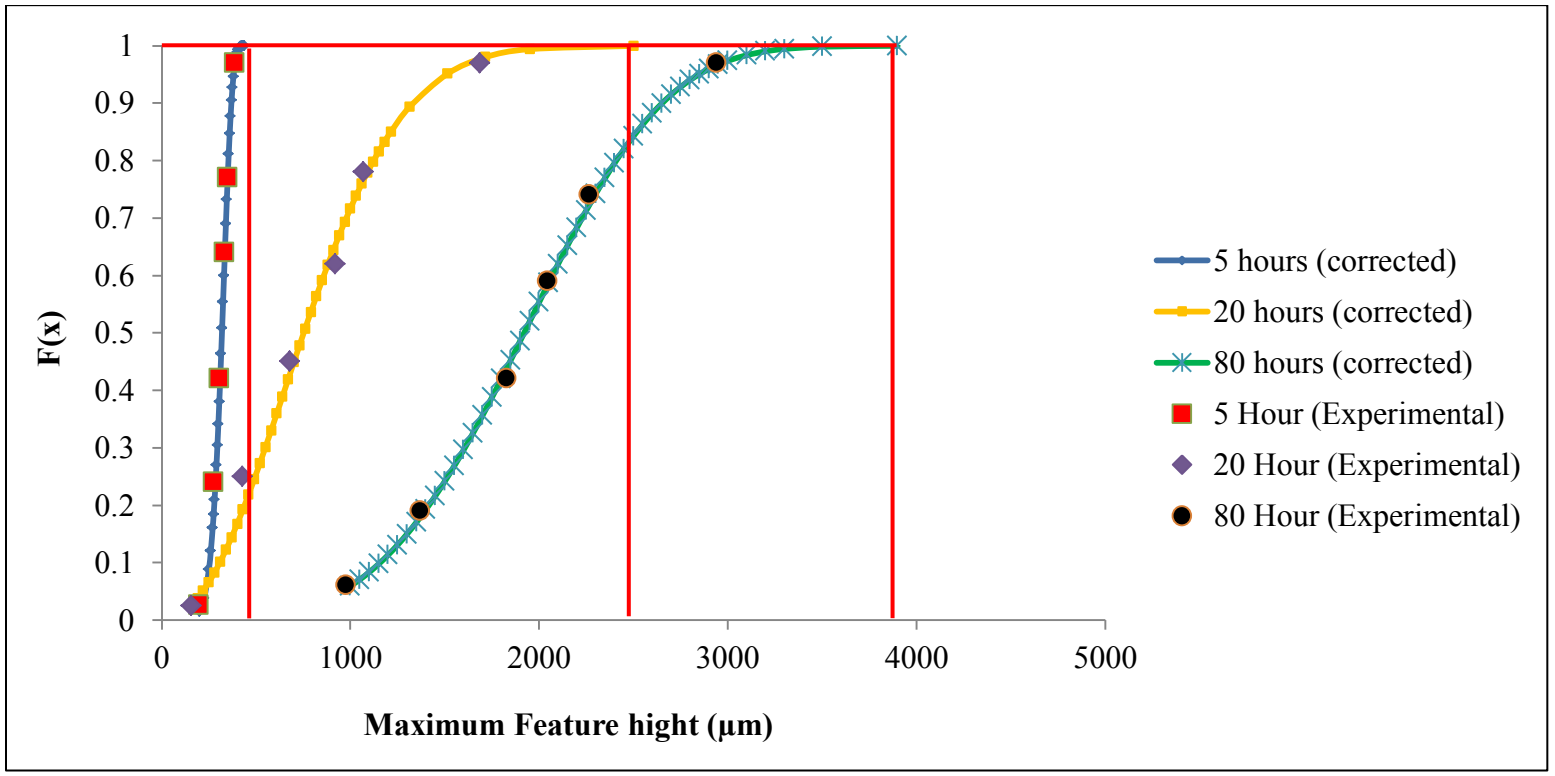

Fig. 33. The corrected from line scan to area scan feature height extrapolation line at F(x) = 0.99, which is shown in red, from small samples to industrial size cathode for Experiment 5 (low temperature, low copper concentration, high current density, and low guar).

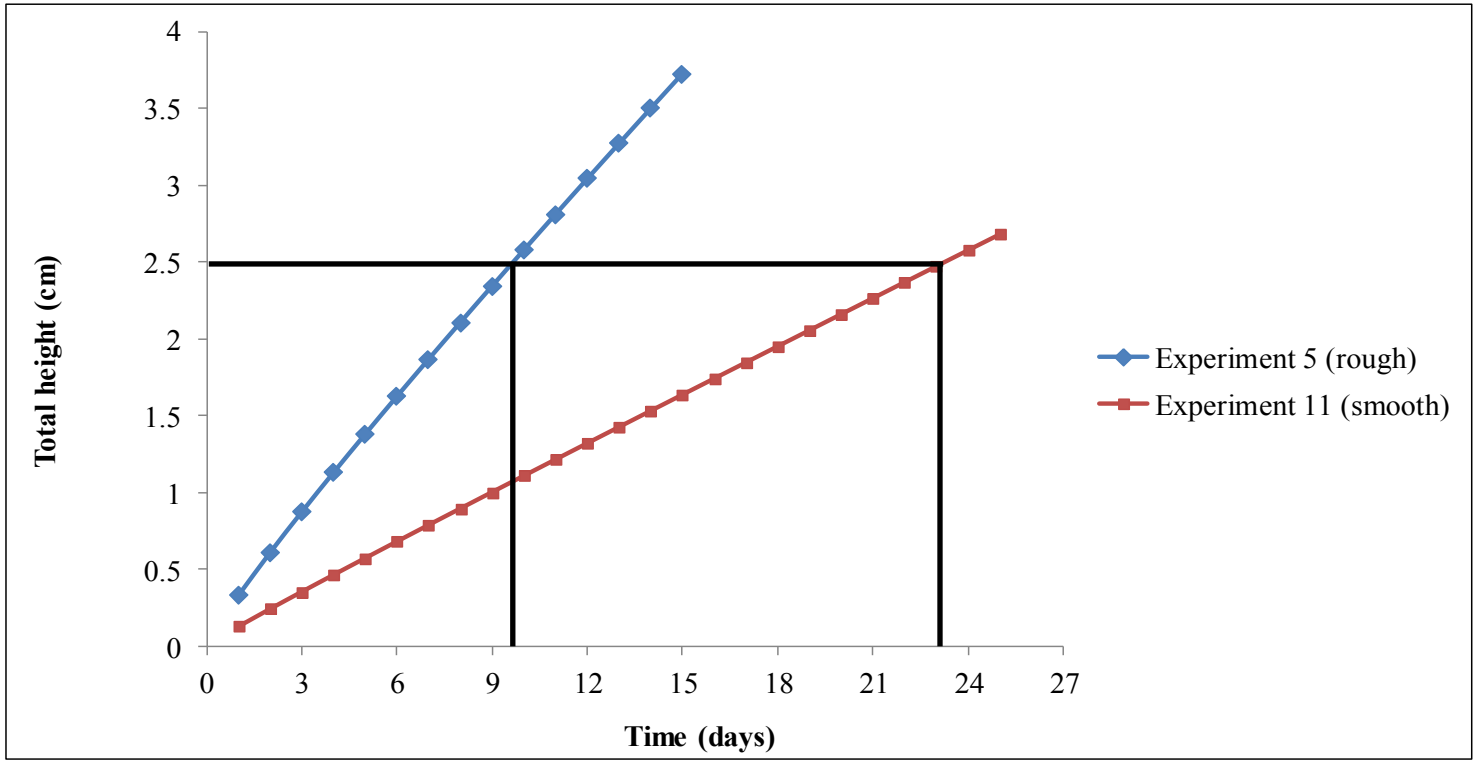

Fig. 34. Predicted time to short-circuiting for Experiment 5 (475 A/m^2, 35 g/L copper, and 175 g/t of guar) and 11 (325 A/m^2, 45 g/L copper, and 325 g/t of guar) for area of 1 m^2 deposition, 2.5 cm electrode distance, and 95% current efficiency based on corrected maximum feature height.

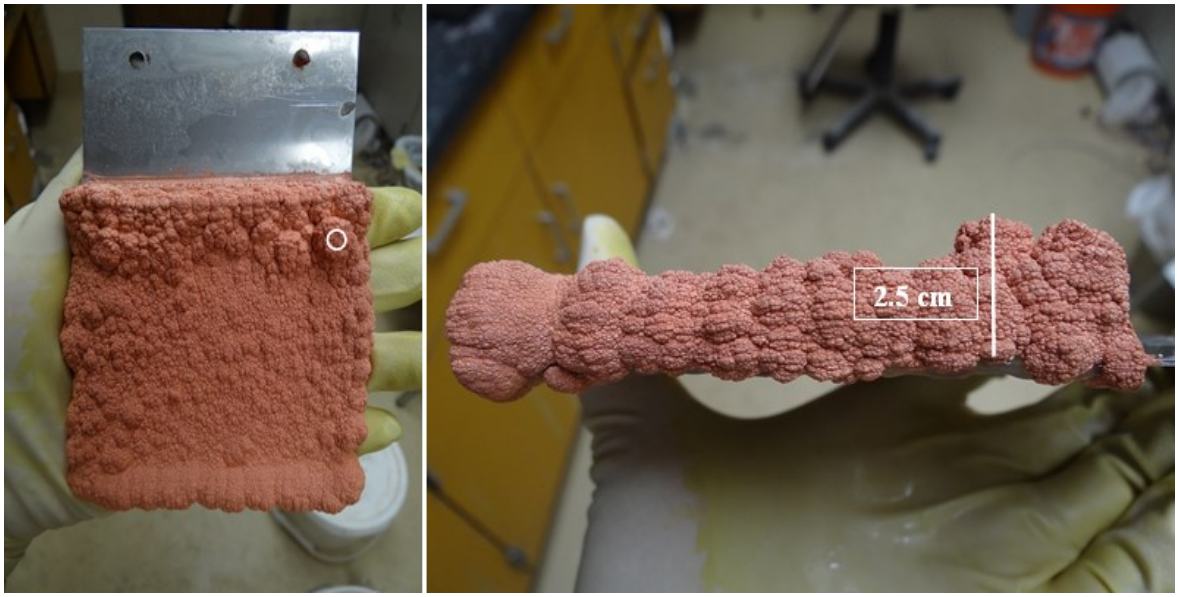

Fig. 35. The first short-circuiting occurred after 8 days of deposition, as shown in white circle (left) and white line (right).

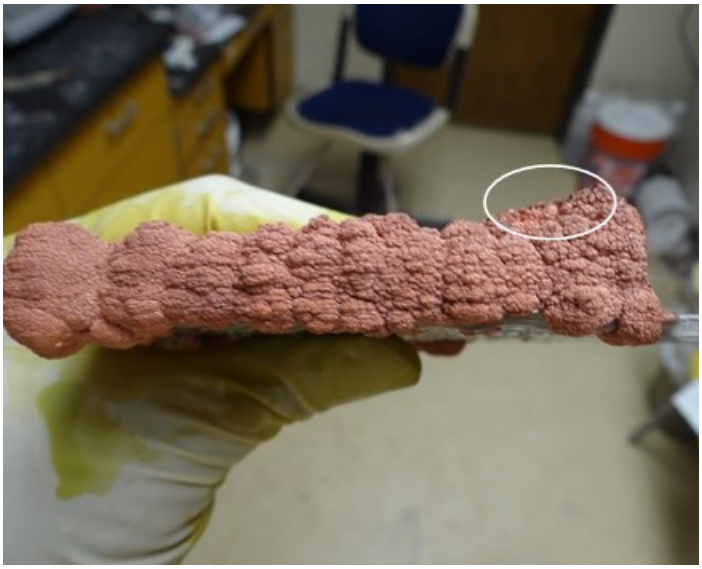

Fig. 36. Undesirable roughness was cut out, as shown in white circle.

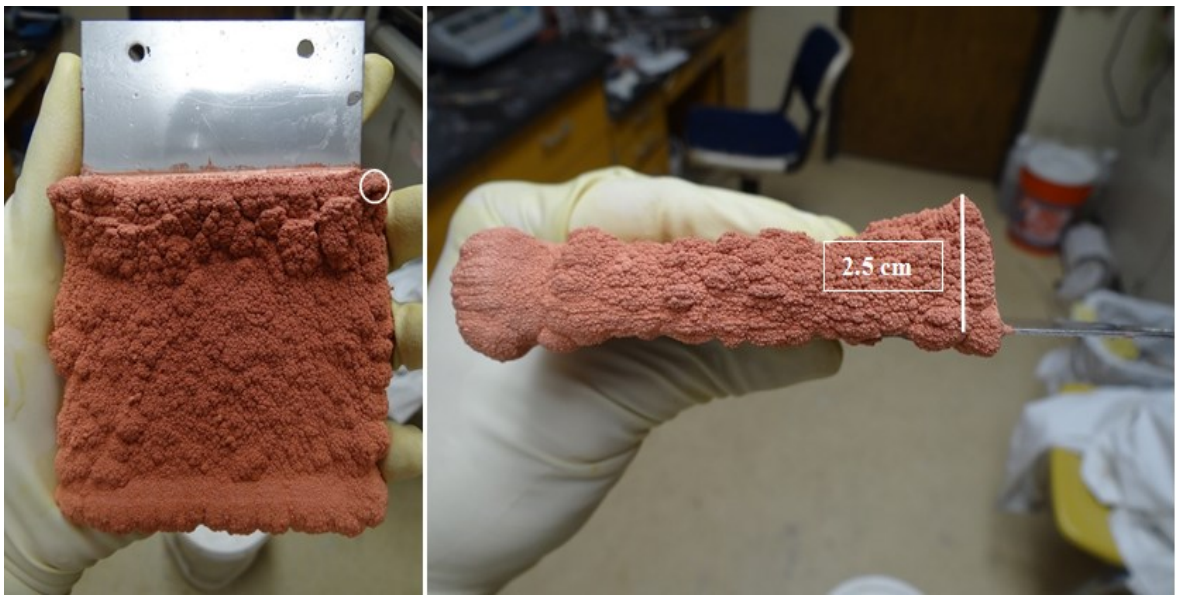

Fig. 37. The second short-circuiting occurred after 9 days of deposition, as shown in white circle (left) and white line (right).

Fig. 38. The third short-circuiting occurred after 9 days of deposition, as shown in white circle (left) and white line (right).

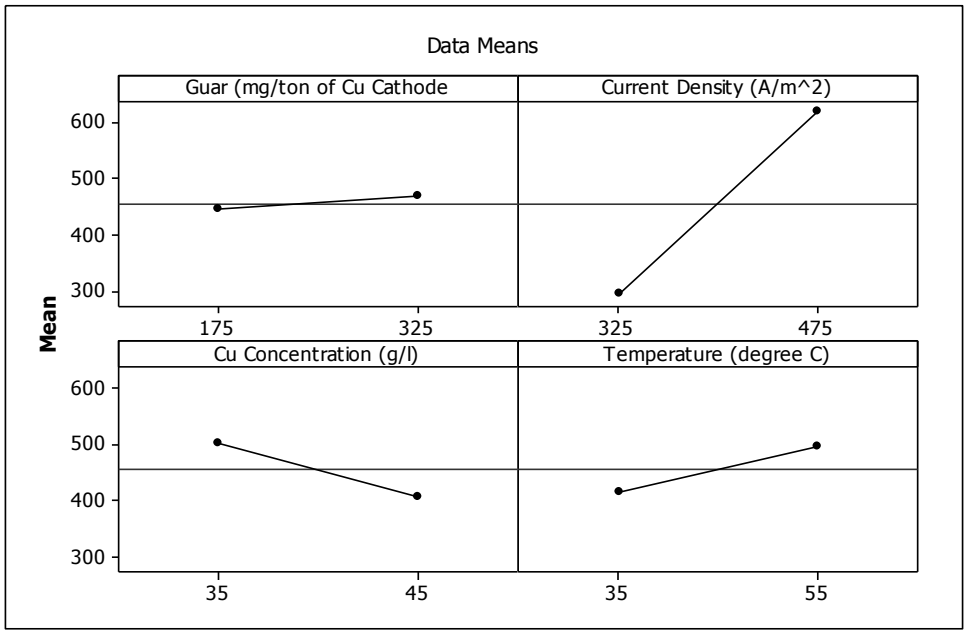

Fig. 39. Main effects plot for maximum feature of 20-hour experiment sample heights 1 cm from the bottom of the cathode.

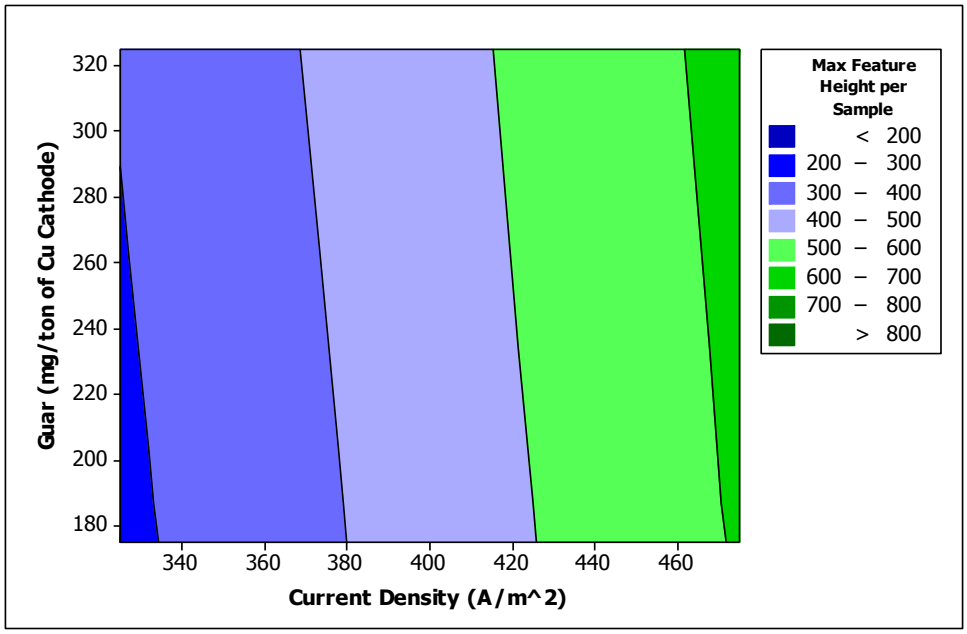

Fig. 40. Contour plot of maximum feature height of 20-hour experiment samples 1 cm from the bottom of the cathode vs. guar and current density.

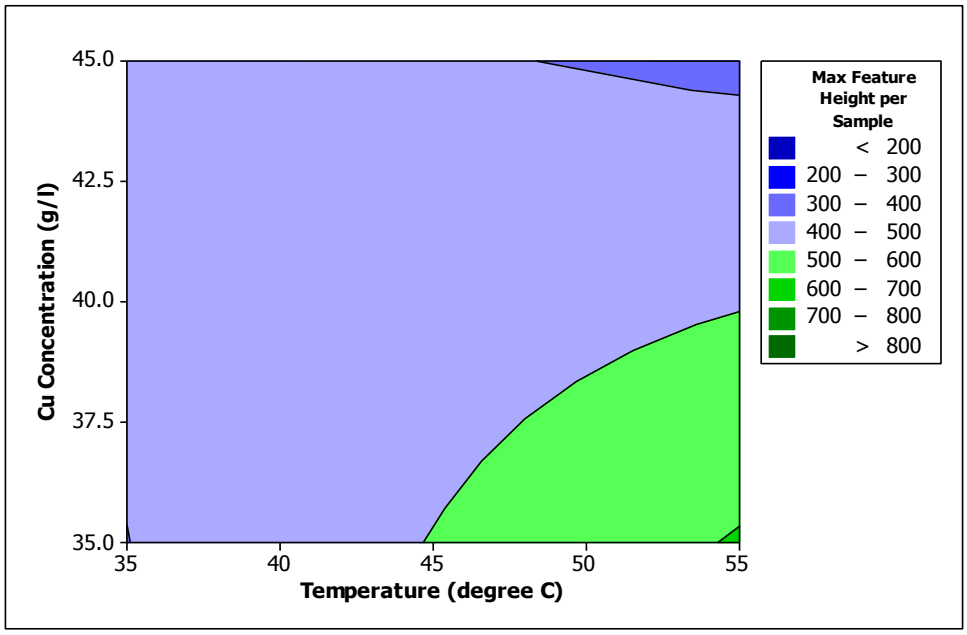

Fig. 41. Contour plots of maximum feature height of 20-hour experiment samples 1 cm from the bottom of the cathode vs. Cu concentration and Temperature.

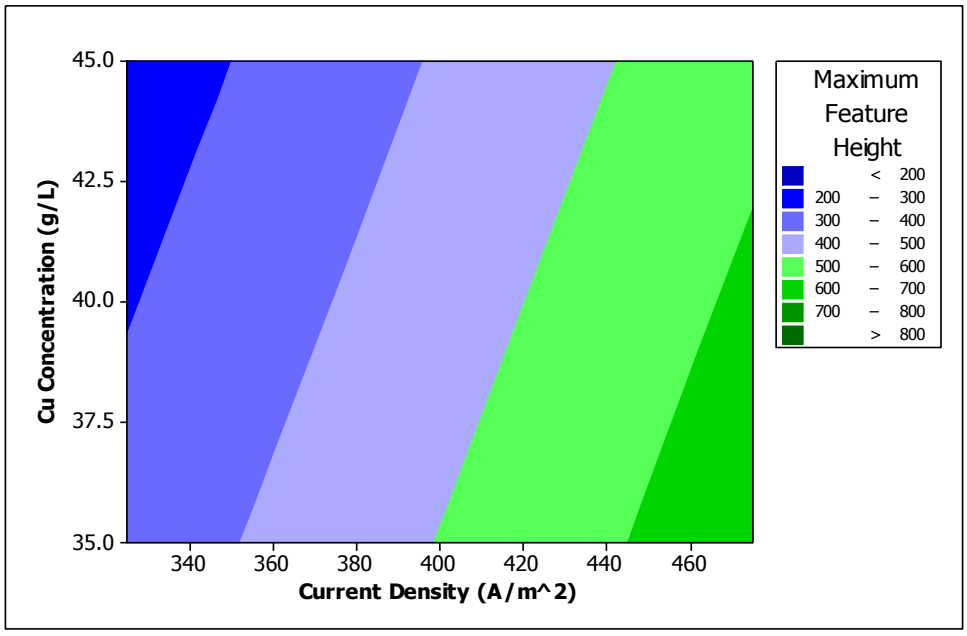

Fig. 42. Contour plots of maximum feature height of 20-hour experiment samples 1 cm from the bottom of the cathode vs. Cu concentration and Current Density.

Analysis of Variance for Max Feature Height (coded units)

Source	DF	Seq SS	Adj SS	Adj MS	F	P
Main Effects	4	486456	486456	121614	540.51	0.032
2-Way Interactions	6	108894	108894	18149	80.66	0.085
3-Way Interactions	4	98719	98719	24680	109.69	0.071
Residual Error	1	225	225	225		
Total	15	694294				

Fig. 43. Analysis of variance for maximum feature height.

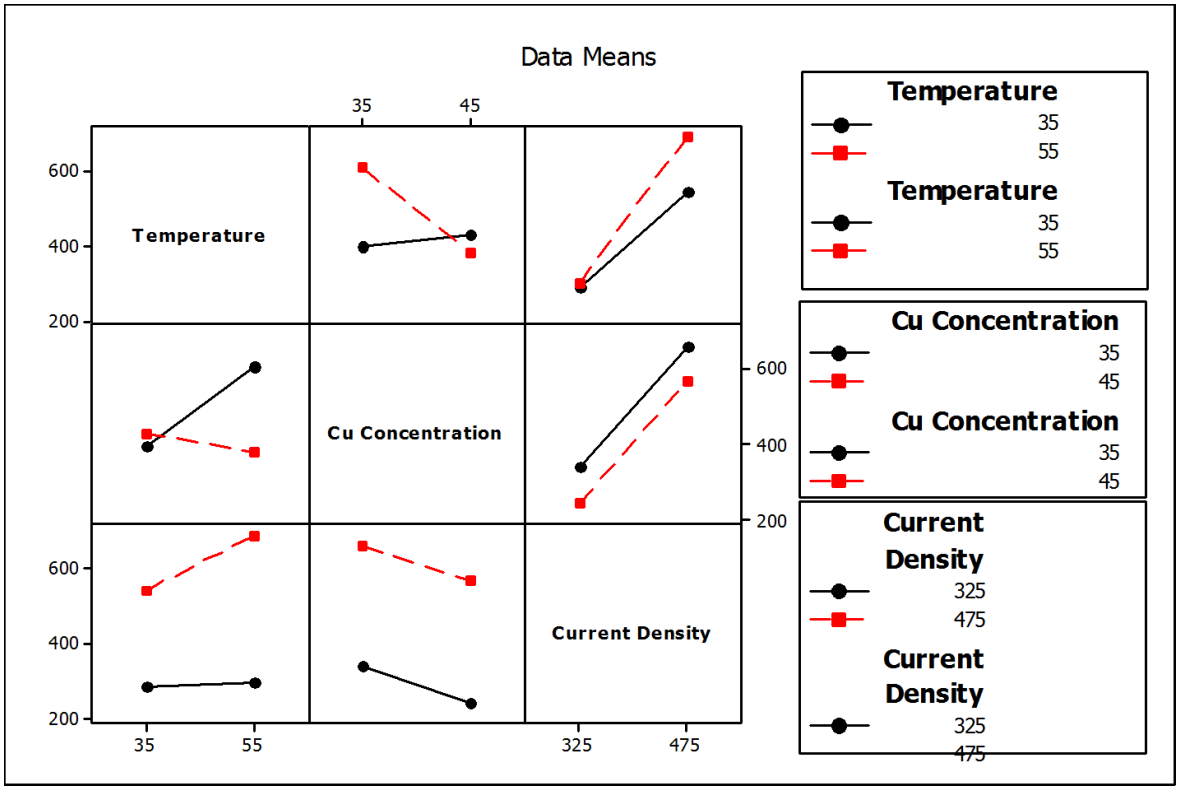

Fig. 44. Interaction plot of various parameters.

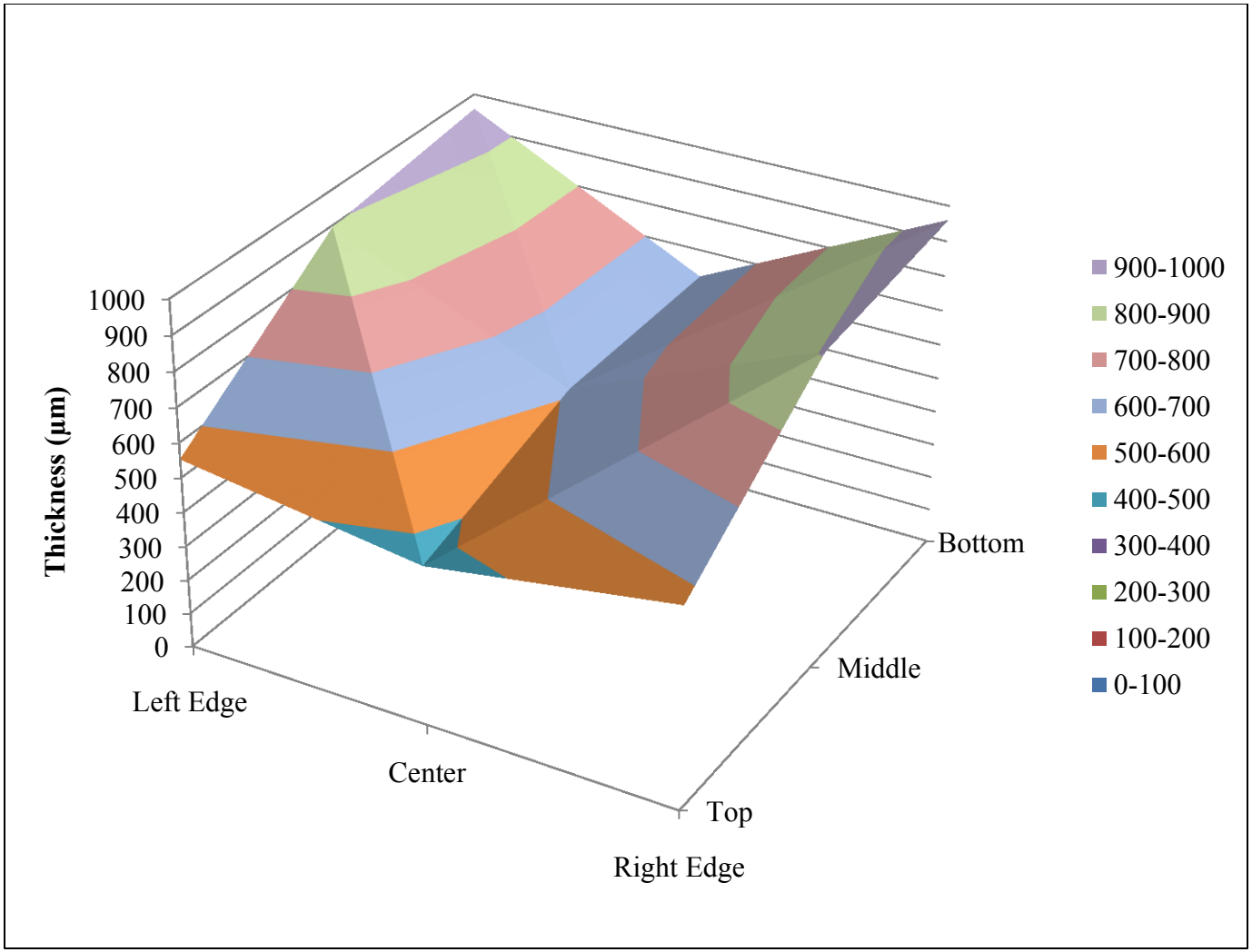

Fig. 45. Thickness map of copper deposit obtained at 475A/m^2 current density, 35 g/l of Cu concentration at 35°C temperature.

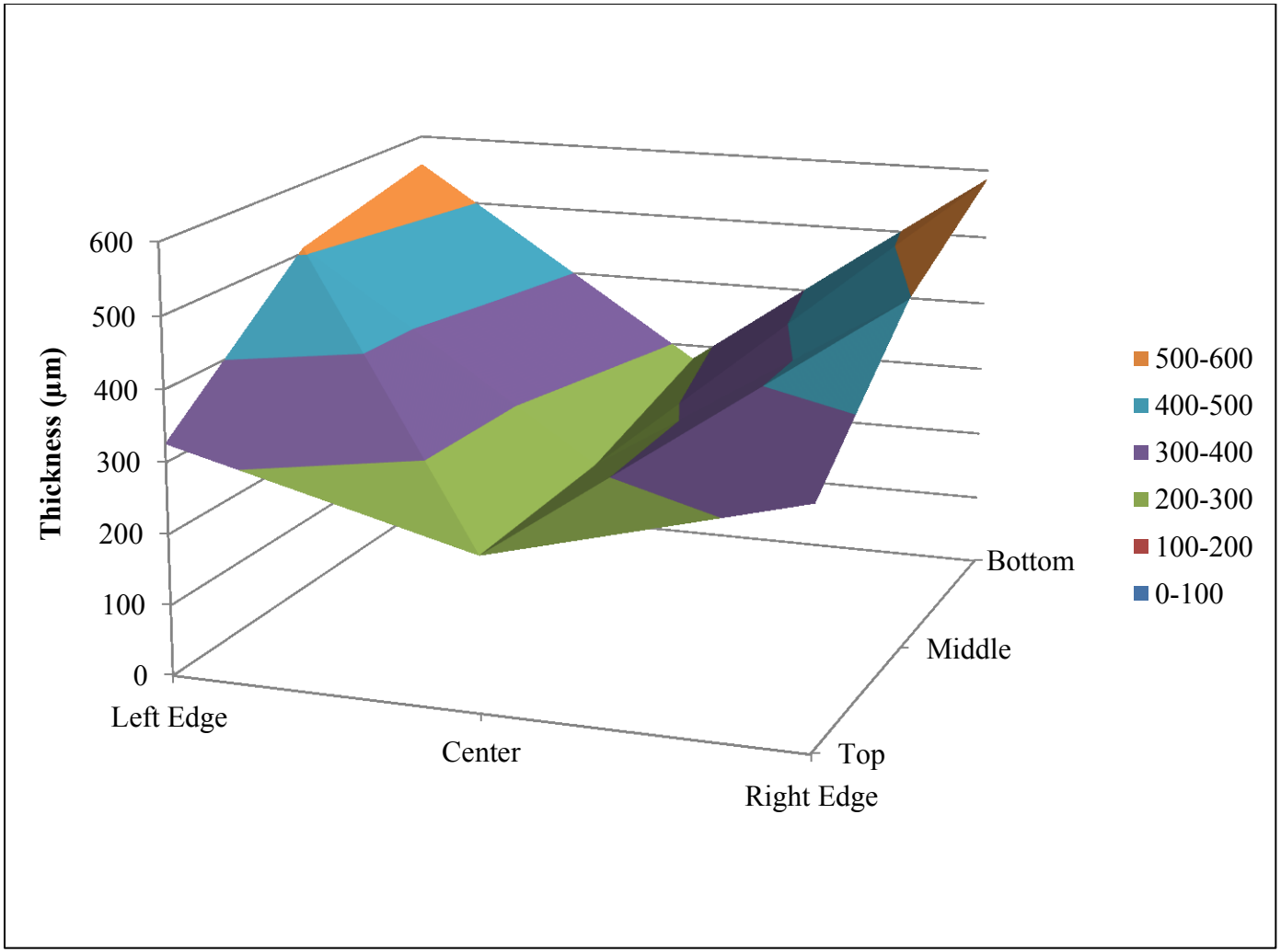

Fig. 46. Thickness map of copper deposit obtained at 325A/m^2 current density, 35 g/l of Cu concentration at 35°C temperature.

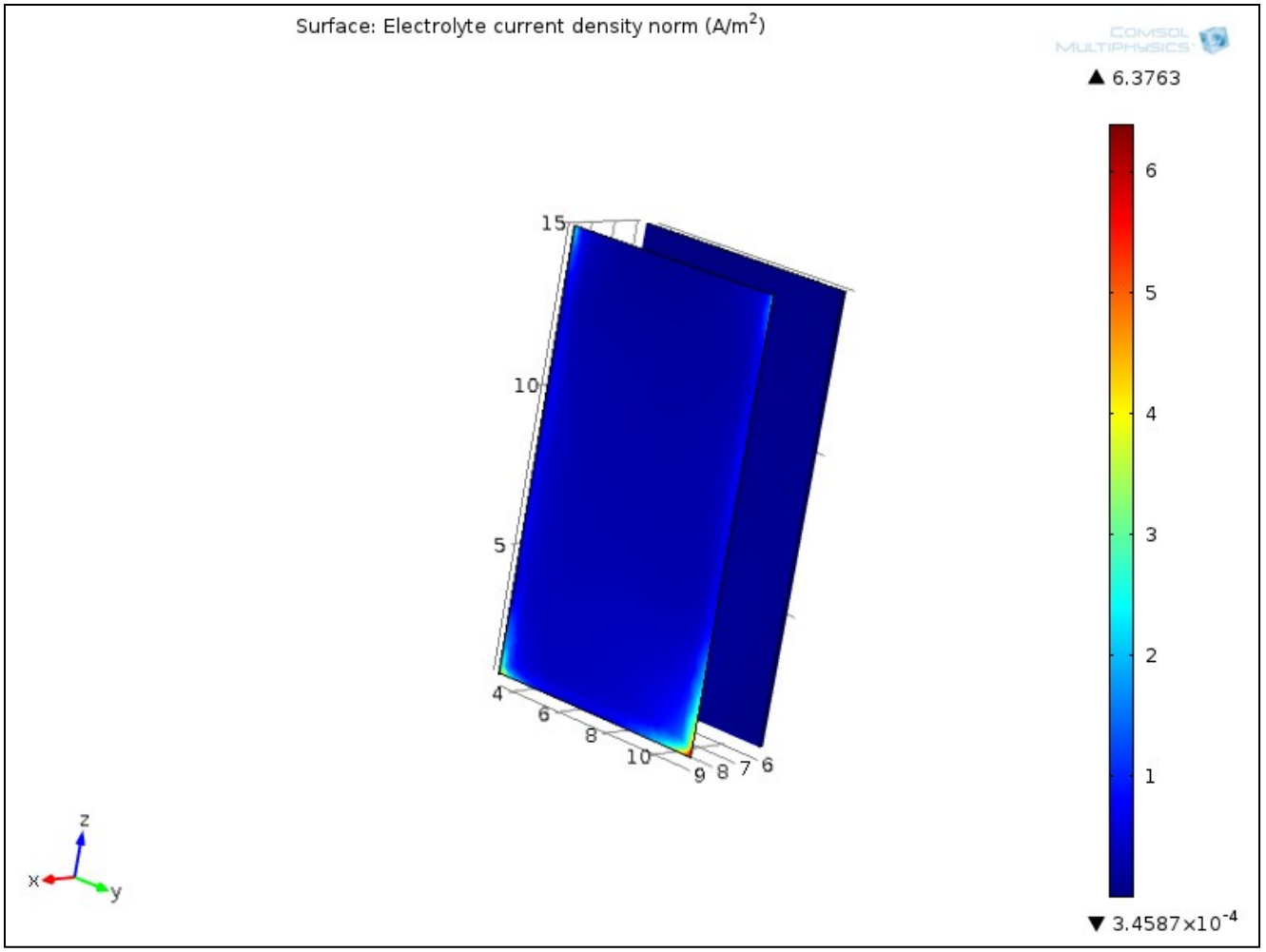

Fig. 47. Current distributions across the electrodes in an electrowinning cell at 325A/m^2 current density, 35g/l of Cu concentration at 35°C temperature.

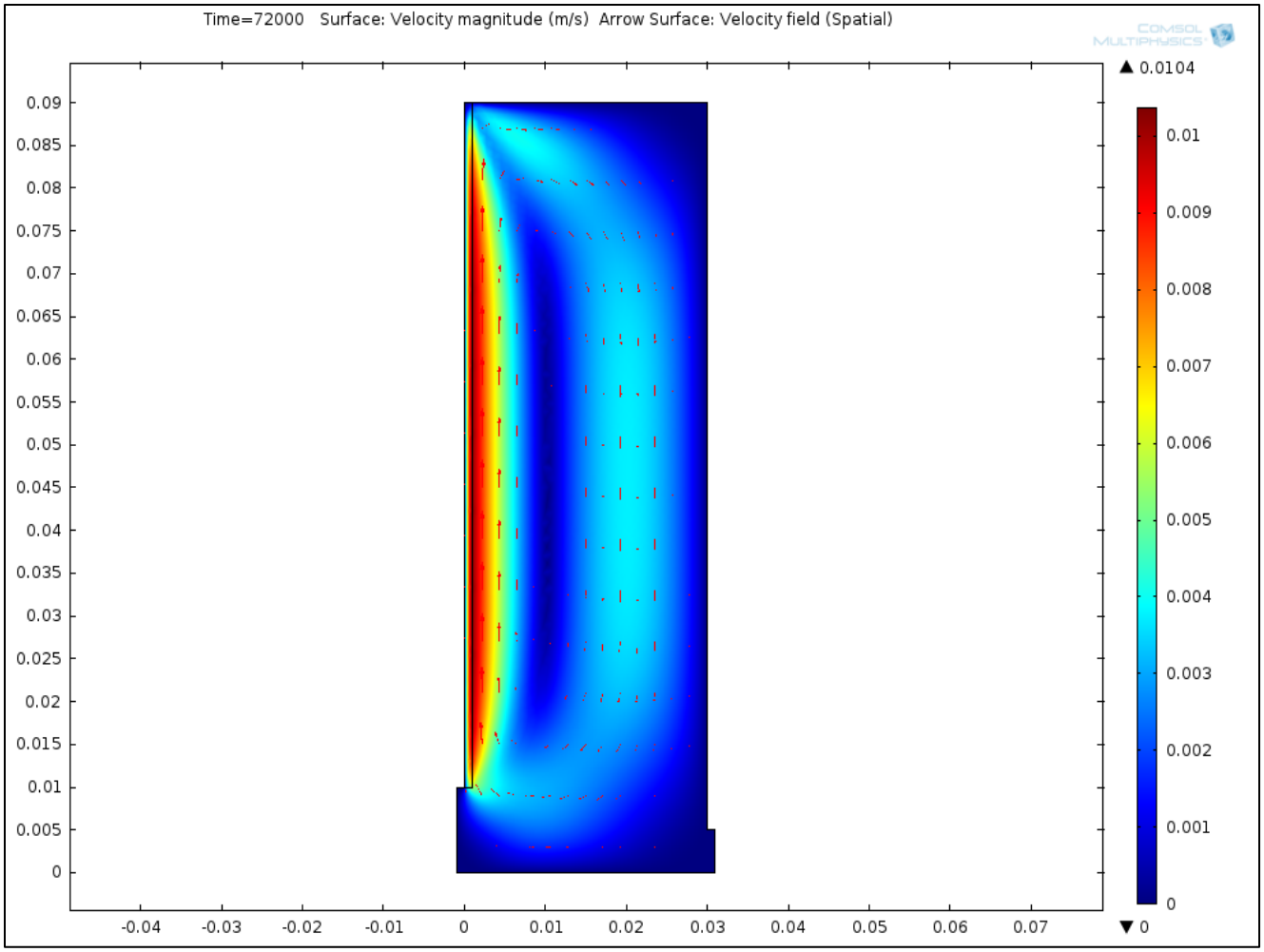

Fig. 48. Velocity distributions across the planar vertical electrodes at 475A/m^2 current density, 35 g/l of Cu concentration at 35°C temperature.

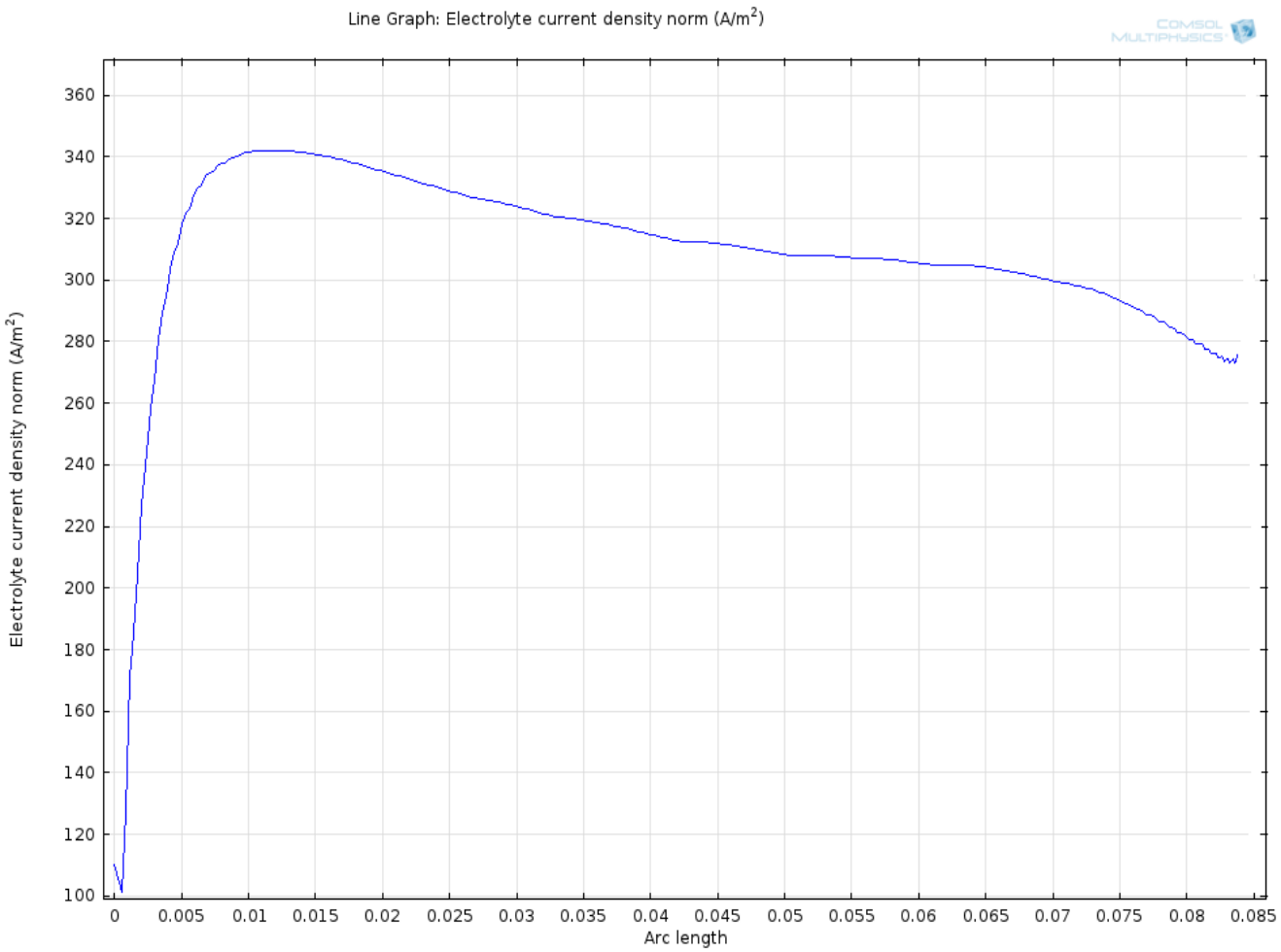

Fig. 49. Current density distributions along the cathode surface at 475A/m^2 current density, 35 g/l of Cu concentration at 35°C temperature.

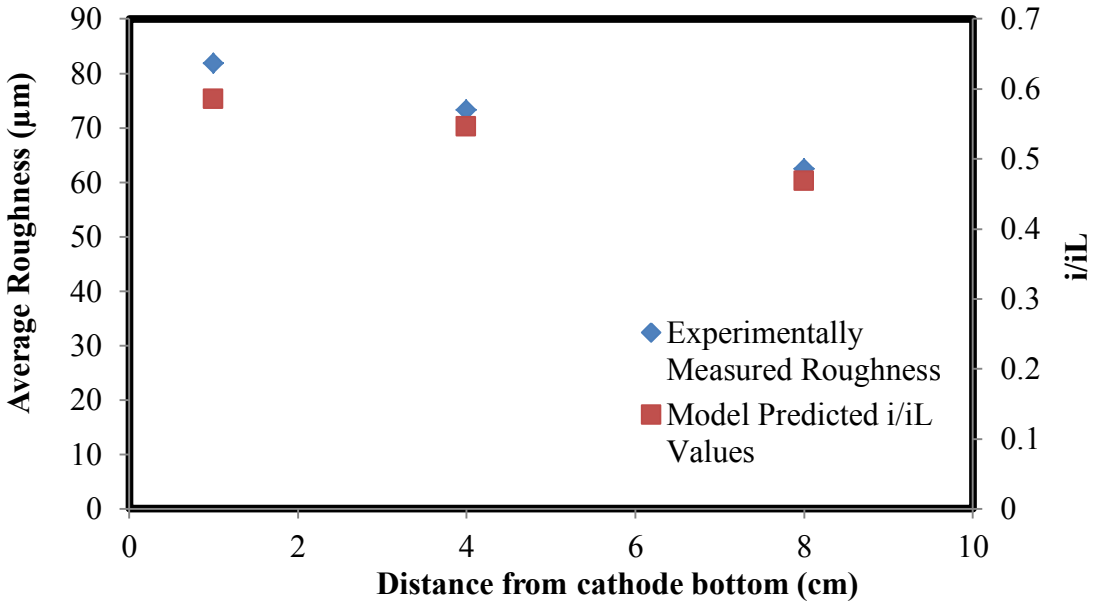

Fig. 50. Comparison of experimentally-measured roughness and model-predicted i/i_L values against the distance from cathode bottom for the experiment with 35 g/l of Cu, 55°C Temperature, 475 A/m^2 Current Density, and 175 g of guar per ton of copper cathode.

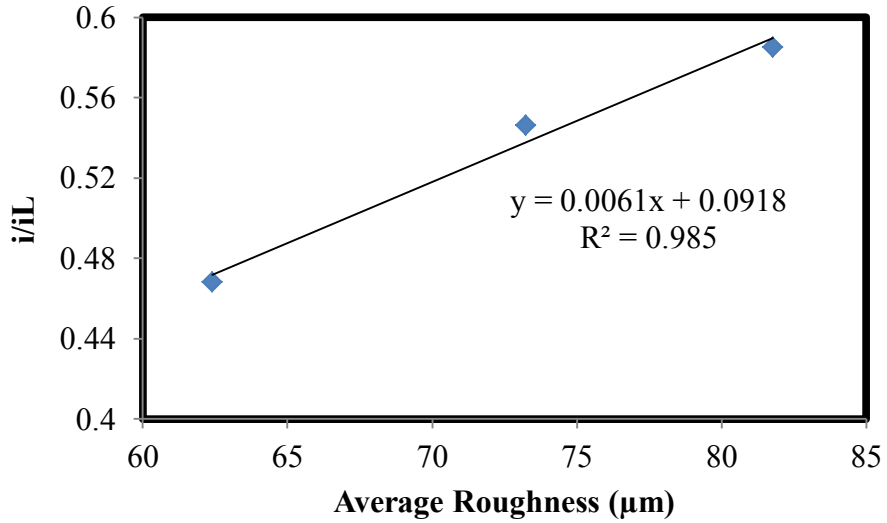

Fig. 51. Plot of model-predicted i/i_L versus experimentally-predicted average roughness for the experiment with 35 g/l of Cu, 55°C Temperature, 475 A/m^2 Current Density, and 175 g of guar per ton of copper cathode.

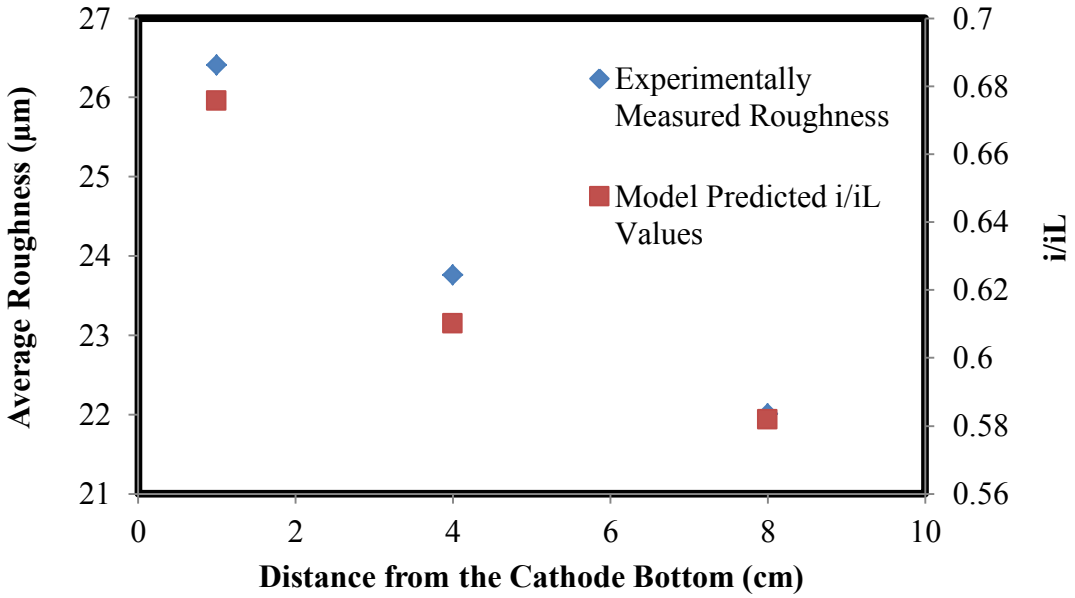

Fig. 52. Comparison of experimentally-measured roughness and model-predicted i/i_L values against the distance from cathode bottom for the experiment with 45 g/l of Cu, 55°C Temperature, 325 A/m^2 Current Density, and 325 g of guar per ton of copper cathode.

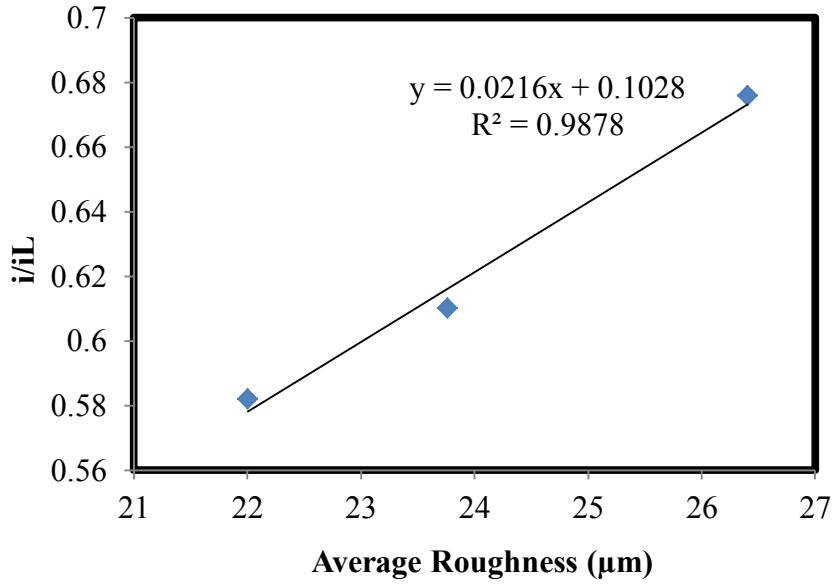

Fig. 53. Plot of model-predicted i/i_L versus experimentally-predicted average roughness for the experiment with 45 g/l of Cu, 55°C Temperature, 325 A/m^2 Current Density, and 325 g of guar per ton of copper cathode.

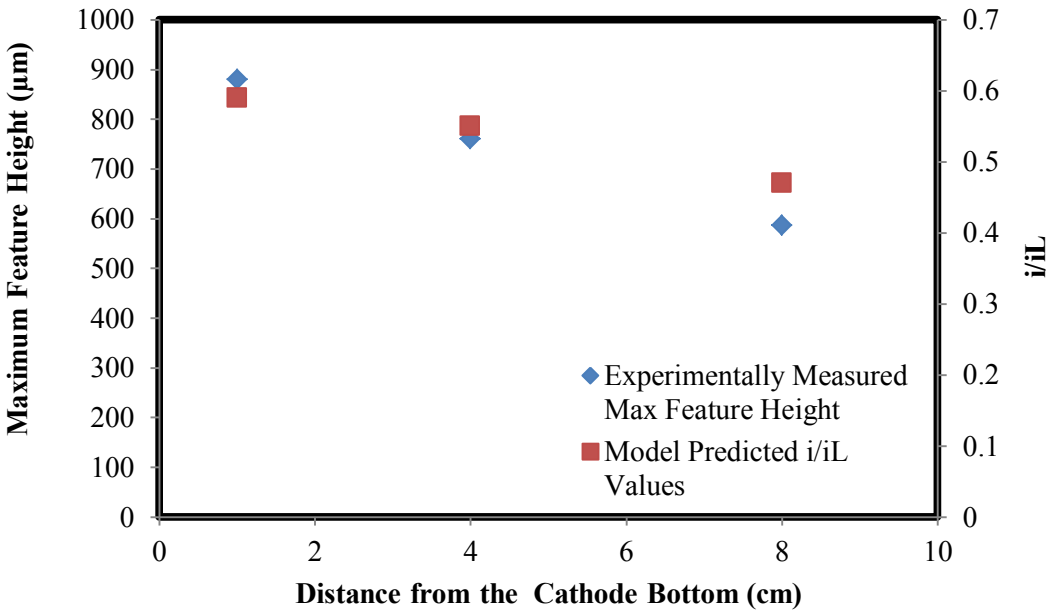

Fig. 54. Comparison of experimentally-measured Maximum Feature Heights and model-predicted i/i_L values versus the distance from cathode bottom for the experiment with 35 g/l of Cu, 55°C Temperature, 475 A/m^2 Current Density, and 175 g of guar per ton of copper.

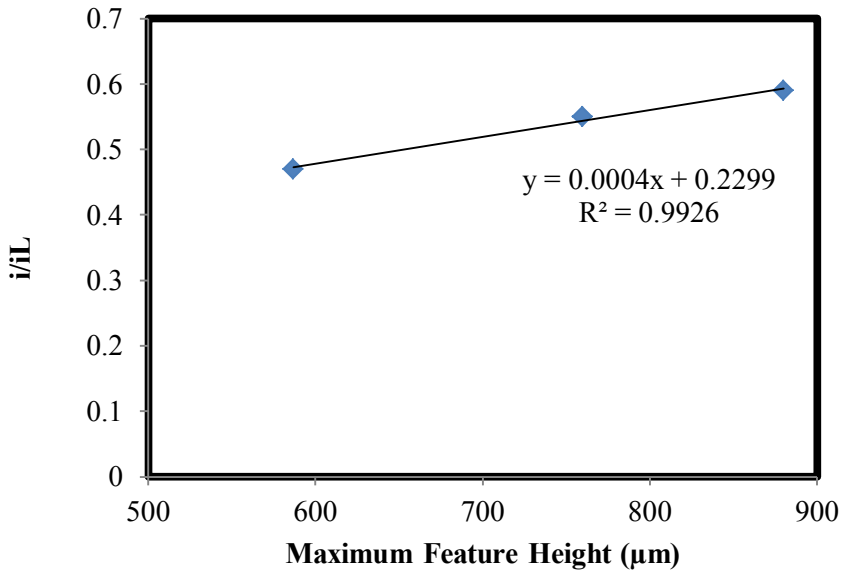

Fig. 55. Plot of model-predicted i/i_L versus experimentally-predicted average roughness for the experiment with 35 g/l of Cu, 55°C Temperature, 475 A/m^2 Current Density, and 175 g of guar per ton of copper cathode.

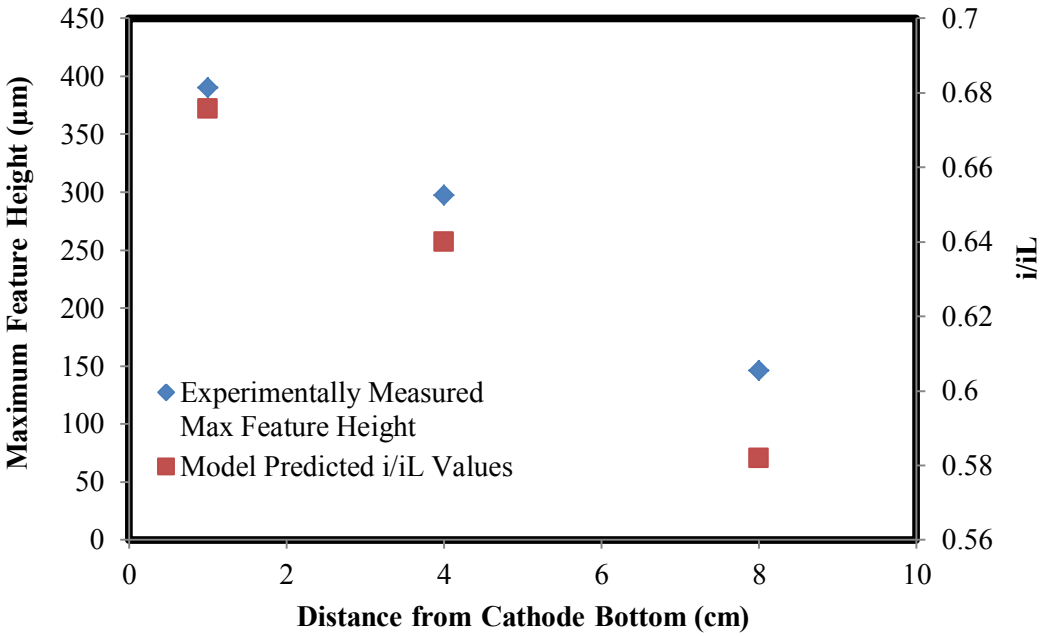

Fig. 56. Comparison of experimentally-measured Maximum Feature Height and model-predicted i/i_L values versus the distance from cathode bottom for the experiment with 45 g/l of Cu, 55°C Temperature, 325 A/m^2 Current Density, and 325 g of guar per ton of copper cathode.

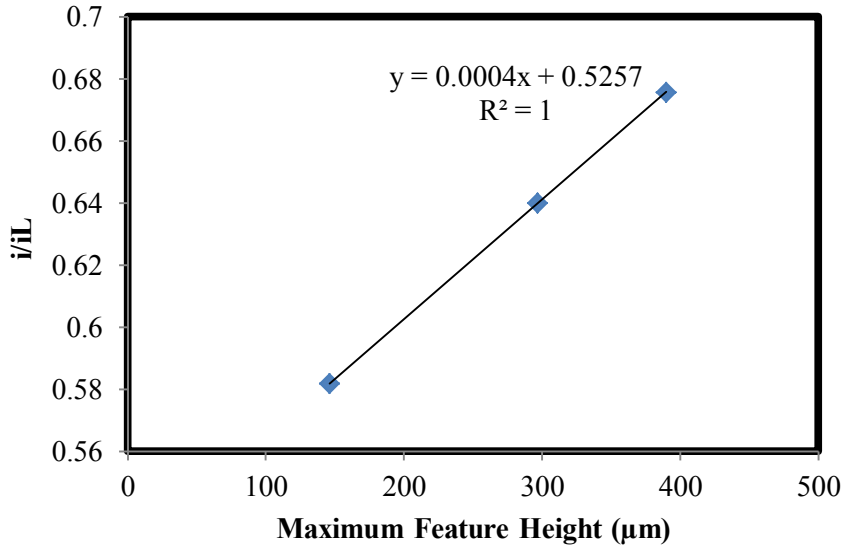

Fig. 57. Plot of model-predicted i/i_L versus experimentally-predicted maximum feature height for the experiment with 45 g/l of Cu, 55°C Temperature, 325 A/m^2 Current Density, and 325 mg of guar per ton of copper cathode.

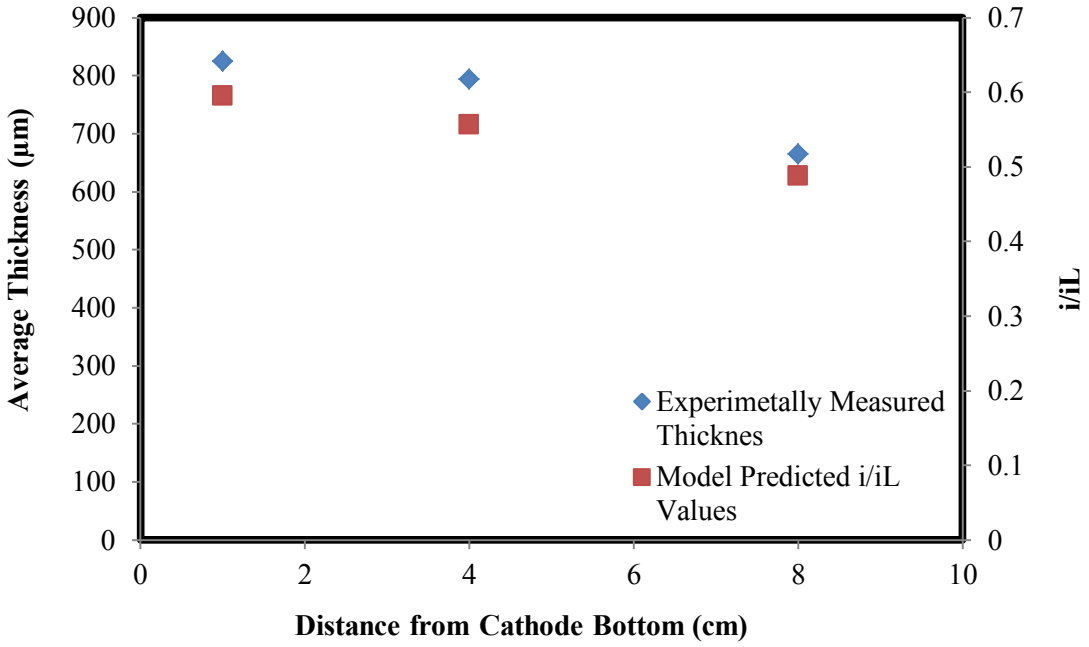

Fig. 58. Comparison of experimentally-measured thickness and model-predicted i/i_L values versus the distance from cathode bottom for the experiment with 35 g/l of Cu, 55°C Temperature, 475 A/m^2 Current Density, and 175 g of guar per ton of copper cathode.

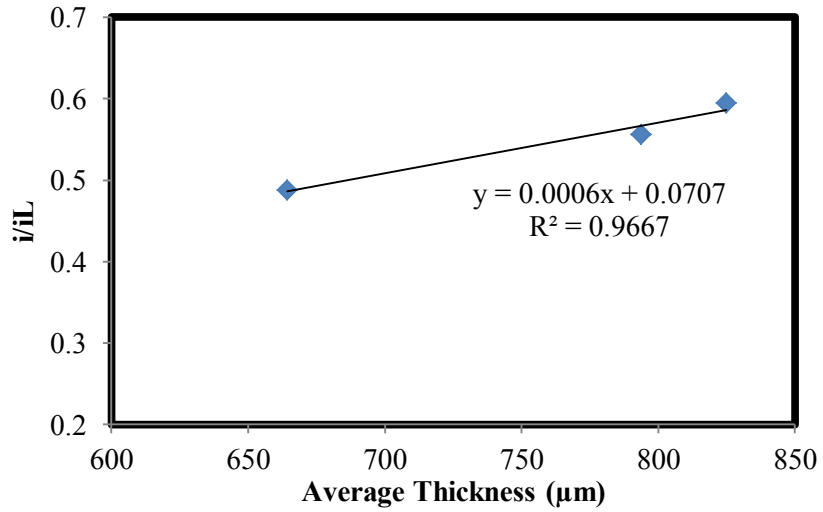

Fig. 59. Plot of model-predicted i/i_L versus experimentally-measured average thickness for the experiment with 35 g/l of Cu, 55°C Temperature, 475 A/m^2 Current Density, and 175 g of guar per ton of copper cathode.

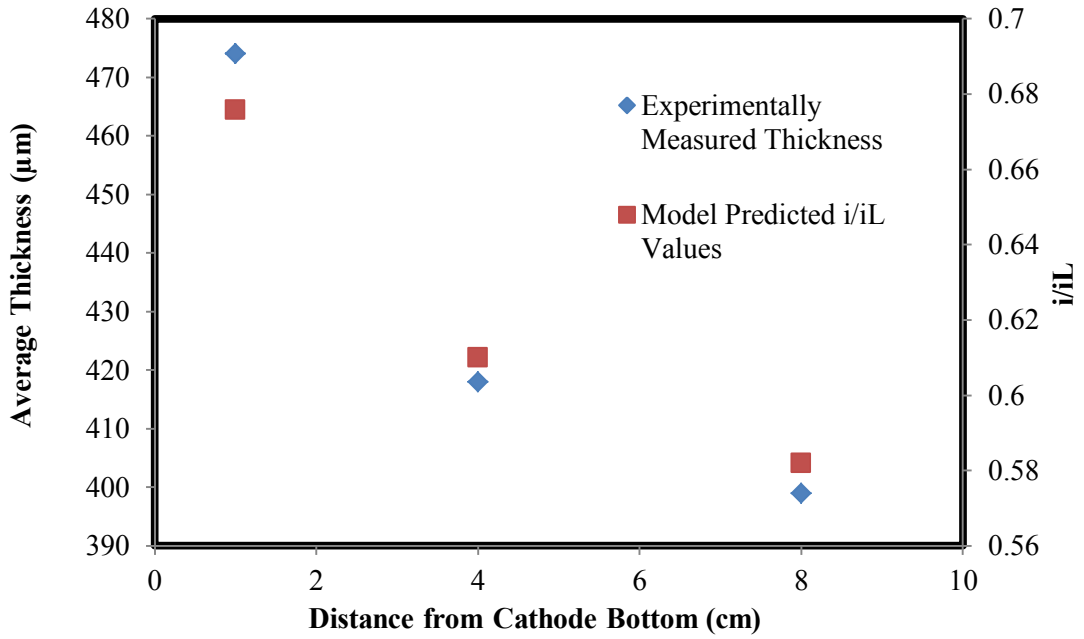

Fig. 60. Comparison of experimentally-measured thickness and model-predicted i/i_L values versus the distance from cathode bottom for the experiment with 45 g/l of Cu, 55°C Temperature, 325 A/m^2 Current Density, and 325 g of guar per ton of copper cathode.

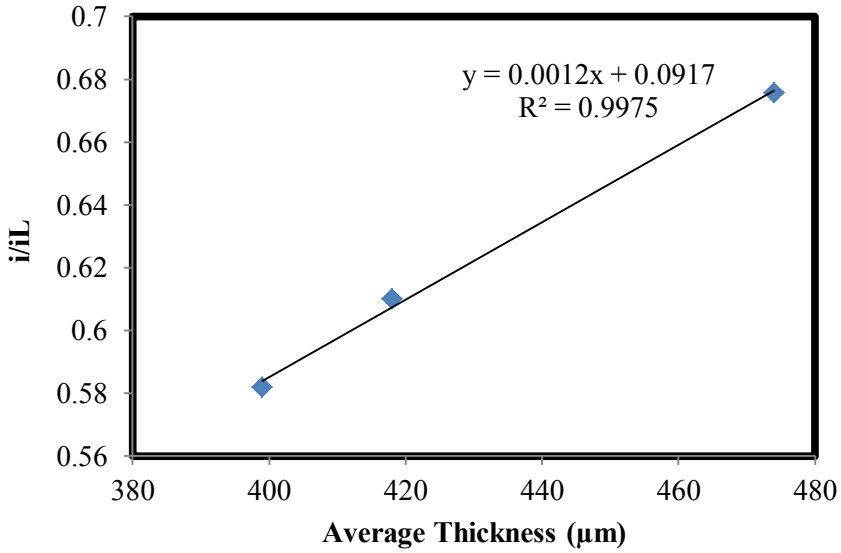

Fig. 61. Plot of model-predicted i/i_L versus experimentally-measured average thickness for the experiment with 45 g/l of Cu, 55°C Temperature, 325 A/m^2 Current Density, and 325 g of guar per ton of copper cathode

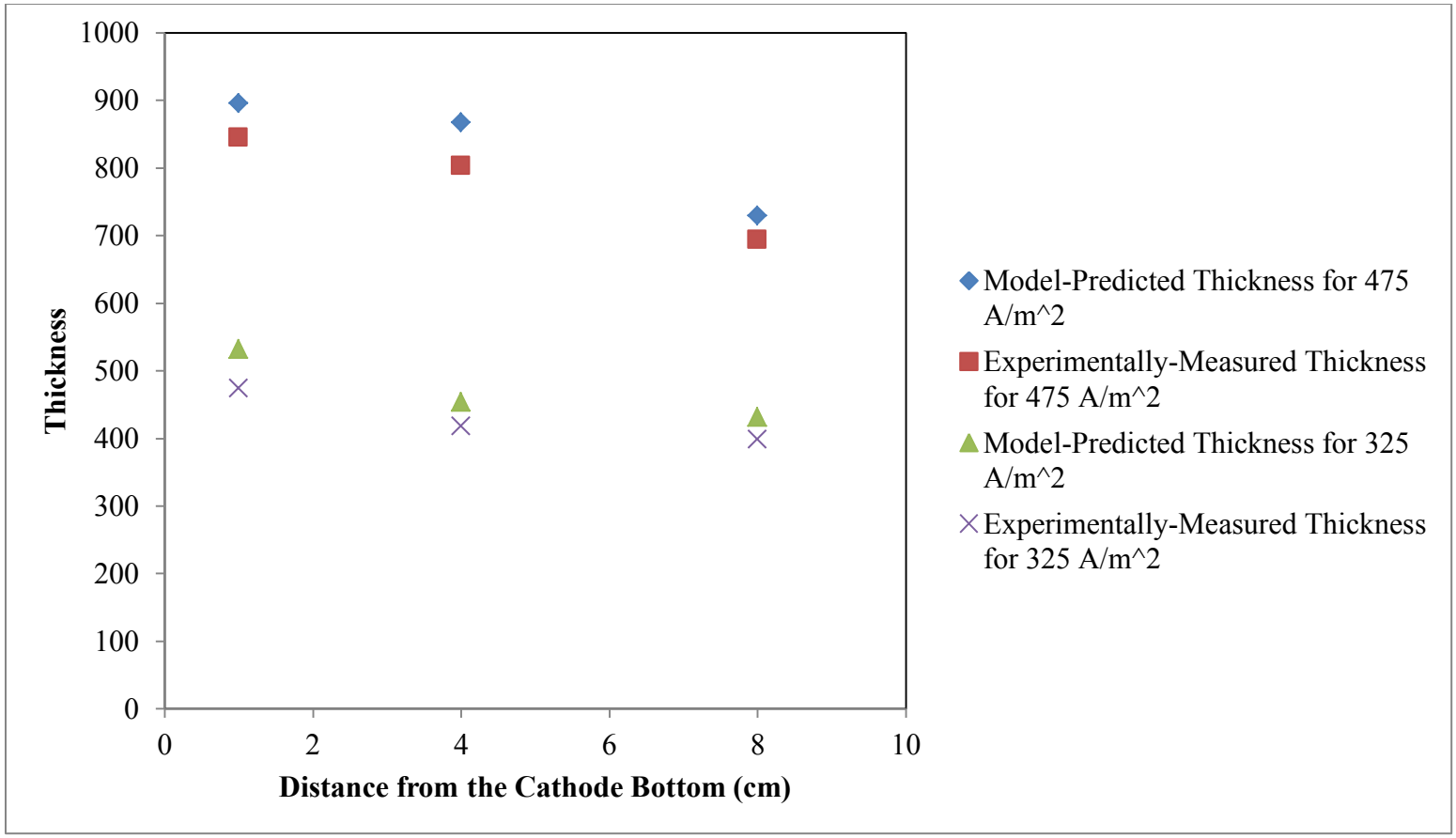

Fig. 62. Comparison of model-predicted and experimentally-measured thickness for 5-hour tests at 325 A/m^2 and 475 A/m^2.

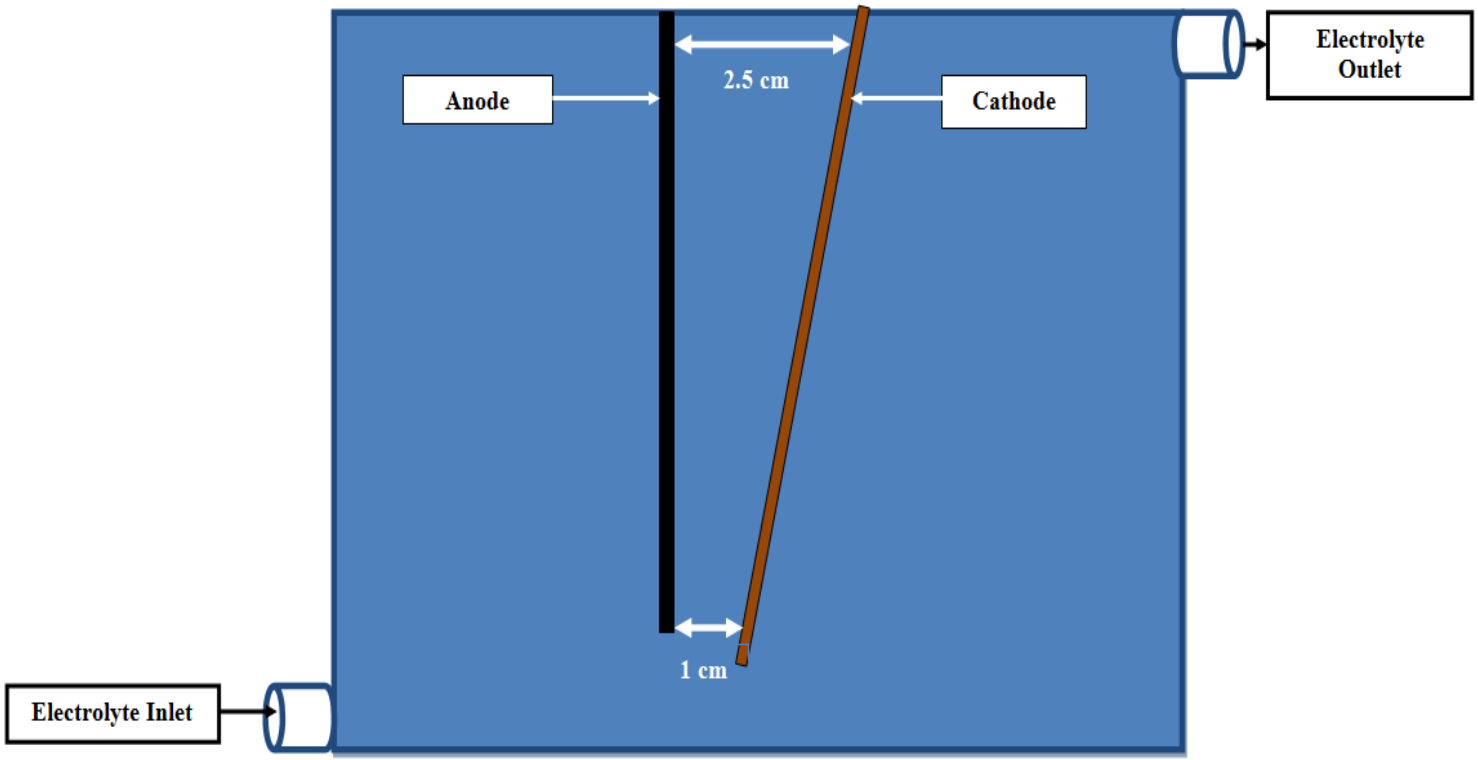

Fig. 63. Electrode setup for tilted cathode experiment.

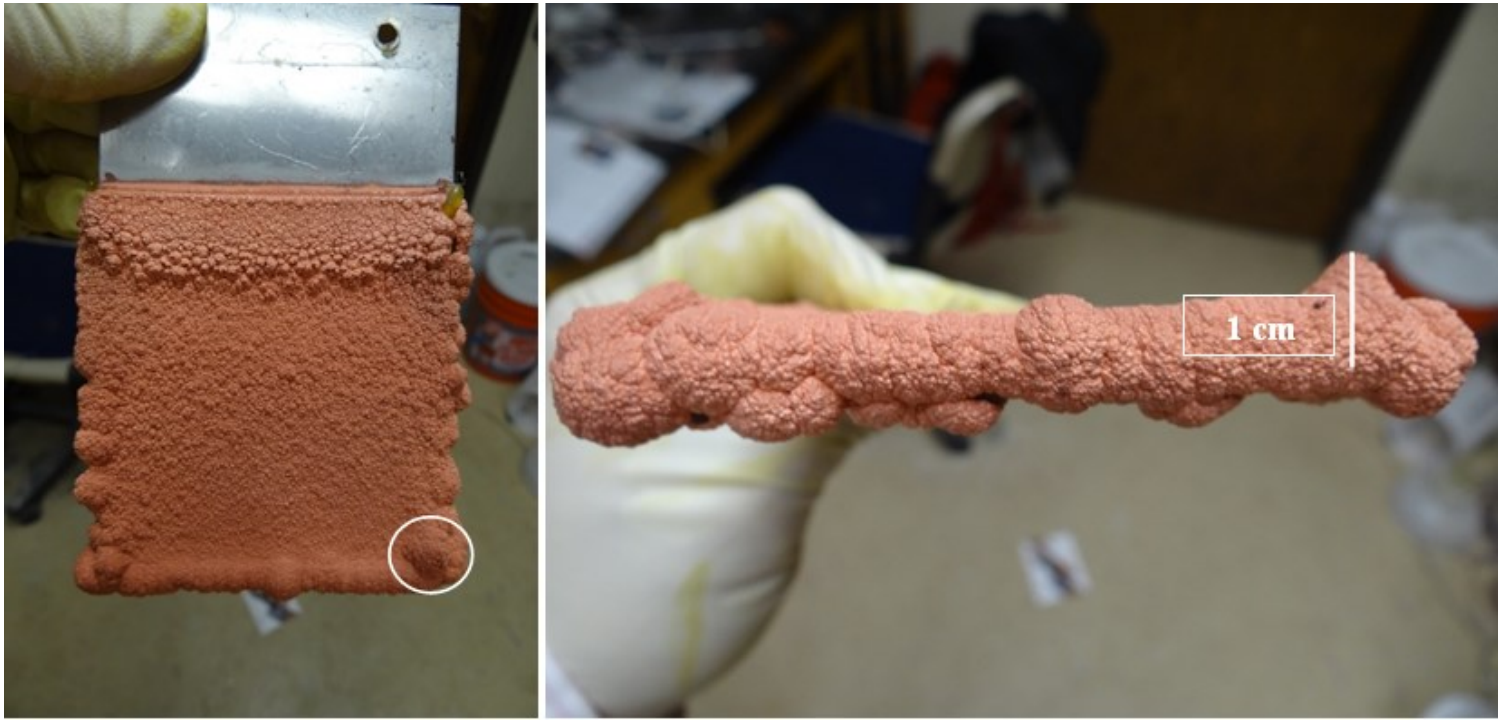

Fig. 64. The first short-circuiting for tilted cathode experiment occurred after 3 days of deposition, as shown in white circle (left) and white line (right).

CHAPTER 6

CONCLUSIONS

Unusual growth of copper deposit may cause short-circuits in copper electrowinning cells. The aim of this thesis was to investigate the effect of different operating parameters on the roughness of electrodeposited copper in an electrowinning cell and validate these experimental results with results obtained from modeling. Despite the variety of results proposed for the smooth deposition of copper, consensus exists that current density plays a determining role. Another influential operating parameter is electrolyte temperature. Most of the variation in cathode deposit roughness shown in this study can be explained by changes in these two parameters. To a lesser extent, concentration of guar and concentration of Cu in electrolyte solution also affected the roughness of cathode deposit. The conclusions of this thesis are grouped under two sections, statistical analysis of cathode deposits and FEA simulation.

6.1 Statistical Analysis of Cathode Deposits

According to the results presented in the results and discussions section, the following conclusions can be made:

- ✓ Statistical analysis of cathode deposit shows that edges of the cathode are thicker and rougher than the middle section of cathode. This higher thickness and roughness is caused by the higher current density in these areas.
- ✓ Statistical analysis of the deposits shows that current density is the most influential parameter affecting roughness of the deposit and Guar is the least affecting parameter.
- ✓ Interaction data for the cathode deposits suggests that current density and Cu concentration together affect the roughness of deposit more than the combined effect of guar and temperature.
- ✓ Short-circuiting occurs when the total growth of electrodeposit plus the maximum feature height exceeds the electrode separation distance. Based on 2.5 cm electrode separation distance and 95% current efficiency, the predicted time to short-circuiting for the experiment conducted at 325 A/m^2 current density, 45°C temperature, 250 gm of guar per tonne of copper cathode, and 45 g/l of copper is 23 days based on single line scan.
- ✓ The predicted time to short-circuiting for the experiment conducted at 475 A/m^2 current density, 55°C temperature, 175 gm of guar per tonne of copper cathode, and 35 g/l of copper is 12 days based on single line scan.
- ✓ Extrapolation of short-term, small sample area data into long-term, full-scale area data for maximum feature height predicted the time to short-circuit for the experiment at 475 A/m^2 current density, 55°C temperature, 175 gm of guar per tonne of copper cathode, and 35 g/l of copper to be 9.5 days, which is 2.5 days earlier than the line

scan data prediction. This prediction was verified by the experimental analysis and the results are in close proximity.

✓ A tilted cathode experiment was also carried out to see the effect of misaligned or bent cathodes on the time to short-circuit. The first short-circuit was obtained after 3 days of experiment, which is significantly less than the time to short-circuit without having a misaligned cathode.

6.2 Mathematical Modeling and Simulation

Simulation was performed on a 2D geometry of a copper electrowinning cell and these simulation results were compared with experimentally-obtained data. The comparison made between these two suggests that the model is a good predictor of the effect of operating parameters. The following conclusions can be made from these comparisons:

✓ The model suggests that the oxygen bubble generation at the anode has a significant effect on the conductivity of the solution. The electrolyte containing oxygen bubbles has less conductivity than the electrolyte without oxygen bubbles.

✓ As seen in statistical analysis of measured cathode deposit, edges are thicker and rougher than the middle section. The model predicted the same trend by showing the higher current densities at these areas of thicker deposits.

✓ The model-predicted flow of electrolyte between two electrodes is in close proximity to the results obtained from Ziegler and Evans[39].

✓ If the ratio of current density to limiting current density (i/i_L) is high at some point of the cathode, these areas have more thickness and roughness[50]. Thickness,

roughness, and maximum feature heights were compared with the simulation-obtained i/i_L values and similar trends were observed.

REFERENCES

1. Walker, A. Plant for the electrodepositación of metals. Dec 3, 1901.

2. Laitinen, I. S.; Tanttu, J. T., Modelling and simulation of a copper electrolysis cell group. *Simulation Modelling Practice and Theory* **2008,** *16* (8), 900-909.

3. W. G. Davenport, M. K., M. Schlesinger and A. K. Biswas, *Extractive Metallurgy of Copper*. 4th ed.; Elsevier Science Ltd.: Oxford, 2002.

4. Scully, J. C., *The Fundamentals of Corrsion*. 2nd ed.; Pergamon Press: Oxford, UK, 1975.

5. Jones, D. A., *Principles and Prevention of Corrosion*. Macmillan Publishing Company: New York, 1992.

6. Allen J Bard, L. R. F., *Electrochemical Methods - Fundamentals and Applications*. 2nd ed.; John Wiley & Sons, INC.: New York, 2001.

7. Parthasaradhy, N. V., *Practical Electroplating Handbook*. Prentice Hall: New Jersey, 1989.

8. Free, M. L., *Chemical Processing and Utilization of Metals in Aqueous Media*. 2nd ed.; Copley Custom Textbooks: USA, 2004.

9. Msindo, Z. S. An investigation of the electrowinning of copper with dimensionally stable titanium anodes and conventional lead alloy anodes. University of the Witwatersrand, 2010.

10. Fierro, S.; Nagel, T.; Baltruschat, H.; Comninellis, C., Investigation of the oxygen evolution reaction on Ti/IrO2 electrodes using isotope labelling and on-line mass spectrometry. *Electrochemistry Communications* **2007,** *9* (8), 1969-1974.

11. Shakarji, R. A.; He, Y.; Gregory, S., Statistical analysis of the effect of operating parameters on acid mist generation in copper electrowinning. *Hydrometallurgy* **2011,** *106* (1-2), 113-118.

12. Stanke, P., Guar concentration measurement with the CollaMat system. In *Copper 99 - Cobre 99 proceedings of the fourth international conference, TMS*, Dutrizac, J. E., Ji, J. and Ramachandran, V., Ed. Warrendale, PA, 1999; Vol. 3.

13. R.D Prengaman, A. S., Improved copper electrowinning operations using wrought Pb-Ca-Sn anodes. In *Copper 99- Cobre 99 proceedings of the fourth international conference, TMS*, J.E. Dutrizac, J., J. and Ramachandran, V., Ed. Warrendale, PA, 1999; Vol. 3.

14. Maki, T., Evolution of cathode quality at Phelps Dodge Mining Company. In *Copper Leaching, Slovent Extraction and Electrowinning Technology, SME*, Jergensen II, G. V., Ed. Littleton, CO, 1999.

15. Laitinen, I. S. Modeling, simulation and optimization of electrolysis cell group. Tampere University of Technology, 2009.

16. COMSOL Electrodeposition Module. www.comsol.com.

17. COMSOL, ELectrodeposition Module User Guide. 2013. www.comsol.com.

18. COMSOL, COMSOL Multiphysics Users Guide. 2013. www.comsol.com.

19. Gupta, C. K., Mukherjee, T.K., *Hydrometallurgy in Extraction Processes*. 2nd ed.; CRC Press: Florida, USA, 1990.

20. Wiechmann, E. P.; Morales, A. S.; Aqueveque, P., Full measuring system for copper electrowinning processes using optibar intercell bars. *IEEE Transactions on Industry Applications* **2009,** *45* (5), 1575-1582.

21. Das, S. C.; Krishna, P. G., Effect of Fe(III) during copper electrowinning at higher current density. *International Journal of Mineral Processing* **1996,** *46* (1-2), 91-105.

22. Khouraibchia, Y.; Moats, M. S. In *Evaluation of the effect of copper electrowinning parameters on current efficiency and energy consumption using surface response methodology*, 2010; pp 295-306.

23. Owais, A., Effect of electrolyte characteristics on electrowinning of copper powder. *Journal of applied Electrochemistry* **2009,** *39*, 1587-1595.

24. Robinson, T., Davwnport, W., Moats, M., Karcas, G., Demetrio, S., World tankhouse operarting data. Houlachi, G. E., Edwards, J.E., Ed. 2007; Vol. V, pp 375-424.

25. Mishra, K., Copper, W.C.,, Electrochemical aspects of the direct electrowinning of copper from sulfuric acid leach solutions in the prsence of iron using gas sparging. In *TMS*, Robinson, D. J., James, S.E., Ed. Los Angeles, 1984; pp 13-36.

26. Pradhan, N., Krishna, P.G., Das, S.C., Influence of chloride ions on the electrocrystallization of copper. *Plating and Surface Finishing* **1996,** *83* (3), 56-63.

27. Fabian, C. P. Copper elctrodeposition in the presence of guar or activated polyacrylamide. James Cook University, 2005.

28. Panda, B., Effects of added chloride ion on electrodeposition of copper from a simulated acidic sulfate bath containing cobalt ions. Amity School of Engineering and Technology: Noida, Uttar pradesh, India.

29. Ilgar, E., O'Keefe, T. J., Surface rouhning of electrowon copper in the presence of chloride ions. In *The Minerals, Metals & Materials Society*, Dreisinger, D. B., Ed. 1997; pp 51-62.

30. (a) Fabricius, G., Sundholm, G., The effect of additives on the electrodeposition of copper studied by the impedence technique. *Journal of applied Electrochemistry* **1984,** *14* (6), 797-801; (b) Yao, Y. L., Functions of chloride in copper refining electrolyte. **1944**, 371-382.

31. Subbaiah, T., Kammel, R., **1986,** *XXVIII* (4).

32. Anderson, T. N., Wright, C.N., Richards, K.J., Important electrochemical aspects of electrowinning copper from acid leach solution. In *International Symposium on Hydrometallurgy*, Evans, D. J. I., Shoemaker, Ed. A.I.M.E.: New York, 1973.

33. Gruenfelder, A. S., Ettel, V.A., Shinichiro, A., The science and technology of the metal, its alloy and compounds. *ACS* **1960**, 319.

34. Greenwalt, W. C., *Trans. of AIME* **1924**.

35. Mantell, C. L., *Electrochemical Engineering*. McGraw Hills: New York, 1960.

36. Winand, R., Electrocrystallization of copper. *Trans. Inst. Min. Metall.* **1975,** *84*, 67-75.

37. Gil, A. F., Galicia, L.,Gonzalez, I., Diffusion coefficients and electrode kinetics parameters of different Fe(III)-sulfate complexes. *Journal of Electroanalytical Chemistry* **1996,** *417*, 129-134.

38. Hiskey, J. B., Principle and practical consideration of copper electrorefining and electrowinning. In *Society for Mining, Metallurgy and Exploration*, Jergenson, G. V., Ed. 1999; pp 169-186.

39. Ziegler, D., Evans, J.W., <Mathematical Modeling of Electrolyte Circulation in Cells with.pdf>. *Journal of Electrchemical Society* **1986,** *133* (3), 567-576.

40. Jennings, D.; Kuhn, A. T.; Stepanek, J. B.; Whitehead, R., A mass-transfer study of two-phase flow in an electro・chemical reactor. *Electrochimica Acta* **1975,** *20* (11), 903-907.

41. (a) Ettel, V. A.; Tilak, B. V.; Gendron, A. S., Measurement of Cathode Mass Transfer Coefficients in Electrowinning Cells. *Journal of The Electrochemical Society* **1974,** *121* (7), 867-872; (b) Gendron, A. S.; Ettel, V. A., Hydrodynamic studies in natural and forced convection electrowinning cells. *The Canadian Journal of Chemical Engineering* **1975,** *53* (1), 36-40.

42. Sides, P. J.; Tobias, C. W., Resistance of a Planar Array of Spheres: Gas Bubbles on an Electrode. *Journal of The Electrochemical Society* **1982,** *129* (12), 2715-2720.

43. Vogt, H., The incremental ohmic resistance caused by bubbles adhering to an electrode. *Journal of Applied Electrochemistry* **1983,** *13* (1), 87-88.

44. Tobias, C. W., Effect of Gas Evolution on Current Distribution and Ohmic Resistance in Electrolyzers. *Journal of The Electrochemical Society* **1959,** *106* (9), 833-838.

45. Philippe, M.; Jérôme, H.; Sebastien, B.; Gérard, P., Modelling and calculation of the current density distribution evolution at vertical gas-evolving electrodes. *Electrochimica Acta* **2005,** *51* (6), 1140-1156.

46. Cross, M.; Croft, T. N.; Djambazov, G.; Pericleous, K., Computational modelling of bubbles, droplets and particles in metals reduction and refining. *Applied Mathematical Modelling* **2006,** *30* (11), 1445-1458.

47. Montgomery C., D., Runger C., Runger, *Applied Statistics and Probability for Engineers*. 5th ed.; 2011.

48. Filzwieser, A., Hein, K., Hanko, G., Grogger, H., Application of two phse hydrodynamics modeling to an electrowinning cell. University of Leoben: Austria.

49. Mathew, R. J., Increasing oxygen charge transfer resistance on the anode in copper electrowinning. In *The Minerals, Metals & Materials Society*, USA, 2012.

50. Bhide, R. Quantifying the Effects of Mass Transport on Surface Roughness of Copper Electrodeposits from Chloride Media. University of Utah, Salt Lake City, Utah, USA, 2008.